

**Effect of Forskolin on Actin Polymerization
in Cultured Vascular Smooth Muscle**

Thesis submitted to
The Graduate College of
Marshall University

In partial fulfillment of the
Requirements for the Degree of
Master of Science
Chemistry

by
Mary Janay Bailey
Marshall University
Huntington, West Virginia
April 2001

This thesis was accepted on April 19, 2001 as meeting the research requirements for the master's degree.

Department of Chemistry

Advisor Willy P. Ri

Committee Members [Signature]
[Signature]

Dean of the Graduate College Ronald Deutch

Acknowledgements

I would like to express my heart felt thanks to Dr. W.D. Price, Dr. G. L. Wright and Dr. R.T. Wang for their dedication and contribution to this research project and acknowledge my most profound debt of all to Dr. W.D. McCumbee for his unfailing encouragement, patience and support. I would also like to thank my parents, Bill and Danna Bailey and my brothers John and Matthew Bailey.

Index of Text	Page
A. Introduction:	10
1. Overview	10
a. Interactions of Forskolin with the cAMP Signaling Pathway	13
b. Proteins Associated with Smooth Muscle	16
c. Smooth Muscle Proteins and the Contractile Response	18
d. Thin Filament Regulatory Proteins	19
e. Effects of Cell Culture on the Expression of Proteins in the Smooth Muscle Cell	20
f. Forskolin Induced Arborization of Cultured Vascular Smooth Muscle Cells	22
2. Electron Microscope	38
3. Confocal Microscope	41
a. Fluorescein	43
b. Rhodamine Fluorophores	43
4. Immunoprecipitation	45
B. Statement of Problem	47
C. Methods	48
1. Animals	48
2. Cell Culture	
3. Confocal Microscopy	49
4. Light Microscopy	49

5. Light Microscopy Staining	50
6. Transmission Electron Microscopy	50
7. Immunoblot Analysis	51
8. Two-dimensional Electrophoresis	52
a. First Dimension	52
b. Second Dimension	53
9. Radiolabeling	53
10. Immunoprecipitation	54
D. Results	55
1. Transmission Electron Microscope Images	55
2. Light Microscopy Images	58
3. Confocal Microscopy Images	64
4. Western Blot Analysis for the Expression of Actin in Vascular Smooth Muscle Cells	72
5. Western Blot Analysis of Immunoprecipitated Alpha-actin in Stimulated VSM	75
6. Analysis of ^{33}P Radiolabeled Immunoprecipitated Alpha-actin in Stimulated Vascular Smooth Muscle Cells in Comparison with the Coomassie Brilliant Blue Stained Gel	78
7. Two-dimensional Comparison of the Expression of Actin in Forskolin Treated Vascular Smooth Muscle Cells	81
8. Time Course Study	82
9. Concentration Study	84

E. Conclusion	86
F. Appendix	87
1. Mass Spectrometry Background	87
2. Millipore ZipTip	94
3. Mass Spectrometry Sample Preparation	94
4. Trypsin In-Gel Digestion of Proteins	95
5. Reverse-phase ZipTip Sample Preparation	96
6. MALDI-MS Analysis	96
7. Actin Standard	97
8. Mass Spectrum Identification	97
9. Trouble Shooting	98
G. Works Sited	101

Index of Figures	Page
Figure 1. 7b-acetoxy-8, 13-epoxy-1a, 6b,9a-trihydroxy-labd-14-en-11-one (Forskolin).	24
Figure 2. cAMP Pathway.	25
Figure 3. Conversion of ATP to cyclic AMP via Adenylate Cyclase.	26
Figure 4. Adenylate Cyclase.	27
Figure 5. Protein Kinase A.	28
Figure 6. The Effect of cAMP on Calcium Mobilization and Contraction in Smooth Muscle. (Calmodulin is abbreviated as CaM).	29
Figure 7. The Sarcoplasmic (Endoplasmic) Reticulum Associated Calcium Pump.	30
Figure 8. G-Actin.	31
Figure 9. F-Actin and Its Associated Proteins.	32
Figure 10. Myosin.	33
Figure 11. The Spatial Relationship of Actin and Myosin to the Cell Membrane.	34
Figure 12. Cross Bridge Formation and the Effects of Calcium Concentration.	35
Figure 13. Smooth Muscle Contraction.	36
Figure 14. The Tropomyosin and Actin Complex.	37
Figure 15. The Transmission Electron Microscope.	40
Figure 16. The Confocal Microscope.	44
Figure 17. Principles of Immunoprecipitation.	46
Figure 18. Vascular Smooth Muscle Cells Imaged on the Electron Microscope.	56

Figure 19. Electron Microscope Image of Vascular Smooth Muscle Cells	
Exposed to 5×10^{-6} M Forskolin for a One Hour Interval.	57
Figure 20. Vascular Smooth Muscle Control Cells Imaged on a Light Microscope.	59
Figure 21. Light Microscopy Image of Vascular Smooth Muscle Cells	
Exposed to 5×10^{-6} M Forskolin for a Thirty Minute Interval.	60
Figure 22. Light Microscopy Image of Vascular Smooth Muscle Cells	
Exposed to 5×10^{-6} M Forskolin for a One Hour Interval.	61
Figure 23. Light Microscopy Image of Vascular Smooth Muscle Cells	
Exposed to 5×10^{-6} M Forskolin for a Three Hour Interval.	62
Figure 24. Light Microscopy Image of Vascular Smooth Muscle Cells	
Exposed to 5×10^{-6} M Forskolin for a Twenty-Four Hour Interval.	63
Figure 25. Vascular Smooth Muscle Control Cells Imaged on the Confocal Microscope.	66
Figure 26. Confocal Microscopy Image of Vascular Smooth Muscle Cells	
Exposed to 5×10^{-6} M Forskolin for a Ten Minute Interval.	67
Figure 27. Confocal Microscopy Image of Vascular Smooth Muscle Cells	
Exposed to 5×10^{-6} M Forskolin for a Thirty Minute Interval.	68
Figure 28. Confocal Microscopy Image of Vascular Smooth Muscle Cells	
Exposed to 5×10^{-6} M Forskolin for a One Hour Interval.	69
Figure 29. Confocal Microscopy Image of Vascular Smooth Muscle Cells	
Exposed to 5×10^{-6} M Forskolin for a Three Hour Interval.	70

Figure 30. Confocal Microscopy Image of Vascular Smooth Muscle Cells Exposed to 5×10^{-6} M Forskolin for a Twenty-Six Hour Interval.	71
Figure 31. Western Blot for the Expression of Actin by Control and Forskolin Stimulated Vascular Smooth Cells.	73
Figure 32. Expression of Actin by Control and Forskolin Stimulated Vascular Smooth Cells.	74
Figure 33. Western Blot of Immunoprecipitated Alpha-actin in Stimulated Vascular Smooth Muscle Cells.	76
Figure 34. The Expression of Actin in Immunoprecipitated Alpha-actin in Stimulated Vascular Smooth Muscle Cells.	77
Figure 35. Coomassie Brilliant Blue Stained Immunoprecipitated Alpha-actin in Stimulated Vascular Smooth Muscle Cells.	79
Figure 36. ^{33}P Radiolabeled Immunoprecipitated Alpha-actin in Stimulated VSM.	80
Figure 37. Forskolin Effects on Vascular Smooth Muscle Arborization. A Time Course Study.	83
Figure 38. Forskolin Concentration Effects On Arborization Following a Thirty Minute Incubation.	85
Figure 39. The Finnigan LCQ Mass Spectrometer.	92
Figure 40. The Matrix Assisted Laser Desorption Ionization Time of Flight Mass Spectrometer (MALDI-TOF MS).	93

A. Introduction

1. Overview

Forskolin, a diterpene derivative of the labdane family, has been found to have a profound influence on cardiovascular function within mammals (Lindner et. al., 1978). When administered to experimental animals, forskolin not only increases the force (inotropic effect) and rate (chronotropic effect) of cardiac contraction but is found to decrease blood pressure (hypotensive effect) as well. The inotropic and chronotropic effects results from the direct action of forskolin on the heart whereas the hypotensive effect stems from the relaxing influence of forskolin on vascular smooth muscle. Both the cardiac and vascular effects are thought to be due to a stimulatory action of forskolin on adenylate cyclase (Daly, 1984), the enzyme that catalyzes of the formation of cAMP (cyclic adenosine monophosphate) from ATP (adenine triphosphate) in the cAMP regulatory pathway.

Forskolin was originally extracted from the roots of *Coleus forskolii*, a perennial herb used in folk medicines on the Indian subcontinent (Seamon and Daly, 1981). The name forskolin specifically applies to the principal diterpene obtained from a methanol extract of the Coleus root. The chemical name of this compound is 7 beta-acetoxy-8, 13-epoxy-1alpha, 6 beta, 9 alpha-trihydroxy-labd-14-en-11-one (The Merck Index, 1996). The chemical structure is demonstrated in figure 1. Studies comparing synthetic derivatives of forskolin with the naturally occurring diterpene indicate that there are specific stereochemical requirements for eliciting a maximal physiological response. In particular, the 1 and 9 a-hydroxy groups are thought to be necessary for the complete activation of adenylate cyclase (de Souza, 1983).

The impact of forskolin on cardiac function has been investigated both in

experiments with animals and clinical studies with humans. Lindner et al. (1978) demonstrated that forskolin increases heart rate, the force of cardiac muscle contraction and blood flow in the coronary vessels of the heart wall in a dose dependent manner in isolated guinea pig hearts. Using isolated papillary muscles from the left ventricle of the guinea pig heart, they also showed that forskolin shortens the duration of the action potential and refractory period. Moreover, they revealed increases in cardiac contractility, heart rate and cardiac output in anesthetized dogs upon forskolin administration. In clinical studies, forskolin was shown to improve left ventricular function when given to patients with dilated cardiomyopathy (Kramer et. al., 1980). Similarly, Bauman et.al. (1990), observed an increase in cardiac output in patients with congestive cardiomyopathy.

The effects of forskolin on blood pressure and blood flow in specific arteries have also been explored through human and animal studies. Baumann et. al. (1990), reported that forskolin reduced systolic, diastolic and mean arterial pressure in a dose-dependent manner in patients with congestive cardiomyopathy. Lindner et.al. (1978), showed that forskolin elicited a fall in blood pressure in anesthetized dogs, cats and in rats with experimentally-induced hypertension. In addition, Linder et.al. (1978) observed that forskolin increased coronary blood flow in the isolated guinea pig heart. These effects are due to the ability of forskolin to bring about a potent relaxation of arterial smooth muscle. A direct effect of forskolin on smooth muscle relaxation has been demonstrated in different arterial segments from a variety of animal species (Lincoln and Fisher-Simpson, 1983; Vegesna and Diamond, 1984; Vegesna and Diamond, 1986).

The direct action of forskolin on the adenylate cyclase-cyclic AMP signaling pathway in vascular smooth muscle suggests that this diterpene derivative may be a useful tool for studying pathophysiological mechanisms associated with hypertension. A key characteristic of hypertension in man (Karsner, 1938; Furuyama, 1962) and

experimental animals (Wolinsky, 1970) is that arterial smooth muscle cells undergo hypertrophy. The hypertrophy of vascular smooth muscle cells, in turn, increases the overall thickness of the arterial wall and is thought to contribute to the maintenance of hypertension. The increased thickness of the arterial wall, decreases the lumen size of the vessel restricting volume flow. In many different experimental models of hypertension, an increase in the cellular content of cyclic AMP has also been observed in the thickened arterial walls of the hypertensive animals relative to corresponding normotensive control animals (Chatelain, 1983; Mangiarua et. al. 1989). Data from several different laboratories suggest that the elevated cyclic AMP levels in vascular smooth muscle cells of hypertensive animals exist prior to the development of vessel hypertrophy (Chatelain, 1983; Chatelain et. al., 1985). Moreover, McCumbee and Mangiarua (1991) have demonstrated that cyclic AMP is able to induce changes in nutrient transport and macromolecule synthesis in vascular smooth muscle that are consistent with the development of vascular hypertrophy.

In a recent report by Wright and Battistella-Patterson (1998), it has been suggested that the cytoskeleton is involved in calcium-dependent stress relaxation of aortic smooth muscle. Specifically, they observed that cytochalasin B, a compound which blocks actin polymerization, was able to inhibit stress-induced relaxation whereas colchicine, a drug that causes microtubules to disassemble, had no effect. These observations suggest that actin polymerization may be involved in relaxation induced by other mechanisms such as forskolin stimulation.

When cultured vascular smooth muscle cells are exposed to hormones or drugs , which elevate intracellular cyclic AMP levels, they undergo a profound morphological change characterized by an arborization of the cell (Smith, 1989). In arborized cells the cytoplasm condenses in the perinuclear area. The cells remain attached to the surface of the cultured dish by means of long dendrite-like processes extending from the compacted

cell body. These changes are reversible and cells tend to resume their normal morphology after a period of hours (Nabika et. al. 1985). A similar response is elicited when vascular smooth muscle cells are exposed to cytochalasin B, a drug that blocks polymerization of actin (Chaldokov et. al., 1989), suggesting the process of arborization involves the disaggregation of actin filaments.

a. Interaction of Forskolin with the Cyclic AMP Signaling Pathway

There are many hormones, neurotransmitters and other chemical messengers that elicit a response in a target cell via the cyclic AMP signaling pathway. Activation of this signaling pathway by a chemical messenger is mediated by an intracellular GTP-binding (guanine triphosphate) regulatory protein called a G protein. G proteins are heterotrimers composed of alpha, beta, and gamma subunits. When in an inactive conformation, the GTP-binding site (located in the alpha subunit) is occupied by GDP (guanine diphosphate). When the inactive G protein associates with a chemical messenger-receptor complex, it undergoes a conformational change enabling it to release GDP and bind GTP. This causes the alpha subunit to dissociate from the remainder of the G protein. The alpha subunit diffuses along the inner surface of the plasma membrane where it serves to activate adenylate cyclase. The G protein, which activates adenylate cyclase, is referred to as a stimulatory G_s protein. There is another member of the G protein family called an inhibitory G_i that inhibits adenylate cyclase. (Garrett and Grisham, 1999) (Figure 2)

Adenylate cyclase is an enzyme that catalyzes the conversion of ATP to cyclic AMP plus pyrophosphate (2 inorganic phosphates). (Figure 3) Adenylate cyclase is a plasma membrane spanning protein composed of two transmembrane domains separating two catalytic domains. The catalytic domains are situated on the inner surface of the plasma membrane (Alberts et. al. 1994). (Figure 4)

When forskolin interacts with the cyclic AMP signaling pathway, it bypasses specific membrane receptors and G-proteins by directly binding to adenylate cyclase (Daly, 1984). The experiments of Schorderet-Slatkine and Baulieu with unfertilized frog (*Xenopus*) oocytes (eggs) suggest that the forskolin binding site is on the external surface of the cell membrane. They observed that if forskolin was injected directly into the *Xenopus* oocyte, cyclic AMP was not generated. On the other hand, if the oocytes were placed in a bath containing forskolin, cyclic AMP was generated. From these studies they concluded that forskolin activation of adenylate cyclase occurs through an external binding site.

The effects of forskolin on adenylate cyclase are rapid and reversible. Moreover, adenylate cyclase does not experience any desensitization with respect to forskolin activation. Forskolin elevates V_{max} of adenylate cyclase while having very little effect on K_m (Seamon and Daly, 1981). V_{max} is defined as the maximum rate of an enzymatic reaction when the substrate is present at saturating levels whereas K_m is defined as the substrate concentration that yields half-maximal velocity.

The cyclic AMP generated via adenylate cyclase acts by binding to the regulatory subunit of a protein kinase located in the cytoplasm called protein kinase A (PKA) (Matthews and Van Holde, 1996). Protein kinase A is a tetramer composed of two regulatory subunits that form a dimer and two separate catalytic subunits (Spaulding, 1993). (Figure 5) Each regulatory subunit has cyclic AMP binding sites. When the four cAMP binding sites are occupied, the catalytic subunits separate from the regulatory subunits. Free catalytic subunits induce a response by phosphorylating specific cellular proteins such as enzymes or other kinases, ion channels, membrane receptors or transcription factors (Devlin, 1997).

The positive inotropic effect of forskolin on cardiac muscle may be related to the effect of cyclic AMP on Ca^{2+} mobilization. Since an influx of calcium into the

cytoplasmic compartment of the muscle cell is the event which triggers the contractile response, intracellular levels of calcium in the resting cell (10^{-7} M) are maintained at a concentration that is several orders of magnitude lower than the concentration of calcium in the extracellular fluid (10^{-3} M) and the calcium storage compartment of the endoplasmic reticulum (Garrett and Grisham, 1999). Calcium may enter the cell to induce a contractile response via voltage-dependent calcium channels in the plasma membrane or ligand-gated calcium channels in the endoplasmic reticulum. The majority of calcium current transported into the smooth muscle cell in response to membrane depolarization is conducted by the L-type calcium channel. The activity of these calcium channels can be potentiated by cyclic AMP-dependent protein kinase A phosphorylation. Forskolin has been shown to stimulate calcium influx via these L-type calcium channels in cardiac myocytes (Mewes et. al., 1993). (Figure 6) A second manner in which the calcium concentration in cytosolic compartment may become elevated is through the cyclic AMP mediated mobilization of calcium stores within the endoplasmic reticulum. Calcium is transported into the endoplasmic reticulum by an active transport mechanism referred to as a calcium pump (Garrett and Grisham, 1999). (Figure 7) Protein kinase A phosphorylation has been shown to increase the activity of this pump. This enhances the calcium availability for use by those contractile agonists, which act by opening the ligand-gated calcium channels of the endoplasmic reticulum (Johnson, 1980).

In addition to increasing the force of cardiac contraction, forskolin also elevates the rate of relaxation following a contractile response by the heart. This action may also be explained by the action of cAMP on the endoplasmic reticulum associated calcium pump. A cAMP-induced transfer of Ca^{2+} from the cytoplasm into the endoplasmic reticulum can potentiate the rate of relaxation by decreasing the calcium concentration within the cytoplasm promoting a dissociation of Ca^{2+} from contractile proteins (Hicks et.

al., 1979). Blood vessel relaxation following the administration of forskolin may also be partly explained by the transfer of calcium from the cytoplasm to the endoplasmic reticulum in response to a cAMP-induced activation of calcium pump activity. McDaniel et al (1990) observed that the relaxation of precontracted blood vessels in response to cyclic AMP is accompanied by a marked reduction in cytoplasmic levels of Ca^{2+} .

A mechanism that completely details how cyclic AMP can induce contraction in cardiac tissue and relaxation in vascular tissue has yet to be proposed. A complete explanation of these apparently paradoxical effects probably lies in the nature of the proteins phosphorylated by PKA in the two different tissues. For example, even though the two tissues both have L-type calcium channels, the subunits of these channel proteins appear to be regulated differently (Hofmann and Klugbauer, 1996). In cardiac muscle PKA phosphorylation of the L-type calcium channel will enhance calcium flux into the cell following membrane depolarization. In contrast, L-type calcium channel activity does not appear to be regulated by PKA phosphorylation in smooth muscle cells. Furthermore, proteins involved in the contractile process itself may be regulated differently. Although some work has been done in this area, the results are very inconclusive at this time.

b. Proteins Associated With Smooth Muscle

Smooth muscle cells contain three types of filaments: thin, intermediate, and thick (Matthews and van Holde, 1996). Thin filaments are approximately six to eight nanometers in diameter and are composed of two intertwined strands of polymerized actin. Regulatory proteins such as tropomyosin, caldesmon and calponin are attached to the actin strands in varying proportions. Thin filaments are attached to cytoplasmic structures called dense bodies within the cell. The major protein of the dense body is alpha actinin, an actin-binding protein (Garrett and Grisham, 1999). Intermediate

filaments have a somewhat larger diameter (ten nanometers) than the thin filaments. Thick filaments are composed primarily of aggregated myosin molecules and have a diameter of twelve to eighteen nanometers. The thin and thick filaments make up the contractile apparatus of the smooth muscle cell. Intermediate filaments are involved in cytoskeleton formation and in the distribution of dense bodies. The intermediate filaments are thought to maintain the shape and structural integrity of the cell, as well as to disperse any stress experienced by the cell. In addition to being composed of intermediate filaments, the cytoskeletal network also contains thin filaments made of a "nonmuscle" isoform of actin.

Actin is composed of globular protein monomers (G-actin) that are combined to form long helical polymers called fibrous actin or F-actin (Matthews and van Holde, 1996). G-actin is composed of two domains and has a molecular mass of approximately 42 KDa. Actin contains a binding site for an adenosine nucleotide and another for a divalent cation. (Figure 8) Polymerization of G-actin into F-actin involves the hydrolysis of ATP. This mechanism entails the binding of ATP to the adenosine nucleotide binding site within G-actin and upon hydrolysis yields the inhabitation of ADP within the adenosine nucleotide binding site of F-actin. (Matthews and van Holde, 1996) The divalent cation binding site is thought to be occupied by Ca^{2+} in vivo. F-actin is the main constituent of thin filaments within smooth muscle cells. (Figure 9) Based on amino acid sequence data and electrophoretic mobility, six different actin isoforms have been identified: three alpha, two beta, and one gamma. The alpha isoform is found mainly in vascular smooth muscle. The beta isoform, is present in most cell types (smooth and nonmuscle) and is thought to contribute to cytoskeleton formation. The gamma isoform is located primarily in enteric smooth muscle. (Devlin, 1997) As vascular smooth muscle cells differentiate in the embryo, there is an increase in the relative content of alpha isoforms (contractile actin) and a decrease in the relative amounts of beta isoforms

(Devlin, 1997).

Molecular myosin is a complex of six chains: two heavy chain subunits having a molecular weight of approximately 200KDa each, two 20 KDa regulatory light chains, and two 17 KDa essential light chains (Matthews and Van Holde, 1996). (Figure 10) Several isoforms of both the heavy and light chains have been described. Each individual myosin molecule is organized into an alpha-helical coiled tail with a pair of globular heads. Each globular head is composed of two domains. The first is an amino-terminal catalytic domain that houses the actin binding site and the nucleotide binding site, which catalyzes the hydrolysis of ATP (myosin ATPase). The second is carboxy-terminal regulatory domain composed of the myosin regulatory light chain and the myosin essential light chain. The rod-like tail is made of heavy chain myosin (Garrett and Garisham, 1999). In the smooth muscle cell, individual myosin molecules link together to form thick filaments with laterally projecting globular heads. Figure 11 demonstrates the spatial relationship of actin and myosin to the cell membrane.

c. Smooth Muscle Proteins and the Contractile Response

Smooth muscle contraction occurs when cross bridges are formed between myosin heads and adjacent actin filaments and is triggered by an elevation in the intracellular Ca^{2+} concentration $\{[\text{Ca}^{2+}]_i\}$ (Matthews and Van Holde, 1996). (Figure 12) Many agonists, which promote smooth muscle contraction, induce a rise in $[\text{Ca}^{2+}]_i$ by activating voltage-gated Ca^{2+} channels in the plasma membrane and/or by opening of ligand-gated channels in the sarcoplasmic (endoplasmic) reticulum, which acts as an intracellular calcium storage compartment. As $[\text{Ca}^{2+}]_i$ becomes elevated, calcium ions begin to associate with a calcium binding regulatory protein called calmodulin. The resultant calcium-calmodulin complex binds to and activates myosin light chain kinase, an enzyme that catalyzes the phosphorylation of myosin regulatory light chains. When

the regulatory light chain is phosphorylated, the myosin head region is able to interact with actin. Energy for cross bridge formation between actin and myosin comes from the hydrolysis of ATP that is induced as actin activates the myosin ATPase. Contraction then occurs as actin and myosin filaments slide past each other through cross bridge cycling. The binding of ATP to the myosin head and its subsequent hydrolysis is believed to cause conformational changes, which move the myosin head, a few nanometers. The ordered formation and breaking of crossbridges enables myosin filaments to slide along adjacent actin filaments, thereby shortening the contractile cell. Relaxation of smooth muscle occurs when Ca^{2+} is removed from the cytoplasm and when the enzyme myosin phosphatase dephosphorylates the myosin regulatory light chain. (Garrett and Grisham, 1999) (Figure 13)

Although the principal regulator of smooth muscle contraction is the intracellular concentration of Ca^{2+} , other factors also appear to be involved in the regulation of the contractile process. For example, the sensitivity of regulatory light chain phosphorylation to intracellular levels of Ca^{2+} can be shifted by the action of factors which modulate the activities of myosin light chain kinase or myosin phosphatase (Word and Kamm, 1997). Moreover, experimental evidence suggests that the regulatory proteins (tropomyosin, caldesmon and calponin) associated with the thin actin filaments may have some modulatory effects on the contractile response (Garrett and Grisham, 1999).

d. Thin Filament Regulatory Proteins

Tropomyosin is a dimer composed of two polypeptides coiled around each other. This protein fits into the grooves between the strands of the actin double helix and occurs at an approximate ratio of one tropomyosin per every seven actin monomers (Garrett and Grisham, 1999). (Figure 14) Evidence suggests that tropomyosin alters the activity of

the actin-activated myosin ATPase. Typically this action functions to enhance ATPase activity. There is also evidence suggesting that tropomyosin may play a role in the formation of actomyosin crossbridges.

Caldesmon is a long thin protein that is located beside tropomyosin in the groove formed by the actin double helix (Devlin, 1997). There is approximately one caldesmon for every seven actin monomers. Calponin, most recently discovered of the regulatory proteins also occurs at approximately the same molar ratio as caldesmon (Devlin, 1997). Both caldesmon and calponin inhibit actin-activated myosin ATPase activity. Indirect experimental evidence suggests that these proteins have an inhibitory effect on the contractile response. Based on the nature of the experiments used to assess the interactions of these regulatory proteins with contractile proteins, it is difficult to discern the real physiological role of these proteins in the contractile process (Chalovich and Pfitzer, 1997).

e. Effects of Cell Culture on the Expression of Proteins in the Smooth Muscle Cell

The smooth muscle cells found in adult mammals are terminally differentiated. Cellular differentiation is defined as the acquisition of the specific cell characteristics that distinguishes a particular cell type from another cell type. The differentiation from the fetal cell type to a vascular smooth muscle cell results in the characteristic expression of marker proteins within the cytoskeleton such as alpha actin and smooth muscle myosin heavy chains.

In fact the expression of alpha actin is considered as the first known marker of differentiated smooth muscle cells during vessel development. Alpha actin has been observed as early as day ten of gestation during blood vessel development (Sawtell and Lessard, 1989). Smooth muscle alpha actin is the most abundant isoform present in

completely differentiated vascular smooth muscle cells. Although the first observable actin isoform in vascular smooth muscle is beta-actin, alpha actin is substantially expressed in greater quantities during development. The cellular content of smooth muscle alpha actin steadily increases from fetal to adult life. The alpha actin isoform accounts for approximately seventy percent of the total actin present in the adult (Fatigati, V. and R. A. Murphy 1984).

When smooth muscle cells are placed in culture and are later passaged, they tend to revert to a dedifferentiated state in which the cells more closely resemble fetal cells. According to Thyberg, the cells structurally reorganize themselves within a few days of seeding in a manner that involves the loss of myofilaments. The dedifferentiation causes a decrease in the expression of contractile proteins and an increase in the expression of the non-muscle variants of these proteins. Gabbiani et. al. 1984 observed a shift in actin isoform expression from the predominance of the alpha isoform in early passages to the beta isoform primarily in older less differentiated cell passages. Actin was not the only protein affected with age of the cultured cell. In fact myosin experienced similar shifts as noted by Chamley et. al. 1977 and Larson et. al. 1984 in which the expression of smooth muscle heavy chains decreased while the expression of nonmuscle myosin heavy chains increased. Altered forms of caldesmon (Shirinsky et. al. 1991), calponin (Birukov et. al. 1993) and vinculin (Shirinsky et. al. 1991) have also been noted.

The changes which occur in smooth muscle cells when placed in culture are similar to those observed by Nakamura and Ohtsubo 1992, when they assessed the morphology of smooth muscle cells of atherosclerotic lesions in blood vessels. A decreased expression in smooth muscle actin, smooth muscle myosin as well as desmin in cells of atherosclerotic lesions was also observed by Gabbiani et. al. 1984; Benzonana et. al., 1988; and Gabbiani et. al., 1982, respectively. In fact, the altered expression of smooth muscle alpha actin is now used as an index for assessing changes in the

phenotypic state of smooth muscle cells during the atherogenic process. The pathogenesis of atherosclerosis begins via a dedifferentiation and migration of vascular smooth muscle cells into the intima layer of the vessel. This results in an accumulation of cells and lesion formation upon the vessel itself (Nakamura and Ohtsuba, 1992; Stary et. al., 1994).

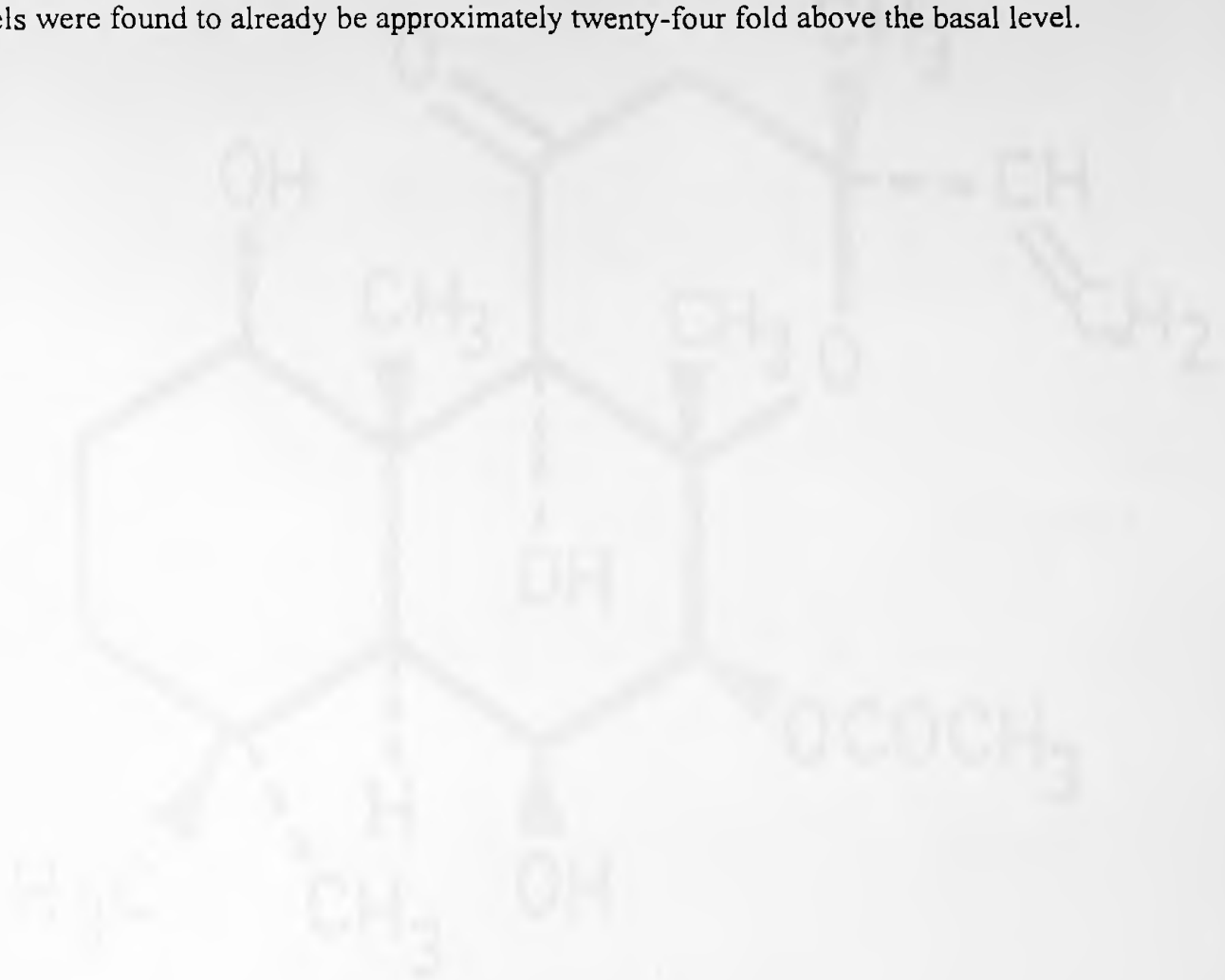
f. Forskolin Induced Arborization of Cultured Vascular Smooth Muscle Cells

Increasing levels of cAMP is associated with the disassembly of stress fibers (Kreisberg et. al. 1985). If forskolin dependent changes in stress fibers are mediated by cAMP and modulate contraction, then alterations in stress fibers should be temporally related to cAMP elevation and relaxation. As cAMP levels become elevated, the cells begin to relax and stress fiber disassembly occurs. In particular, these elevated cAMP levels have been demonstrated to interrupt interaction of actin/myosin (major constituents of the cytoskeletal structure) by inhibiting myosin light-chain kinase activity (Adelstein et. al. 1978 and Lamb et. al. 1988). It has been reported in smooth muscle that myosin-light chain phosphorylation is a prerequisite for actin-activation of myosin-ATPase activity (actin-myosin association) and hence contraction.

It has been observed that a decrease in phosphorylation of myosin light chain plays a role in stress fiber disassembly. The mechanism involves formation and binding of a calcium-calmodulin complex to the catalytic subunit of myosin light chain kinase. This is followed by phosphorylation of the myosin light chain, which then causes the activation of myosin ATPase by actin.

Kelley et.al. demonstrated the correlation of cAMP, stress fibers and relaxation. After a few minutes of forskolin addition, pericyte relaxation occurred with subsequent relaxation of stress fibers. Although this five minute interval of incubation did not

correspond with the peak cAMP levels brought about by forskolin stimulation, cAMP levels were found to already be approximately twenty-four fold above the basal level.



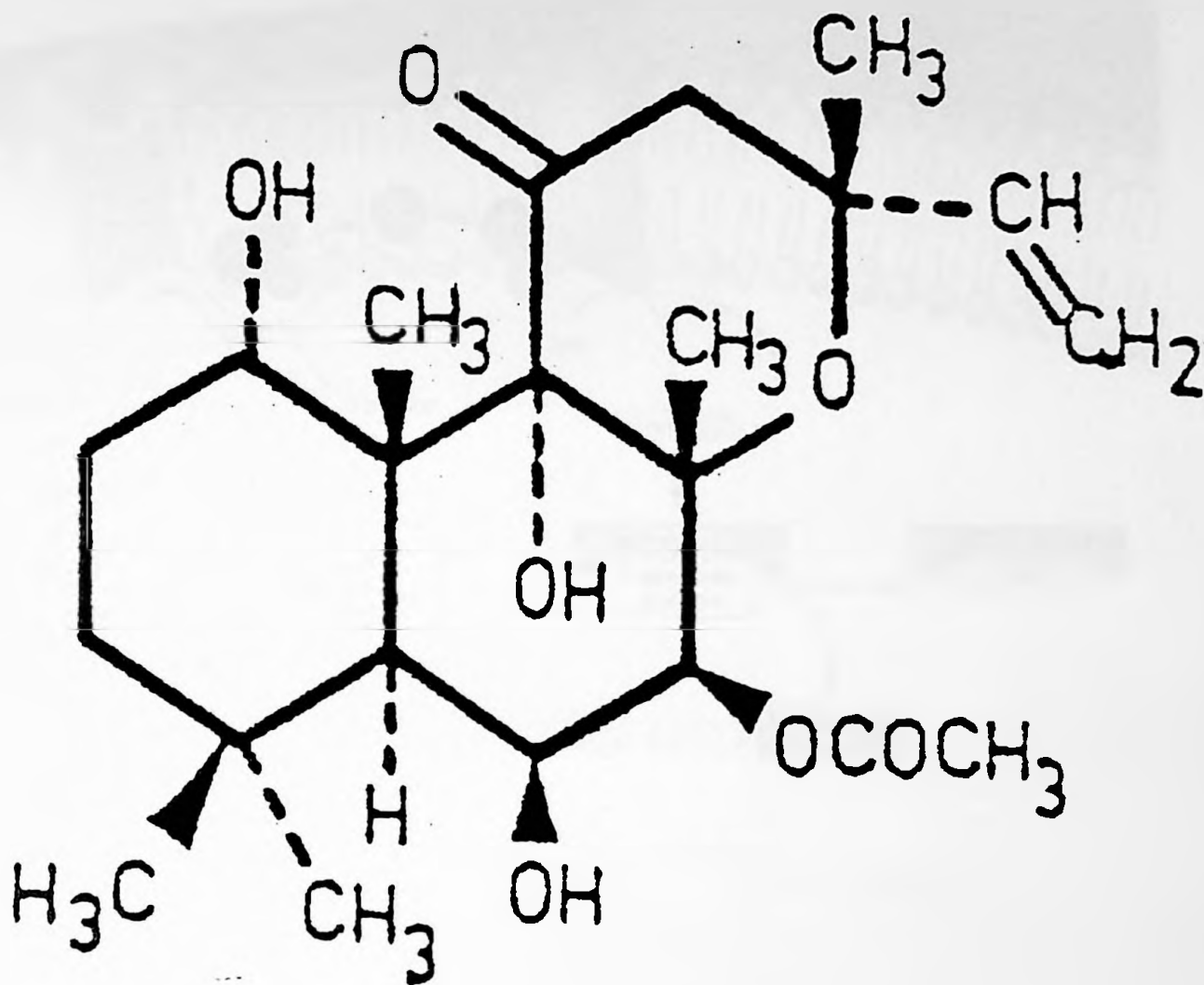


Figure 1. 7b-acetoxy-8, 13-epoxy-1a, 6b, 9a-trihydroxy-labd-14-en-11-one (Forskolin).
The name forskolin specifically applies to the principal diterpene obtained from a methanol extract of the *Coleus forskolii* root.

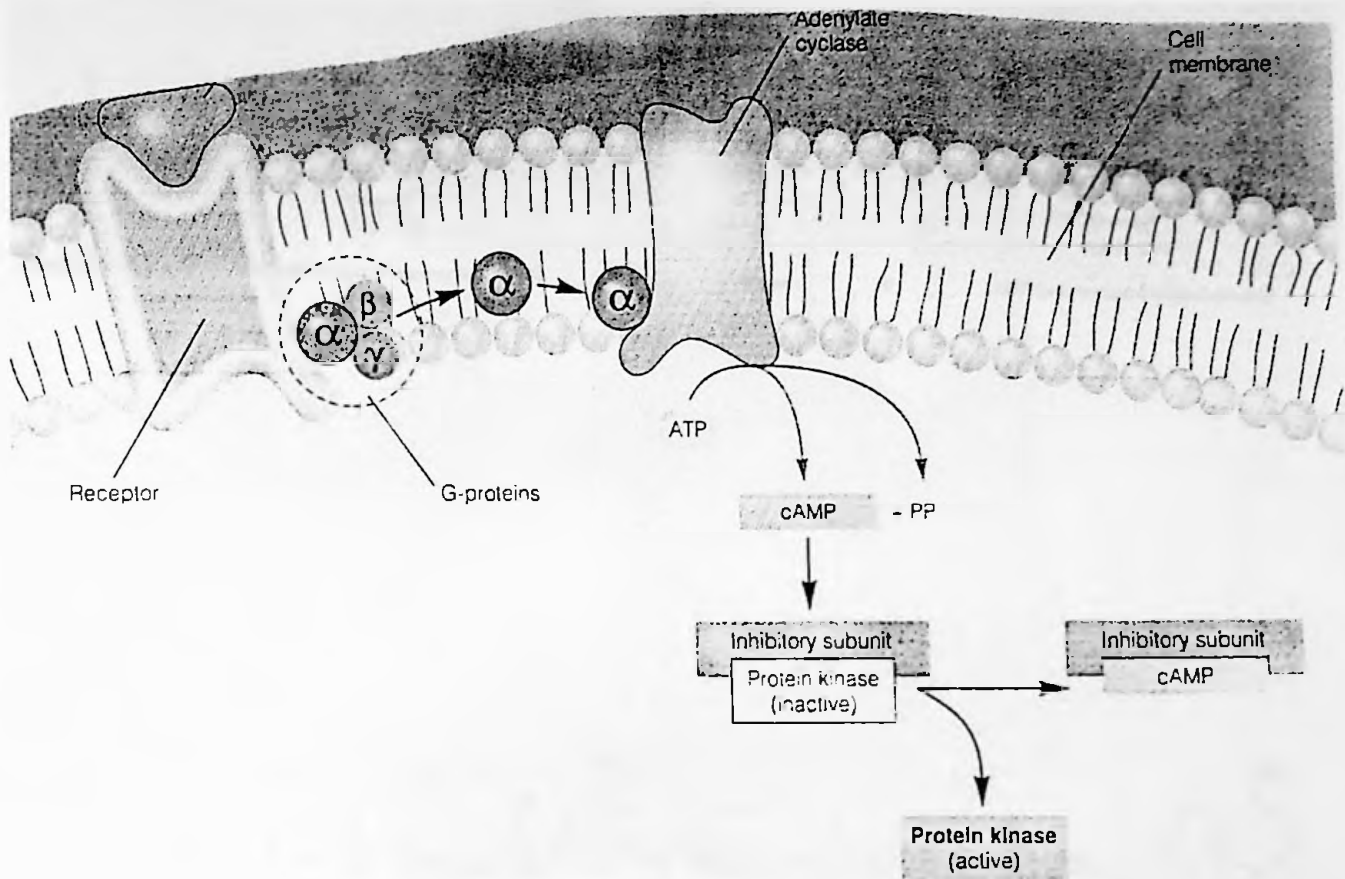


Figure 2. Activation of the cAMP pathway by a chemical messenger is mediated by an intracellular GTP-binding regulatory protein called a G-protein. The alpha subunit of the G-protein is responsible for activating adenylate cyclase, an enzyme that catalyzes the conversion of ATP to cAMP. Protein kinase is activated via cAMP and is responsible for phosphorylating specific cellular proteins.

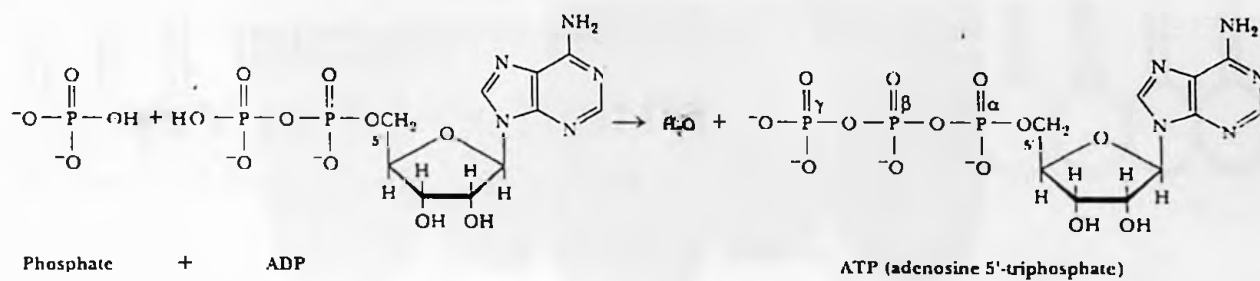
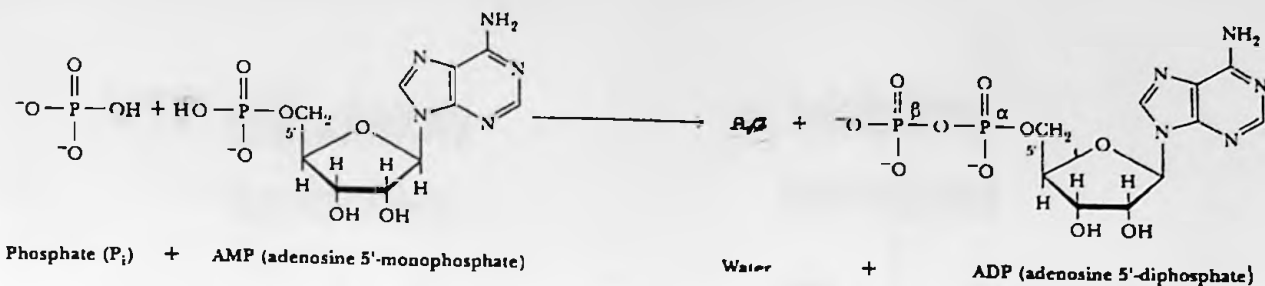


Figure 3. Adenosine 5'-triphosphate (ATP) is created via subsequent additions of phosphate to Adenosine 5'-monophosphate and is converted to cAMP via adenylate cyclase.

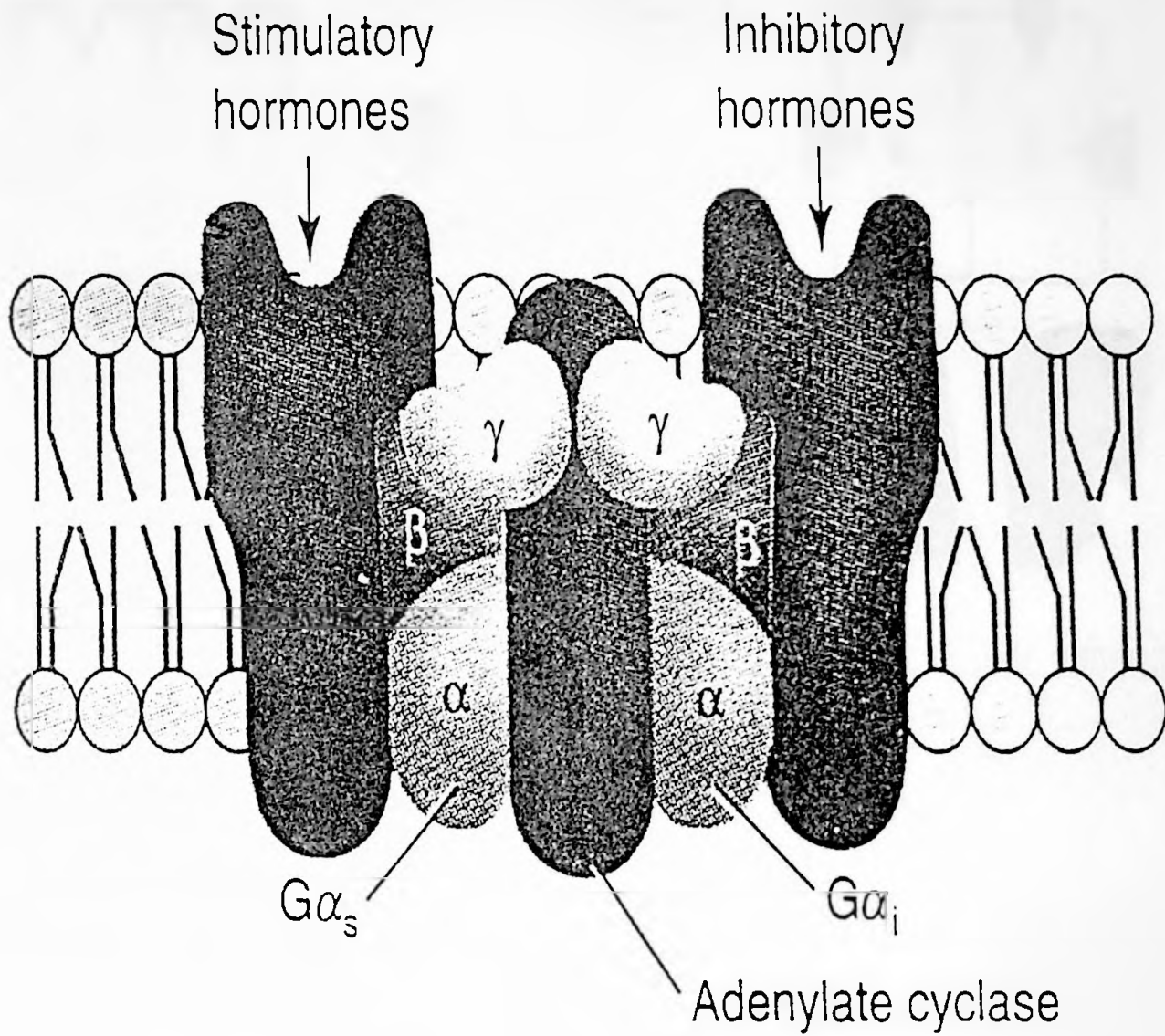


Figure 4. Adenylate cyclase is a plasma membrane spanning protein composed of two transmembrane domains separating two catalytic domains. The catalytic domains are situated on the inner surface of the plasma membrane (Alberts et. al. 1994)

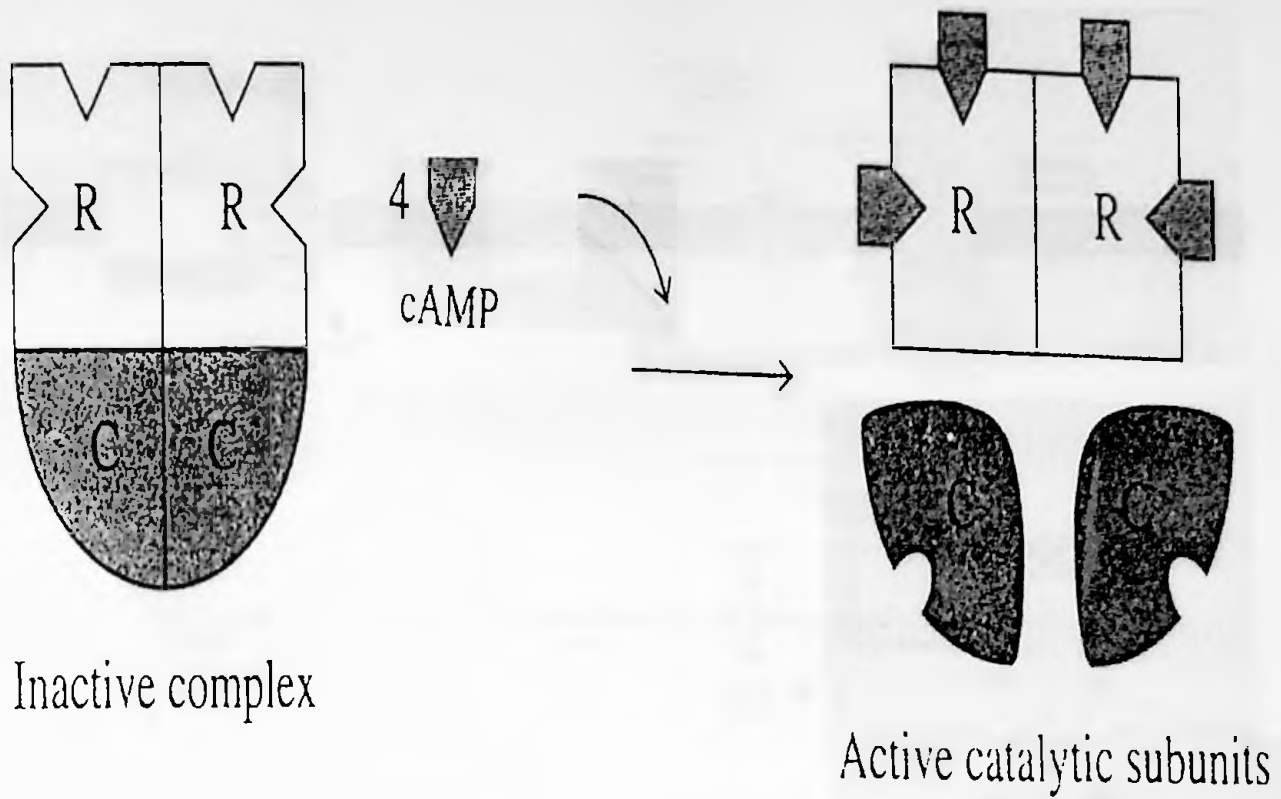


Figure 5. Protein kinase A is a tetramer composed of two regulatory subunits, which form a dimer and two separate catalytic subunits. Each regulatory subunit has cAMP binding sites. When the four cAMP binding sites are occupied, the catalytic subunits separate from the regulatory subunits.

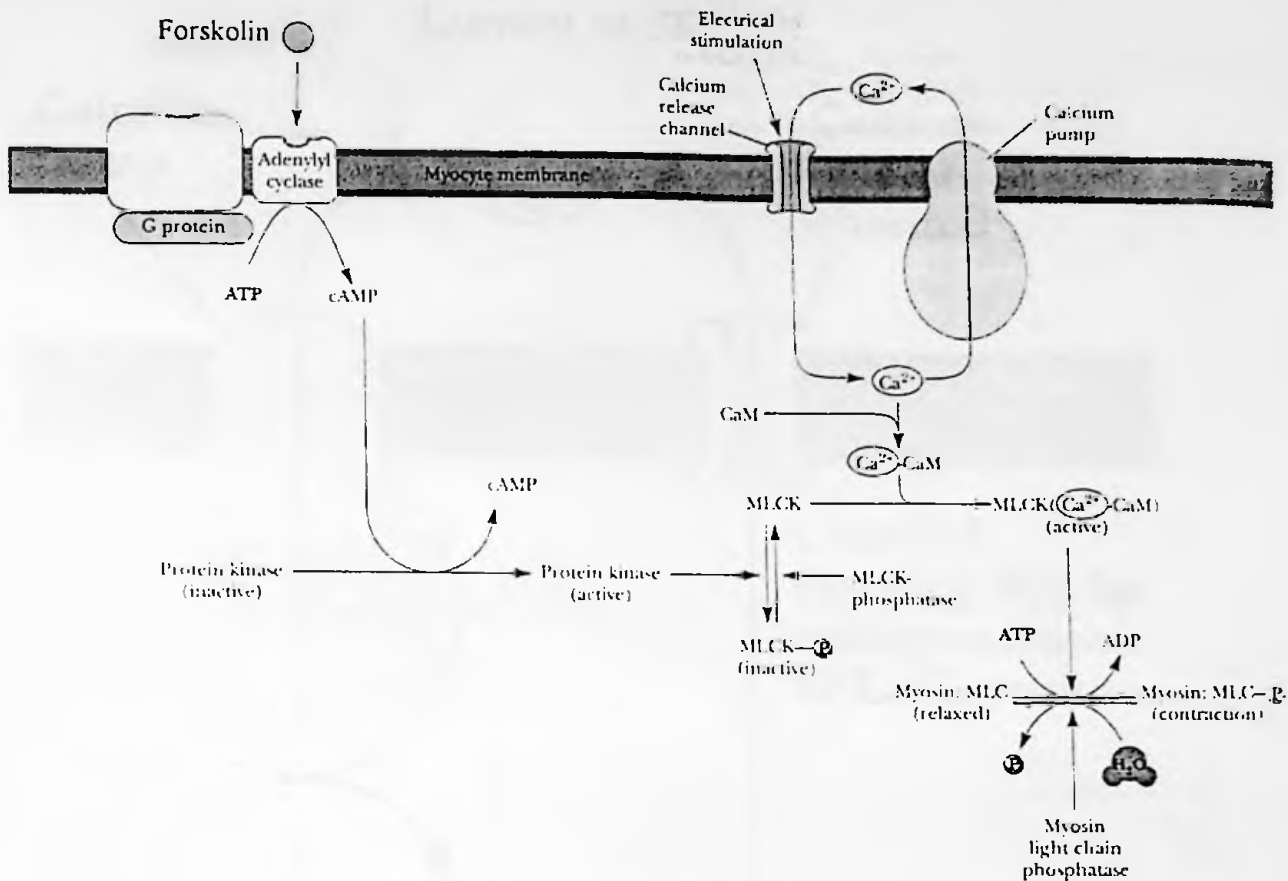


Figure 6. The Effect of cAMP on Calcium Mobilization and Contraction in Smooth Muscle. Calcium may enter the cell to induce a contractile response via voltage-dependent calcium channels in the plasma membrane. The activity of these calcium channels can be potentiated by cAMP dependent protein kinase A phosphorylation. (Calmodulin is abbreviated as CaM and Myosin light chain kinase is abbreviated as MLCK).

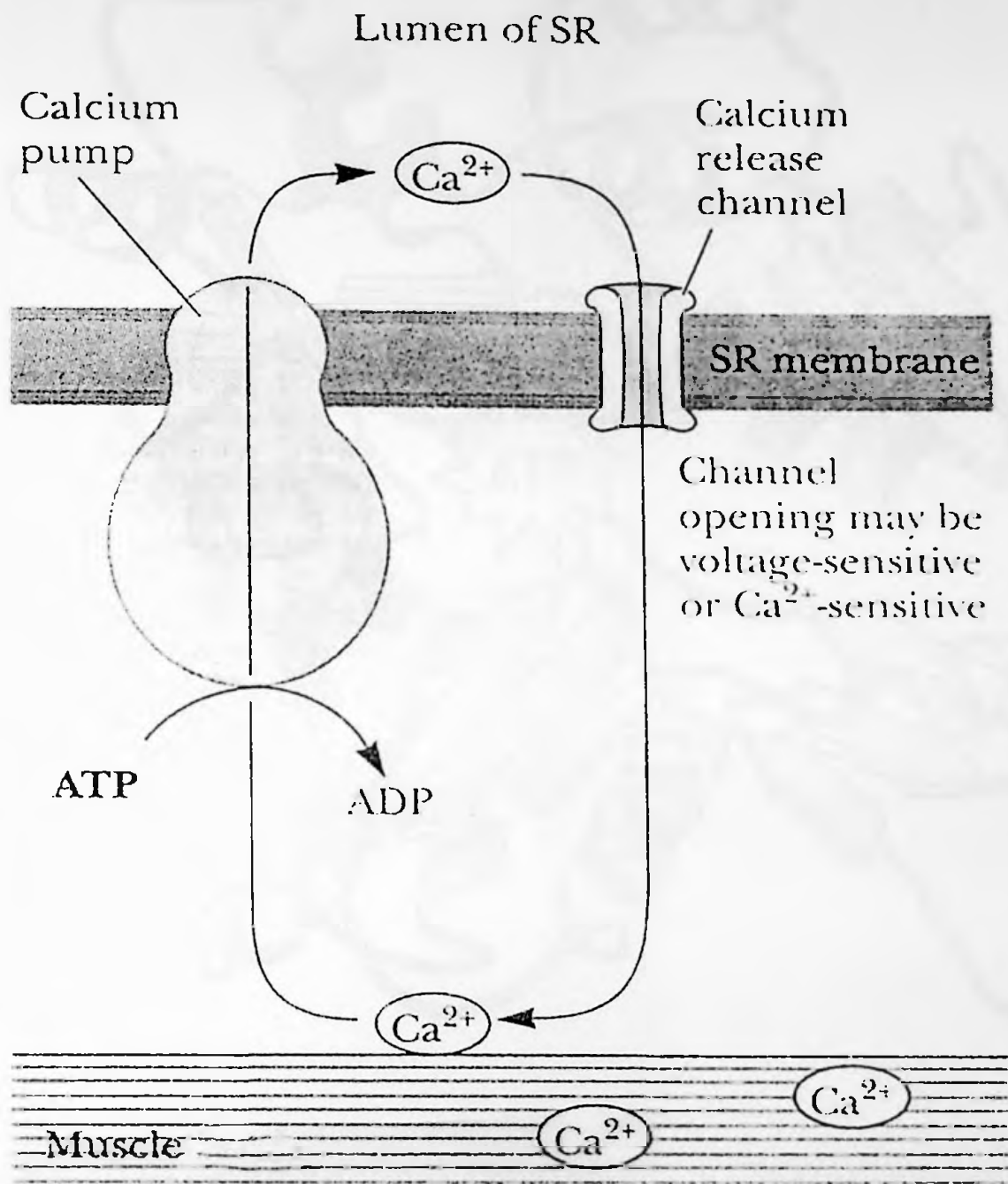


Figure 7. The Sarcoplasmic (Endoplasmic) Reticulum Associated Calcium Pump. Forskolin has been shown to stimulate calcium influx via these L-type calcium channels in cardiac myocytes (Mewes et.al.1993)

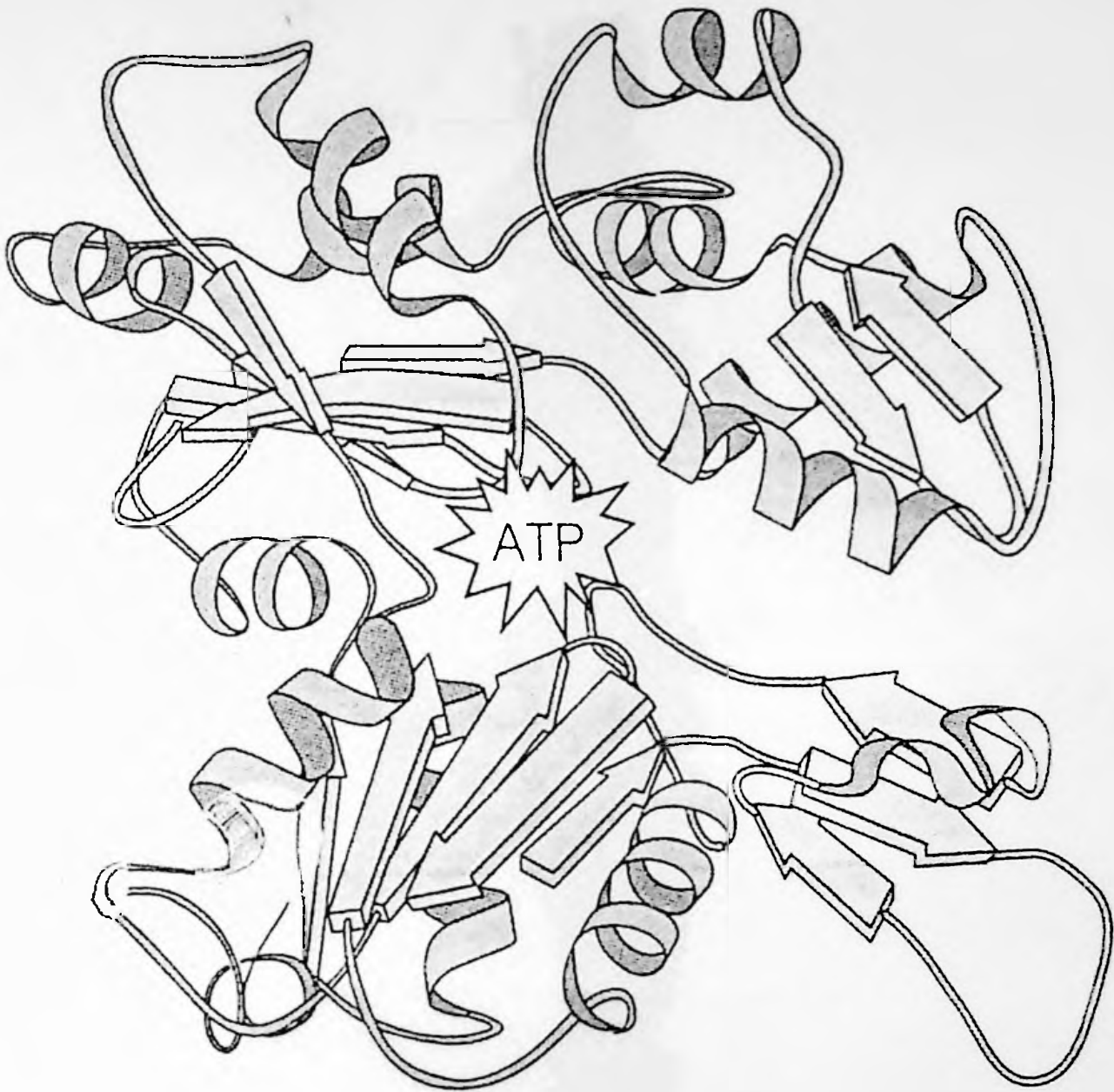


Figure 8. G-actin is composed of two helical domains and forms the basis of actin.

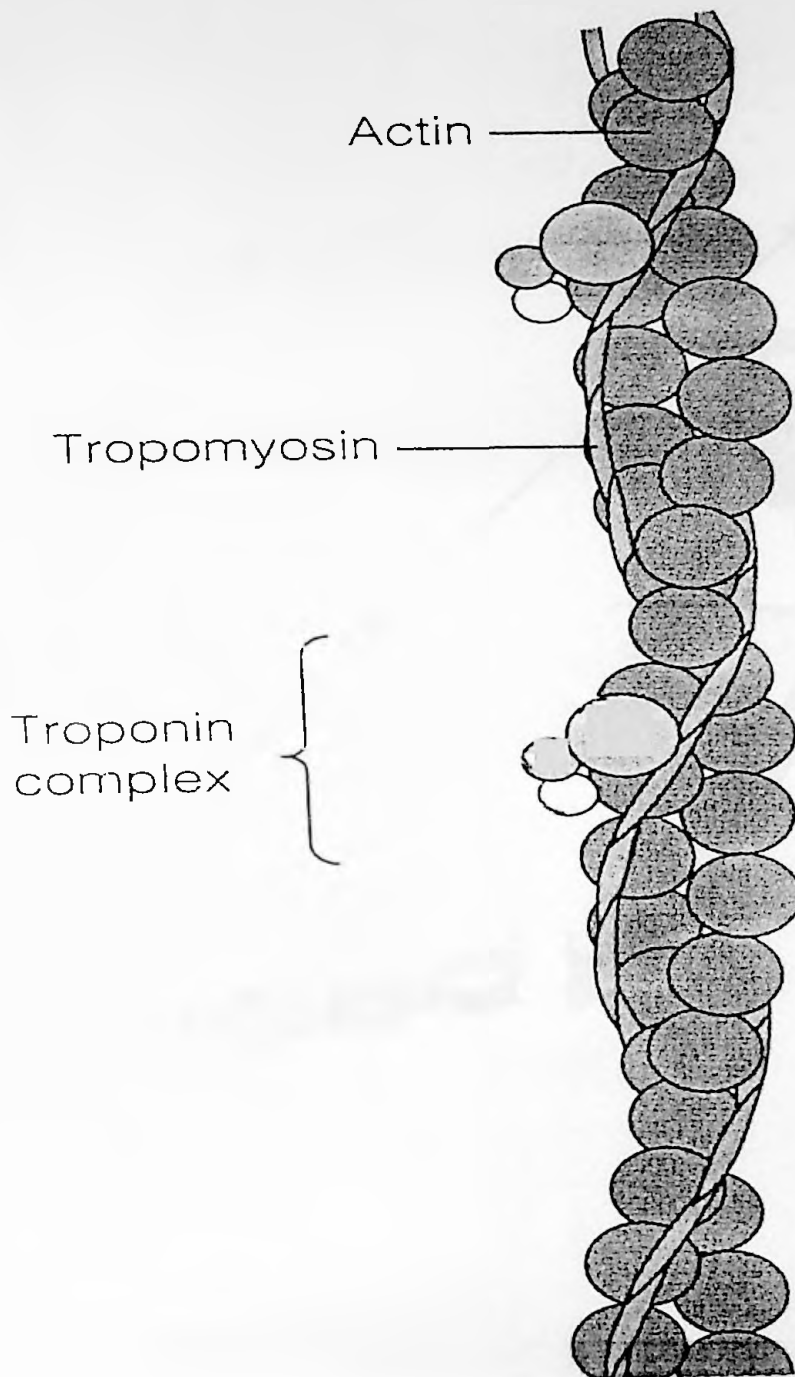


Figure 9. F-Actin and Its Associated Proteins. F-actin is the main constituent of thin filaments within smooth muscle cells.

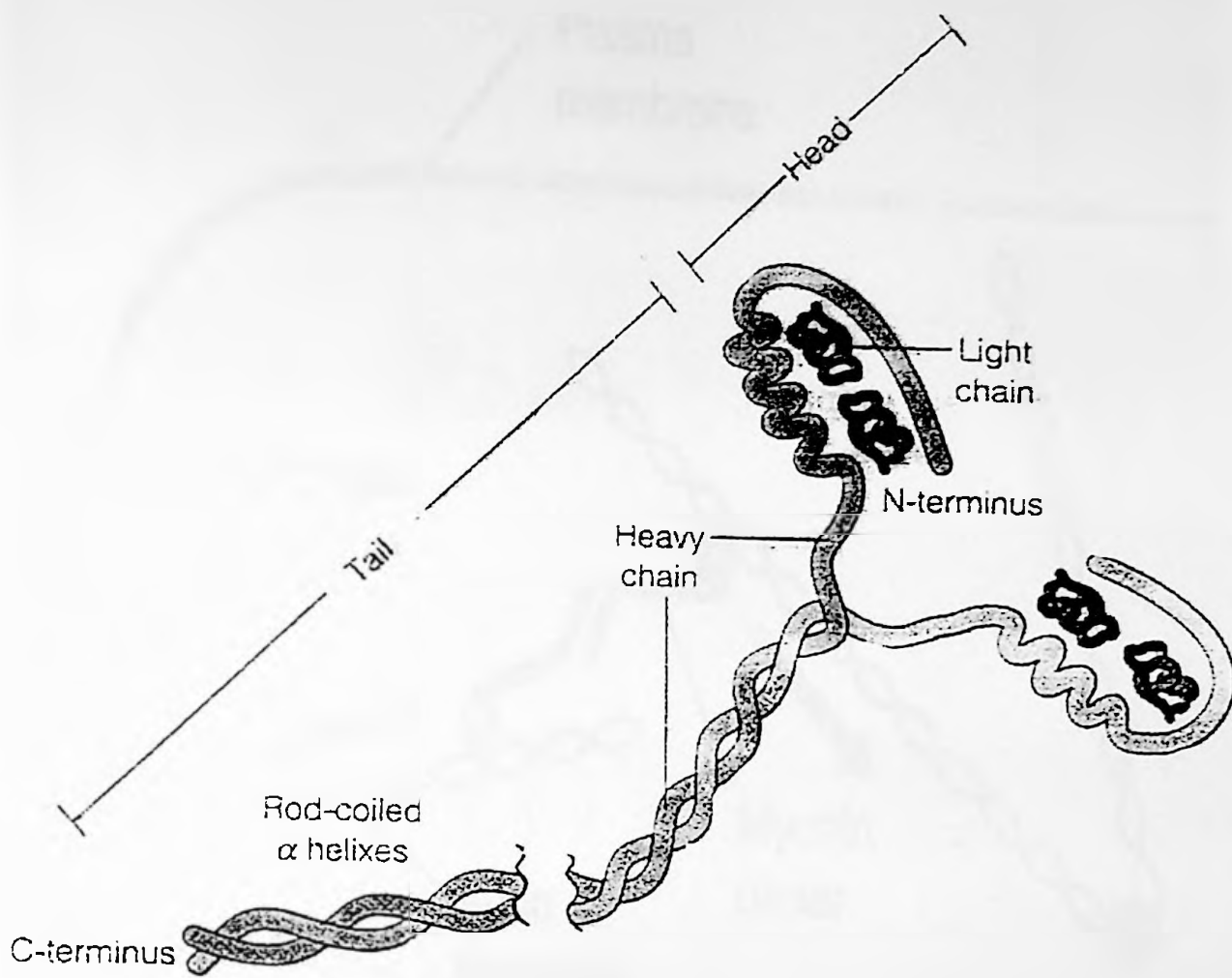


Figure 10. Myosin. Molecular myosin is a complex of six chains: two heavy chain subunits, two regulatory light chains and two essential light chains. (Matthews and Van Holde, 1996).

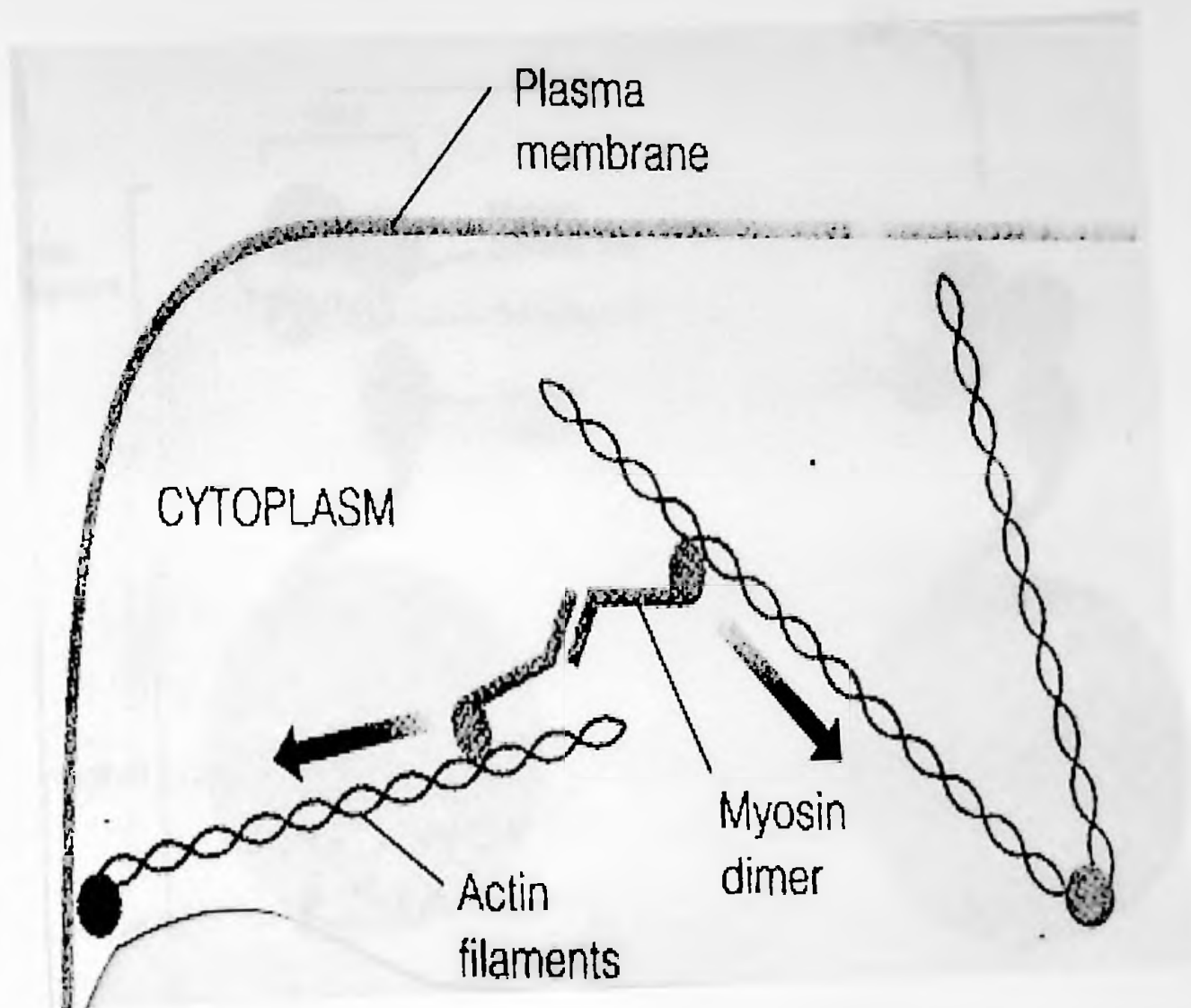


Figure 11. The Spatial Relationship of Actin and Myosin to the Cell Membrane.

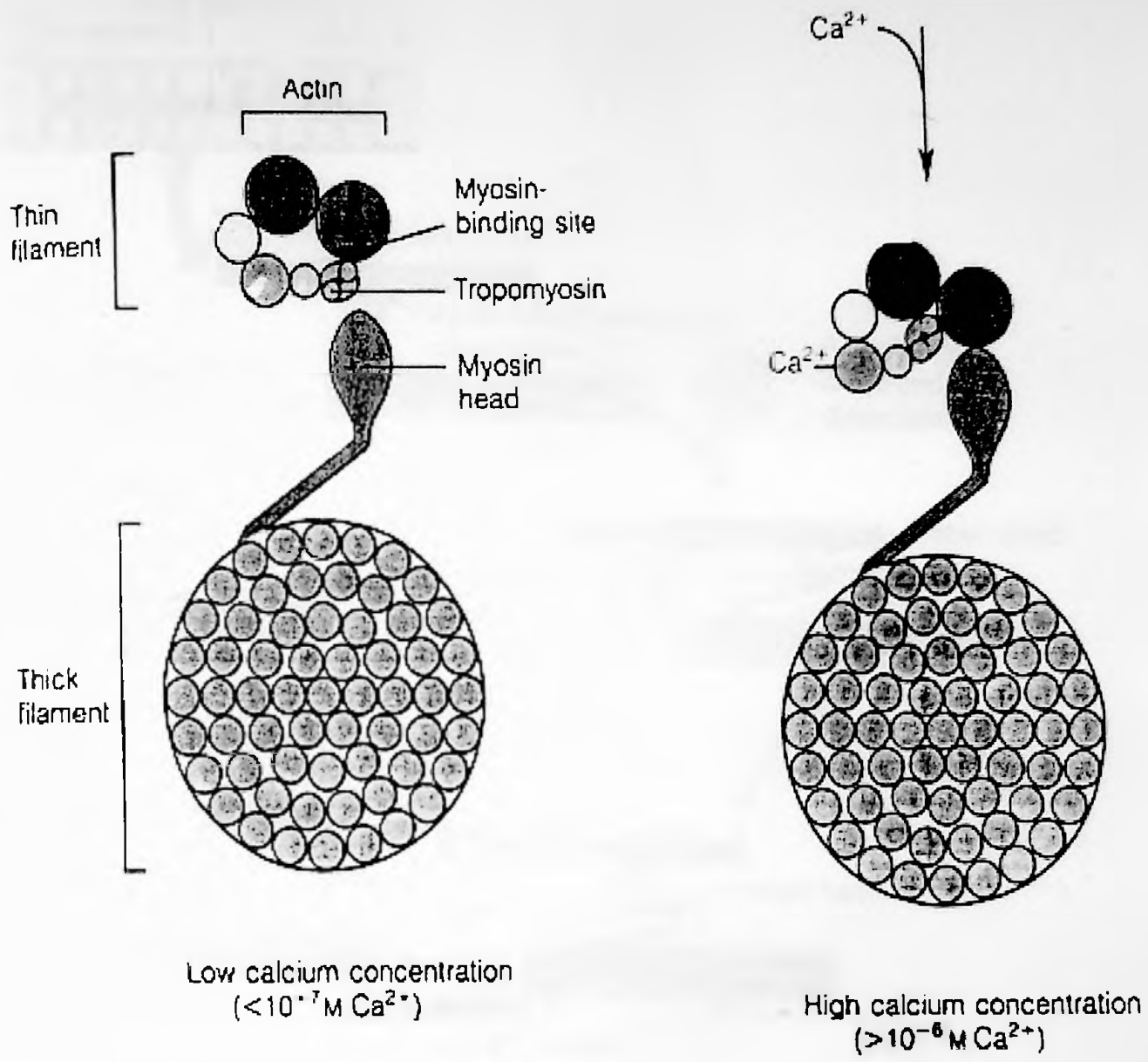


Figure 12. Cross Bridge Formation and the Effects of Calcium Concentration. Smooth muscle contraction occurs when cross bridges are formed between myosin heads and adjacent actin filaments and is triggered by an elevation in the intracellular Ca^{2+} concentration (Matthews and Van Holde, 1996).

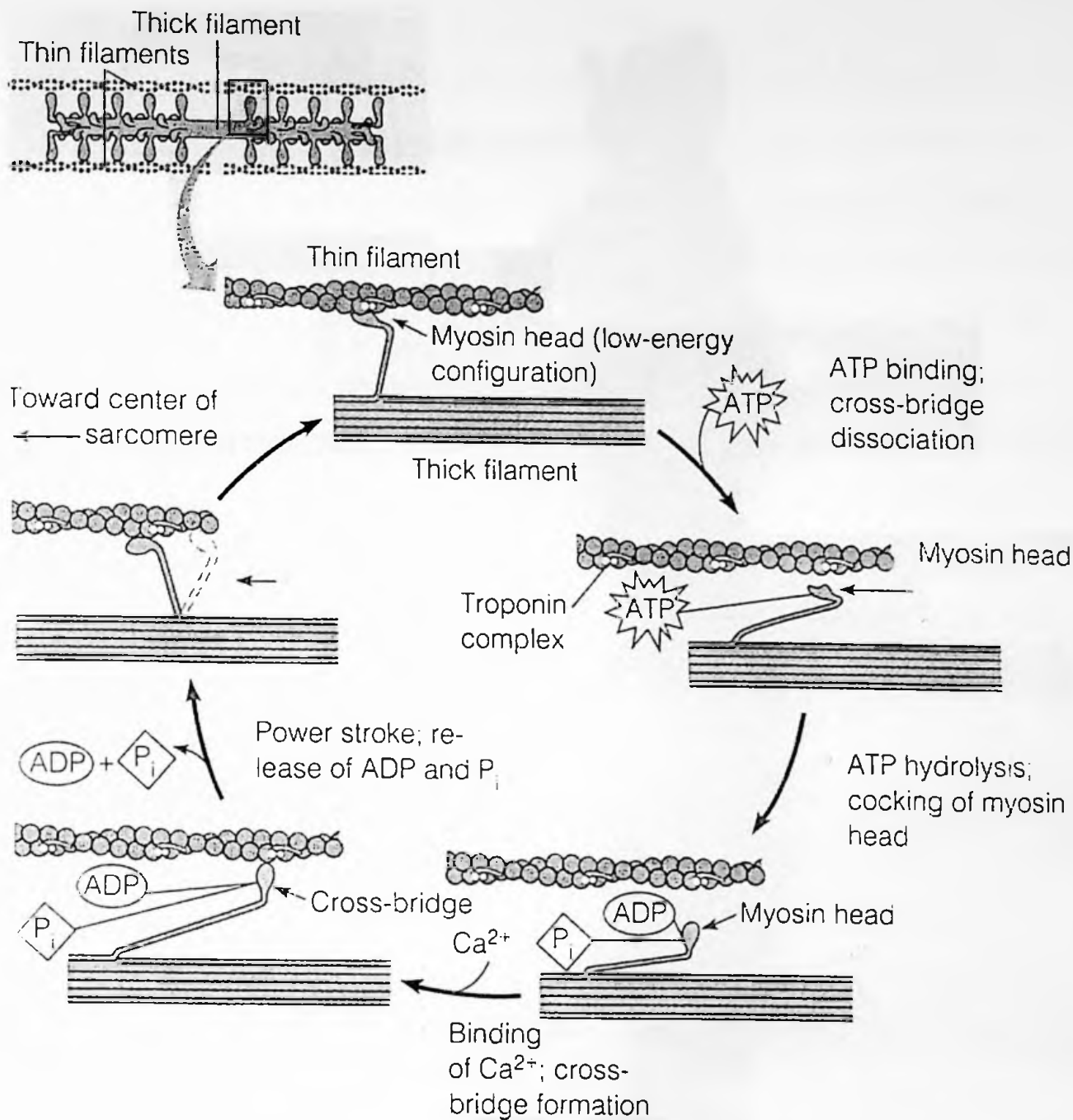


Figure 13. Smooth Muscle Contraction. When the regulatory light chain becomes phosphorylated, the myosin head region is able to interact with actin. Energy for cross bridge formation between actin and myosin comes from the hydrolysis of ATP that is induced as actin activates the myosin ATPase. Contraction then occurs as actin and myosin filaments slide past each other through cross bridge cycling. The binding of ATP to the myosin head and its subsequent hydrolysis is believed to cause conformational changes, which move the myosin head. The ordered formation and breaking of crossbridges enables myosin filaments to slide along adjacent actin filaments, thereby shortening the contractile cell.

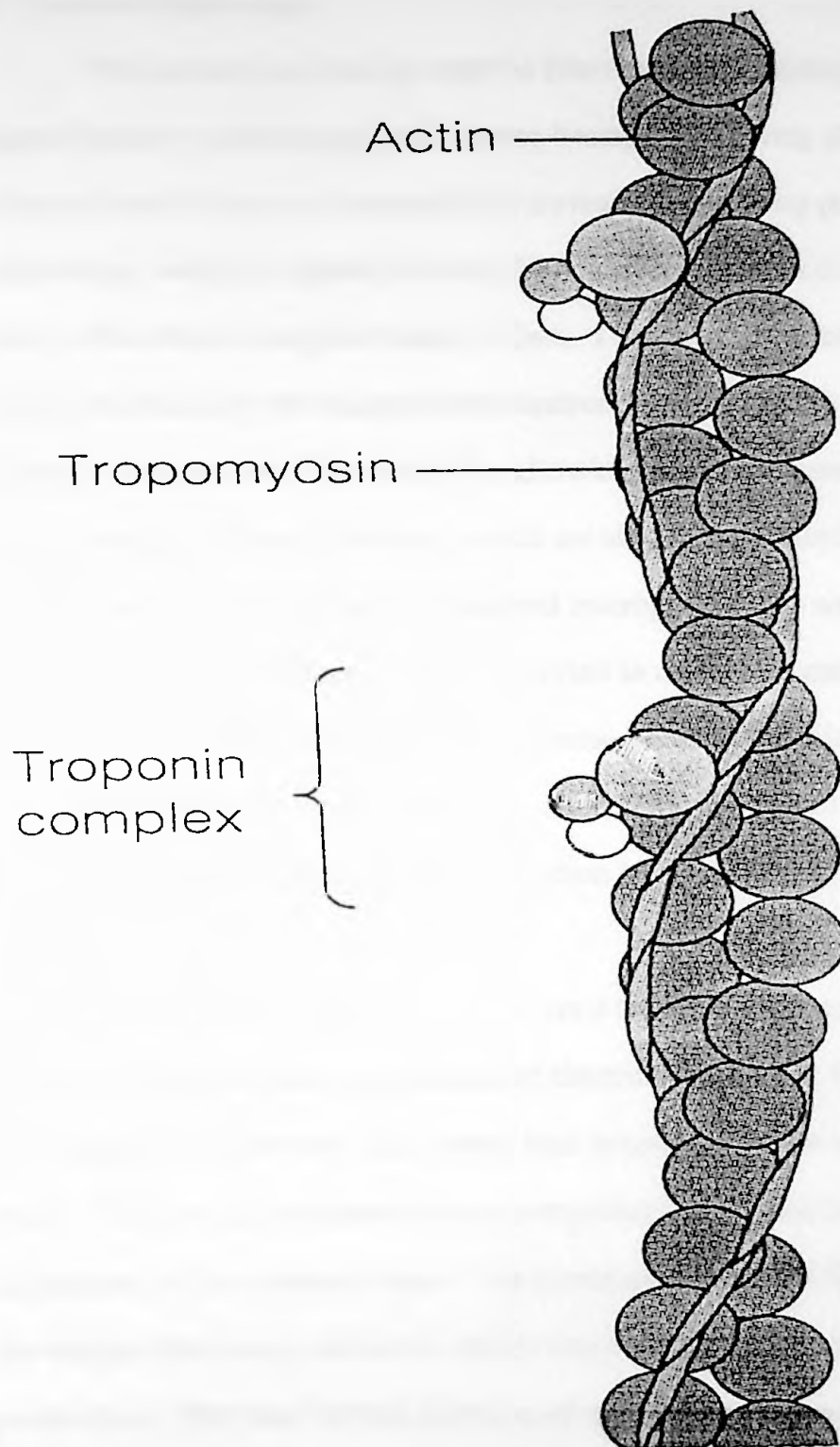


Figure 14. The Tropomyosin and Actin Complex. Tropomyosin is a dimer composed of two polypeptides coiled around each other. This protein fits into the grooves between the strands of the actin double helix and occurs at an approximate ratio of one tropomyosin per every seven actin monomers (Garrett and Grisham, 1999).

2. Electron Microscope

The electron microscope enables fine detail to be distinguished through specimen magnification via electromagnetic lenses because of the very short wavelength. The electrons provide up to a thousand fold increase in resolving power over the light microscope, which is limited to about 200nm. The transmission electron microscope can resolve fine detail to approximately 0.2nm. Like the light microscope, bright field images produced by the transmission electron microscope can provide information on the internal components of the sample by allowing electron beams rather than light through the thin sample. Those electrons, which are able to penetrate and pass through the sample, are used to produce a transmitted micrograph. The source of electrons is provided by a high-voltage supply connected to a filament assembly located at the top of the transmission electron microscope column. Within this filament chamber, a beam volume known as the crossover exists between the anode and the filament. This crossover is responsible for image formation by providing an effective, highly condensed electron source.

The electron beam then encounters a two part condenser-lens system, which is employed to control the illumination of electrons both upon the sample and on the viewing screen. The first high power lens is responsible for condensing the electron beam. The second condenser lens is somewhat weaker and is employed for fine adjustment of the electron beam. The condenser lenses are fitted with apertures to protect the sample from stray electrons, which lead to excessive heat and limitations on x-ray production. The most critical function of a condenser lens and its aperture is to establish the angular aperture of illumination. The maximum angular aperture occurs when the electron beam is the brightest and fullest.

The sample, usually supported by a rod, is inserted into the vacuum chamber above the objective lens and can be moved in X, Y and Z directions to facilitate the

desired angle of interest to be observed for the particular sample.

As the electron beam interacts with the sample, various relationships thereof are considered in regard to the final transmission electron microscope image formation. These considerations include absorption, diffraction, elastic scattering and inelastic scattering. In regard to absorption, uneven coating of the specimen, contaminants such as dirt may lead to particular artifacts. Elastically scattered electrons are produced from interaction of the nuclei of specimen atoms with the electron beam causing large deviations in the original path of the electrons. These elastically scattered electrons contribute to both the amplitude and diffraction contrast of the image. On the other hand, inelastically scattered electrons, come to play when the electron beam collides with the electrons in atoms from the sample. These primary electrons only experience a slight deviation from their original path and are characterized by a loss of energy leading to chromatic aberration and phase contrast. The differential scattering that results between the transmitted and scattered electrons from the specimen causes the contrast seen in the final micrograph in the transmission electron microscopy. Enhancement of contrast can be further achieved by the insertion of an objective aperture below the sample and objective lens.

The objective aperture limits electrons diffracted at large angles from reaching the screen. Impregnation of heavy metal stains (such as osmium and lead) into the sample facilitates wide angle diffraction of the primary electrons and greatly enhances the contrast in the image. The objective lens provides magnifications and focus for the image to the intermediate lenses. The intermediate lens brings about the image formed by the objective lens for further magnification through the variation of its lens current. Finally, the projector lens projects the final magnified image to the viewing screen or to the film of the recording camera. (Figure 15)

2. Electron Microscopy

The Transmission Electron Microscope

The transmission electron microscope (TEM) is a type of electron microscope that uses a beam of electrons to create an image of a specimen. It is used to study the fine structure of materials at the atomic level.

The TEM consists of several main components: a high-voltage power supply, an electron gun, a series of electromagnetic lenses, a specimen stage, and a detector. The electron gun produces a beam of electrons that is accelerated by the high-voltage power supply. The beam then passes through a series of lenses that focus it onto the specimen. The electrons that pass through the specimen are then collected by the detector, which creates an image of the specimen.

The TEM is capable of achieving a resolution of up to 0.2 nm, which is much higher than that of a light microscope. This allows it to study the fine details of biological and materials science specimens.

The TEM is a complex instrument that requires a high level of technical expertise to operate. It is typically found in research laboratories and is used by scientists to study the structure of materials at the atomic level.

The TEM is a powerful tool for studying the fine structure of materials. It has been used to study a wide range of specimens, including biological cells, polymers, and metals. The TEM has provided valuable insights into the structure of these materials and has helped to advance our understanding of the natural world.

The TEM is a complex instrument that requires a high level of technical expertise to operate. It is typically found in research laboratories and is used by scientists to study the structure of materials at the atomic level.

The TEM is a powerful tool for studying the fine structure of materials. It has been used to study a wide range of specimens, including biological cells, polymers, and metals. The TEM has provided valuable insights into the structure of these materials and has helped to advance our understanding of the natural world.

The TEM is a complex instrument that requires a high level of technical expertise to operate. It is typically found in research laboratories and is used by scientists to study the structure of materials at the atomic level.

The TEM is a powerful tool for studying the fine structure of materials. It has been used to study a wide range of specimens, including biological cells, polymers, and metals. The TEM has provided valuable insights into the structure of these materials and has helped to advance our understanding of the natural world.

The TEM is a complex instrument that requires a high level of technical expertise to operate. It is typically found in research laboratories and is used by scientists to study the structure of materials at the atomic level.

The TEM is a powerful tool for studying the fine structure of materials. It has been used to study a wide range of specimens, including biological cells, polymers, and metals. The TEM has provided valuable insights into the structure of these materials and has helped to advance our understanding of the natural world.

The TEM is a complex instrument that requires a high level of technical expertise to operate. It is typically found in research laboratories and is used by scientists to study the structure of materials at the atomic level.

The TEM is a powerful tool for studying the fine structure of materials. It has been used to study a wide range of specimens, including biological cells, polymers, and metals. The TEM has provided valuable insights into the structure of these materials and has helped to advance our understanding of the natural world.

The TEM is a complex instrument that requires a high level of technical expertise to operate. It is typically found in research laboratories and is used by scientists to study the structure of materials at the atomic level.

The TEM is a powerful tool for studying the fine structure of materials. It has been used to study a wide range of specimens, including biological cells, polymers, and metals. The TEM has provided valuable insights into the structure of these materials and has helped to advance our understanding of the natural world.

The TEM is a complex instrument that requires a high level of technical expertise to operate. It is typically found in research laboratories and is used by scientists to study the structure of materials at the atomic level.

The TEM is a powerful tool for studying the fine structure of materials. It has been used to study a wide range of specimens, including biological cells, polymers, and metals. The TEM has provided valuable insights into the structure of these materials and has helped to advance our understanding of the natural world.

The TEM is a complex instrument that requires a high level of technical expertise to operate. It is typically found in research laboratories and is used by scientists to study the structure of materials at the atomic level.

The TEM is a powerful tool for studying the fine structure of materials. It has been used to study a wide range of specimens, including biological cells, polymers, and metals. The TEM has provided valuable insights into the structure of these materials and has helped to advance our understanding of the natural world.

The TEM is a complex instrument that requires a high level of technical expertise to operate. It is typically found in research laboratories and is used by scientists to study the structure of materials at the atomic level.

The TEM is a powerful tool for studying the fine structure of materials. It has been used to study a wide range of specimens, including biological cells, polymers, and metals. The TEM has provided valuable insights into the structure of these materials and has helped to advance our understanding of the natural world.

The TEM is a complex instrument that requires a high level of technical expertise to operate. It is typically found in research laboratories and is used by scientists to study the structure of materials at the atomic level.

The TEM is a powerful tool for studying the fine structure of materials. It has been used to study a wide range of specimens, including biological cells, polymers, and metals. The TEM has provided valuable insights into the structure of these materials and has helped to advance our understanding of the natural world.

The TEM is a complex instrument that requires a high level of technical expertise to operate. It is typically found in research laboratories and is used by scientists to study the structure of materials at the atomic level.

The TEM is a powerful tool for studying the fine structure of materials. It has been used to study a wide range of specimens, including biological cells, polymers, and metals. The TEM has provided valuable insights into the structure of these materials and has helped to advance our understanding of the natural world.

The TEM is a complex instrument that requires a high level of technical expertise to operate. It is typically found in research laboratories and is used by scientists to study the structure of materials at the atomic level.

The TEM is a powerful tool for studying the fine structure of materials. It has been used to study a wide range of specimens, including biological cells, polymers, and metals. The TEM has provided valuable insights into the structure of these materials and has helped to advance our understanding of the natural world.

The TEM is a complex instrument that requires a high level of technical expertise to operate. It is typically found in research laboratories and is used by scientists to study the structure of materials at the atomic level.

The TEM is a powerful tool for studying the fine structure of materials. It has been used to study a wide range of specimens, including biological cells, polymers, and metals. The TEM has provided valuable insights into the structure of these materials and has helped to advance our understanding of the natural world.

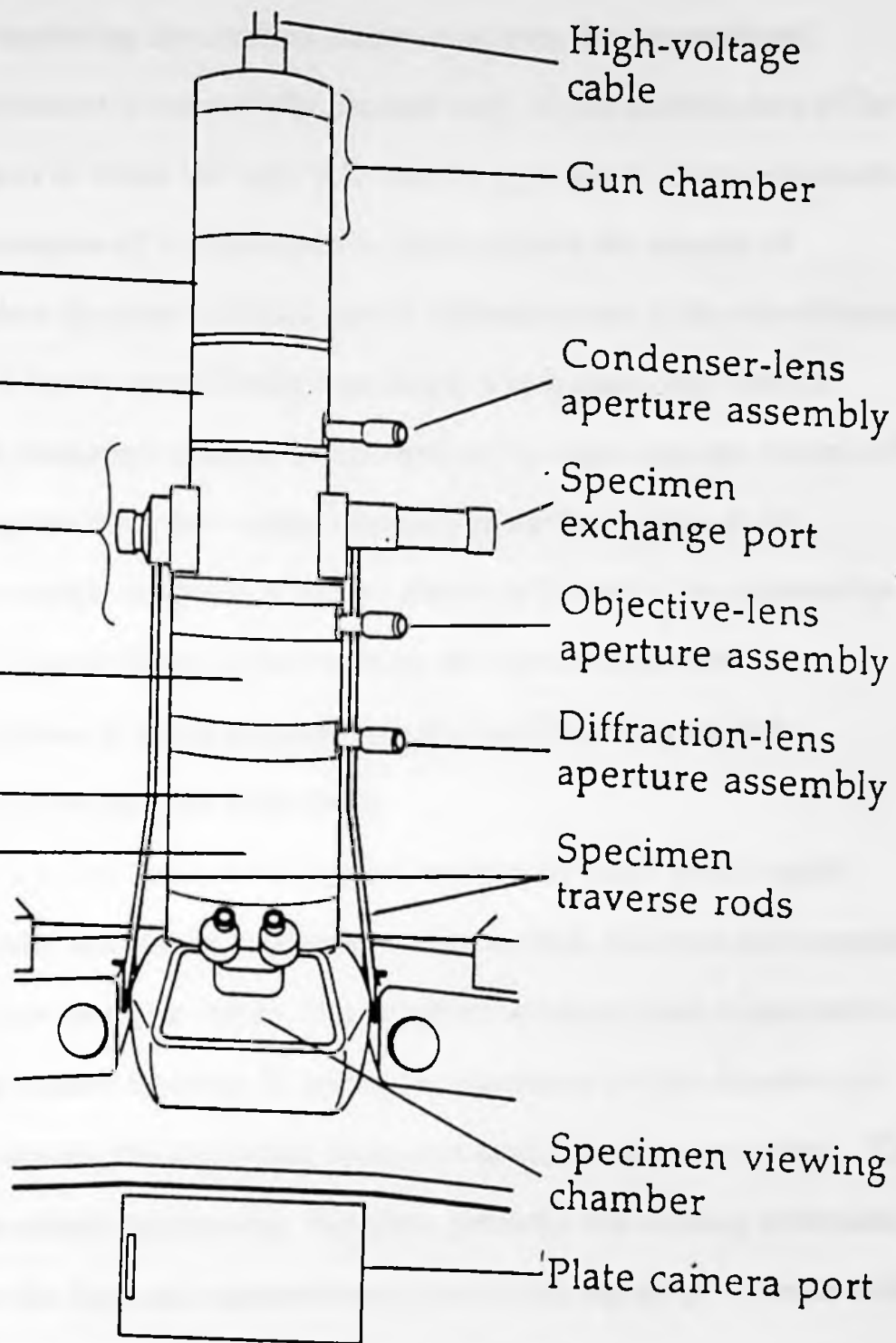


Figure 15. The Transmission Electron Microscope enables fine detail (up to 0.2nm) to be distinguished through specimen magnification via electromagnetic lenses due to a very short wavelength. The electrons provide up to a thousand fold increase in resolving power over the light microscope.

3. Confocal Microscope

The advantage of employing the confocal microscope over the conventional microscope is that its illumination is sequentially focused only on one discrete area of the specimen at a time. The area in which the light is focused is typically 0.25 μ m in diameter and 0.5 μ m deep. The discreteness of the illumination beam reduces the amount of illumination above and below the plane of focus, hence reducing some of the out-of-focus information. This ability is based upon Minsky's principle which states that both the illumination and detection (imaging) systems are focused on the same discrete volume of the specimen, allowing signals from the volume elements in the focal plane to be detected and signals from outside the plane of focus (above or below) to be removed by a spatial filter. The use of spatial filters further reduces the out-of-focus feedback information. The term confocal is hence derived from the fact that the specimen illumination and the detector possess the same focus.

In order to compose a two dimensional optical section, the laser beam rapidly scans the sample horizontally and slowly progresses in the vertical direction and compiles the detected fluorescent light intensity values. These optical sections taken at successive focal planes may be compounded together (Z series) to reconstruct a three dimensional image of the sample by viewing the individual slices as a stack to create a montage. This unique capability of the confocal microscope, therefore, provides the missing information necessary to link together the light and transmission electron micrographs. Z series refers to the acquisition of a series of optical sections taken along the z axis at successively lower or higher focal planes.

Confocal imaging employs laser excitation. This light reaches the objective lens by first passing through the confocal scanning system, which causes the beam to illuminate a discrete volume element of the specimen. Fluorescence created by the sample is emitted in all directions. The objective lens and scanning system together

direct the light from the focal plane of the specimen to reflect off of the dichroic mirror, through appropriately chosen filters, and then onto a detector.

The air-cooled krypton-argon ion laser employed by the Bio-RAD 1024 combines the excitation capabilities of the krypton and argon lasers to cause excitation at 488nm (blue), 568nm (yellow) and 647nm (red). The argon laser (most common) has two major emission lines 488nm (blue) and 514nm (green). The krypton laser, on the other hand, has a wider range of visible emission wavelengths, which can excite most fluorophores requiring excitation by visible light. The emission line capabilities are as follows: red emission lines at 647 and 676nm, a yellow emission line at 568nm, green emission lines at 520 and 531nm and blue emission lines at 468, 476, and 482nm. The combination of argon-krypton laser allows intense excitation of blue fluorophores at a 488nm emission line to allow greater excitation of fluorescein, a higher efficiency 568nm line for excitation of various rhodamines, and the 647nm line provides the capability of exciting far red fluorophores.

The most common detectors used in laser scanning confocal microscopes are photomultiplier tubes (PMTs), which are extremely sensitive to the wavelength of the detected photons. The photomultiplier tube is simply a vacuum tube with a photosensitive cathode and a set of secondary electrodes. The probability of photon detection is strongly determined by the wavelength of light and is given in terms of quantum efficiency, which is the probability that an electron is generated by an incident photon. (Figure 16)

The use of fluorescence in confocal microscopy has advantages for imaging fine details within specimens. The most common means of fluorescence labeling for biological samples involves the use of antibodies labeled with fluorophores (immunofluorescence histochemistry). The samples may be directly or indirectly labeled with fluorophores. Direct immunofluorescence involves the use of a primary antibody

already conjugated with a fluorophore. Indirect immunofluorescence, on the other hand, uses a secondary antibody conjugated with a fluorophore raised against the immunoglobulins of the same species in which the primary antibody was raised.

a. Fluorescein

Fluorescein isothiocyanate (FITC), a xanthene fluorescent dye of great intensity, is maximally excited by blue light and emits green to yellow fluorescence. Its absorbance maximum is between approximately 450 to 500nm, which nicely corresponds to the 488nm line of the argon laser for near-maximal excitation. The fluorescein isothiocyanate is capable of displaying large extinction coefficients and high quantum yields after conjugation. This fluorescein isothiocyanate dye binds approximately 3 to 5 fluoresceins to each IgG antibody before self-quenching. (Brelje et.al. 1993)

b. Rhodamine Fluorophores

Like fluorescein, Rhodamines are also derived from xanthene. The maximal excitation is slightly shifted toward red with an emission peak around 546nm. Due to the hydrophobic nature of rhodamines, less fluorophores are able to bind with the antibody molecule. The interactions between the antibody and fluorophore limit the increase in fluorescence intensity that is possible by conjugating higher numbers of fluorophores to each protein molecule. Although the total fluorescence signal may be enhanced through higher illumination intensities, photochemical side effects such as photobleaching of the fluorophores, denaturation of antibodies and specimen damage become a concern. In comparison to fluorescein, rhodamines are less intense due to lower quantum yields, more photostable and pH insensitivity. Tetramethylrhodamine (TRITC) is one of the most widely used rhodamines. (Brelje et.al. 1993)

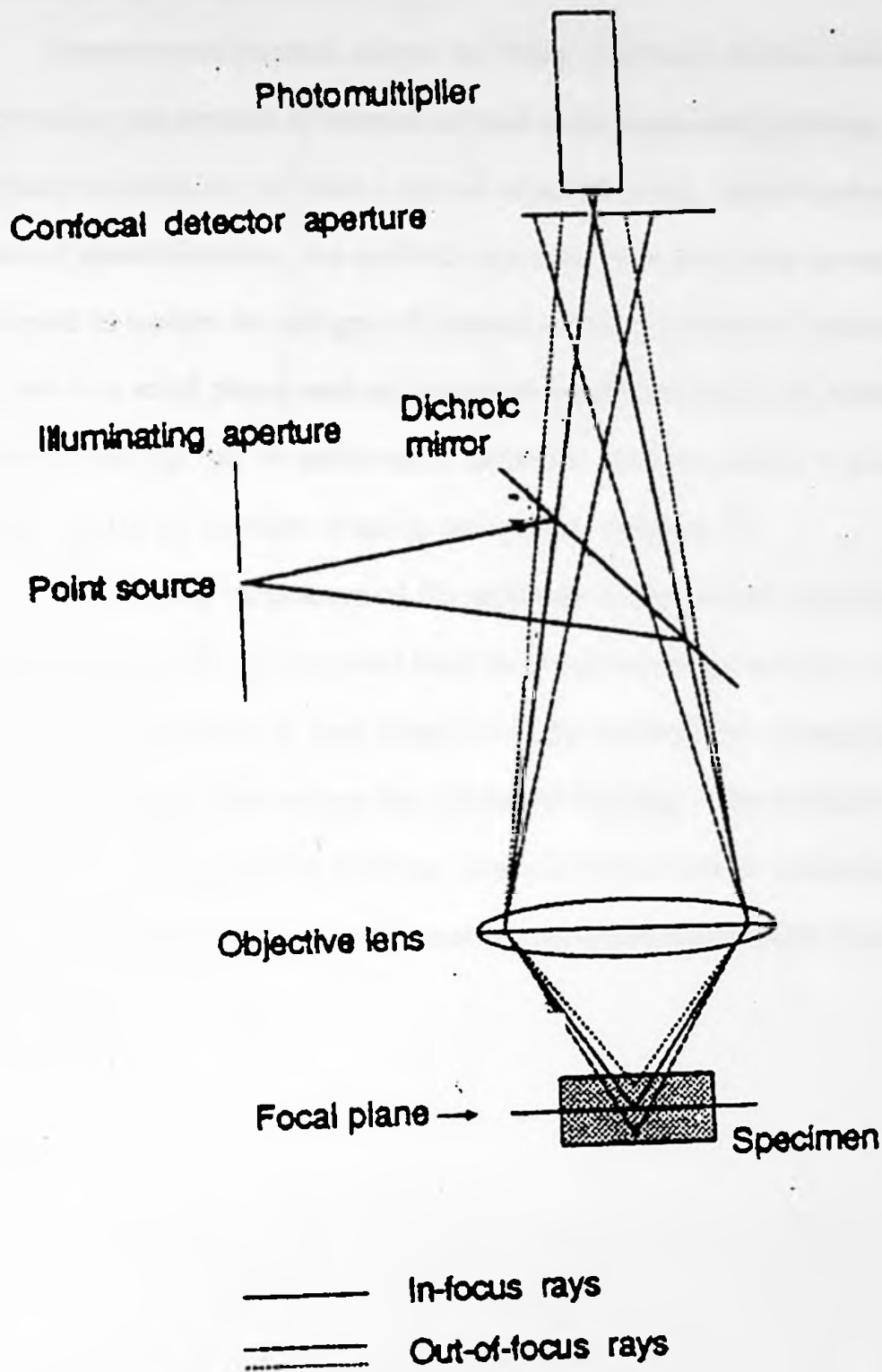


Figure 16. The Confocal Microscope. The illumination of the confocal is sequentially focused on one discrete area of the specimen at a time. The discreteness of the illumination beam reduces the amount of illumination above and below the plane of focus, hence reducing some of the out-of-focus information.

4. Immunoprecipitation

Immunoprecipitation allows the study of protein-protein interactions by precipitating the protein of interest as well as its associated proteins.

Immunoprecipitation provides a means of purification, identification of an antigen and a means of quantification. An antibody specific for a particular protein antigen is employed to isolate the antigen of interest within a mixture of proteins. The antibody is attached to a solid phase such as an agarose bead via a direct or indirect chemical binding. Indirect coupling can be achieved by proteins, such as protein A that have an inherent affinity for the Fc portion of the Ig molecules. (Figure 17)

Following incubation of the antibody coated beads with the solution of antigen, unbound molecules are removed from the bead-antibody-antigen complex by washing. The antigen of interest is then eluted from the antibody by changing the pH or by other solvent conditions that reduce the affinity of binding. The purified antigen can then be analyzed to reveal specific physical characteristics such as molecular weight and isoelectric points by one-dimensional or two-dimensional SDS-PAGE.

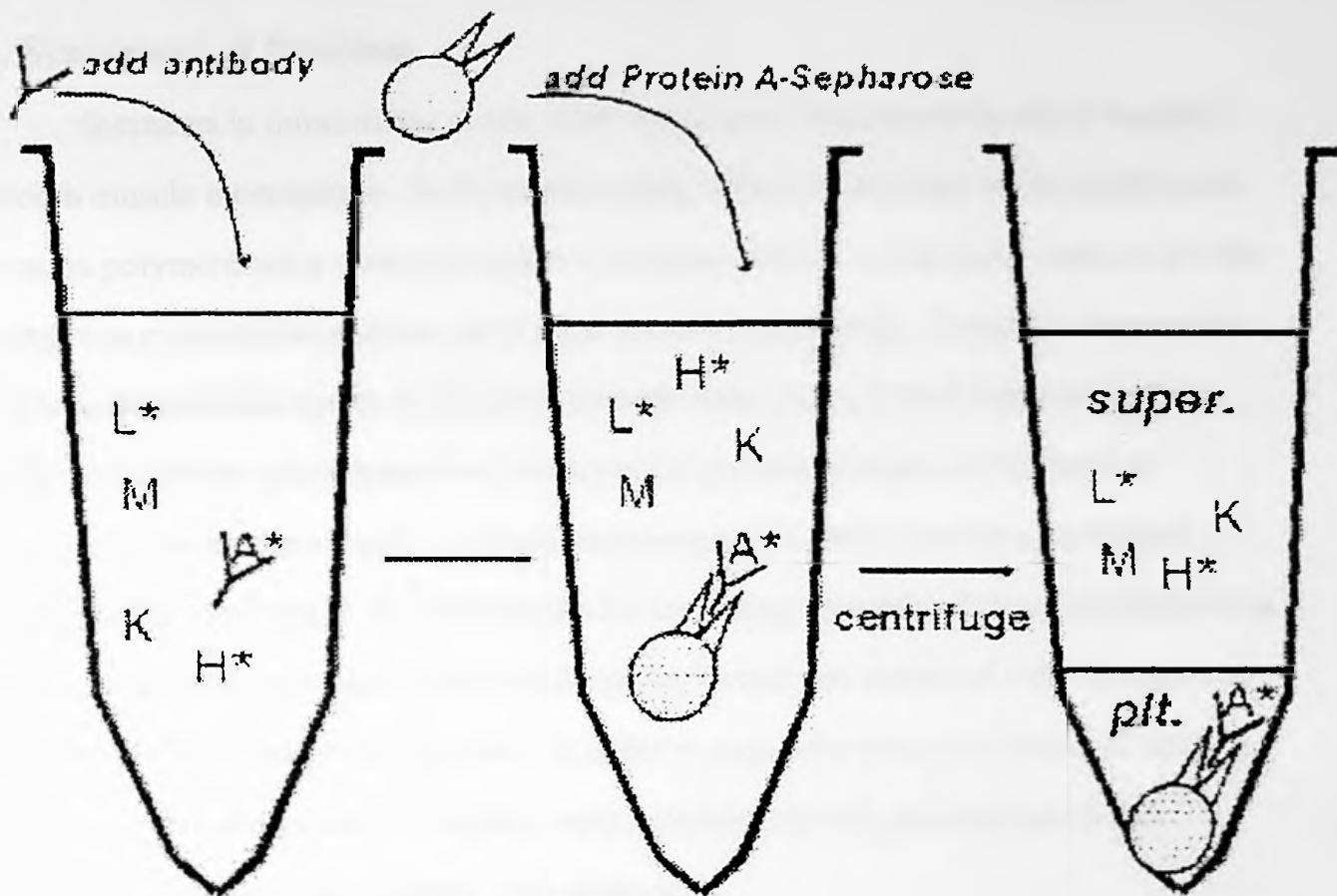


Figure 17. Principles of Immunoprecipitation. An antibody specific for a particular protein antigen is employed to isolate the antigen of interest within a mixture of proteins. The antibody is attached to Protein A-Sepharose beads.

B. Statement of Problem

Increases in intracellular cyclic AMP levels have been shown to affect vascular smooth muscle morphology. In the present study, effects of elevated cyclic AMP levels on actin polymerization were assessed to determine whether cyclic AMP induces specific changes in cytoskeletal proteins of vascular smooth muscle cells. Forskolin was used to increase intracellular cyclic AMP levels through direct activation of adenylate cyclase. Light and Electron microscopy was employed to appraise changes in the shape of vascular smooth muscle cells. Confocal microscopy was used to reveal cytoskeletal changes after exposure to 10^{-6} M forskolin for increasing intervals of time. Differences in the expression of actin were evident in forskolin treated and untreated cells through one and two-dimensional electrophoresis. In order to assess the phosphorylation of actin in response to protein kinase, VSM cells were radiolabeled with phosphorus-33 and subsequently immunoprecipitated with alpha-actin.

C. Methods

1. Animals

Twelve week-old, 225g-250g male Sprague Dawley rats (Hilltop Laboratories, Scottsdale, PA) were used for all experiments except for the radiolabeling and immunoprecipitation studies. Sprague Dawley rats were maintained on a 12:12 hour light:dark cycle at a constant temperature of 23C +/- 2C. The diet of the Sprague Dawley rats consisted of Purina Rat Chow and tap water. Thoratic aortae from rabbit were obtained through an independent source for the radiolabeling and immunoprecipitation studies.

2. Cell Culture

Rats were anesthetized with an intraperitoneal injection of ketamine hydrochloride/ xylazine (45:5 mg/kg) and the thoracic aortae were surgically removed under aseptic conditions. Vascular smooth muscle cells from the tunica media of the thoratic aortae were enzymatically dispersed in a cocktail of Type II collagenase (12mg), elastase (10mg), DNase (1mg), soybean trypsin inhibitor (8mg) and bovine serum albumin (BSA) (32mg) in 8ml of Isolation Buffer (152mg glucose, 357mg Hepes, 100ul CaCl₂ 2H₂O in 990ml of calcium and magnesium free Hanks Buffered Saline Solution (HBSS) for one hour on a 37C water bath shaker. Residual material was removed following dispersion using a fine mesh filter. The digestion media was then extracted following centrifugation at approximately 1000g for 5 minutes. The cell pellet formed was resuspended in 2mL of serum free Dulbecco's Modified Eagle Media (DMEM). This cell suspension was plated in a 25cm² Falcon tissue culture flasks and allowed to incubate for 2 hours to allow for cell attachment. Additional DMEM containing 10% heat inactivated fetal calf serum with penicillin and streptomycin was added to the flask to promote cell growth. Cells were incubated in a humidified

environment of 37°C and 10% CO₂ throughout the course of growth and experimentation. After confluency was achieved cells were passaged at regular intervals using a 1x trypsin solution (0.5% trypsin in 5.0ml EDTA-4Na) in HBSS for cell detachment. Cell passages 3 through 10 were used.

3. Confocal Microscopy

The vascular smooth muscle cells were grown on glass cover slips in six-well Falcon tissue culture plates for a minimum of twenty-four hours to allow for attachment and elongation. Then forskolin (5×10^{-6} M) was added to the tissue culture medium for varying intervals of time. An equivalent volume of carrier was added to control (untreated) cells. Following stimulation, the medium was removed and ice-cold acetone was added to each well to remove lipid soluble cell components and fix the cells. The cytoskeleton was probed for thirty-minutes at room temperature with TRITC-labeled and FITC-labeled phalloidin for visualization of polymerized smooth muscle actin filaments. The cells were observed using a Nikon Diaphot Microscope and BioRad Model 1024 Scanning Laser Confocal System System with a Krypton/Argon laser. Three dimensional images of sequential plane sections were compiled using BioRad Laserssharp and Confocal Assistant Software.

4. Light Microscopy

Vascular smooth muscle cells were grown on glass cover slips in six-well Falcon tissue culture plates for a minimum of twenty-four hours. Then forskolin (5×10^{-6} M) or an equivalent volume of carrier was added to the smooth muscle cells for varying periods of time. Images of the live smooth muscle cells were acquired using a Nikon Diaphot-TMP inverted microscope. Pictures were taken with an attached 35mm Nikon camera.

5. Light Microscopy Staining

After vascular smooth muscle cells (attached to glass cover slips) were incubated with or without (control) forskolin, they were fixed for one hour in 1M glutaraldehyde solution. After washing they were exposed to a 0.2M cacodylate buffer (50ml of 0.4M sodium cacodylate, 8ml of 0.2M HCl, 42ml distilled water) for an additional fifteen minutes. The cells were stained with filtered toluidine blue for forty-five seconds and then rinsed with 0.5% sodium borax. The cells were rinsed again with distilled water and then incubated for ten minutes in xylene. Subsequently, the cells were dehydrated in each of the following for fifteen minute intervals: thirty percent ethanol, fifty percent ethanol, seventy percent ethanol and ninety percent ethanol. The cells were then incubated twice in one hundred percent ethanol for a period of thirty minutes each. Following staining and destaining, the cells were counted based upon the following categories, no change in cell shape, intermediates change indicating partial depolymerization or rounding up with some protoplasmic extensions, or complete change indicating a complete "balling up" of the cells around the perinuclear region with definite protoplasmic extensions.

6. Transmission Electron Microscopy

After vascular smooth muscle cells (grown on glass cover slips in six-well Falcon tissue culture plates) were incubated with 5×10^{-6} M forskolin for varying time intervals, the media was removed and the cells were exposed to 1M glutaraldehyde and 0.2M cacodylate buffer as described as above. The cells were then treated for one hour with two percent osmium tetroxide in 0.1M cacodylate buffer. The cells were then rinsed for fifteen minutes with 0.2M cacodylate buffer followed by an additional fifteen minute rinse with distilled water. Afterwards the cells were rinsed for fifteen minute intervals in each of the following thirty percent ethanol, fifty percent ethanol, seventy percent ethanol

and ninety percent ethanol. The cells were then incubated twice in one hundred percent ethanol for a period of thirty minutes each. Critical dry mass was then conducted. Throughout the above processes the cells were gently rocked and incubated on ice.

7. Immunoblot Analysis

At the end of an experiment, the vascular smooth muscle cells were scraped from the flask and centrifuged at 1000g for five minutes. The supernatant was removed and the cell pellet was resuspended in HBSS. Protein concentrations of the cell homogenate were determined by BCA (Pierce) protein assay according to the manufacturers' instructions following sample sonication. Samples of equal protein concentrations were denatured in sample buffer (1.576g Tris, 10g SDS, 50ml of 5% B-Mercaptoethanol, 100ml of 10% glycerol in 1L distilled de-ionized water at a pH of 7.4) and heated at 40C for five minutes. The samples were electrophoresed on a ten percent sodium dodecyl polyacrylamide gel electrophoresis (SDS-PAGE) for twenty-four hours at fifty volts. Proteins were then electrophoretically transferred at 36 volts for 30 minutes to hybond nitrocellulose membrane (Amersham) using a Biorad transfer apparatus. The membrane was incubated for one hour at room temperature in a five percent nonfat-dry milk/phosphate buffered saline (PBS) pH 7.5, containing 0.5% tween-twenty to reduce non-specific antibody binding. The membrane was then probed with a 1: 1000 dilution on monoclonal anti-actin anti-body (Sigma) for one hour at room temperature. The blot was then washed for one hour with several changes of PBS-0.5% Tween-twenty to remove non-specific anti-actin antibody binding. Afterwards, the membrane was subjected to a one-hour incubation with a 1:1000 dilution of rabbit anti-mouse horseradish peroxidase conjugated secondary antibody (Sigma). Following incubation, the blot was again washed with PBS-0.5% Tween-twenty. Immunoblots were visualized using the ECL Western blotting detection system (Amersham) following manufacturers'

instructions.

8. Two-Dimensional Electrophoresis

a. First Dimension

Isoelectric focusing gels were created within a 130mm by 2.5mm diameter glass tubing sealed at one end with Parafilm. The isoelectric focusing gels consisted of the following 2.75g Urea, 1ml of 10% NP-40, 200ul ampholines (Ph 5-7), 50ul of ampholines (pH 3.5-10), 0.633ml of 30% acrylamide, 0.5ml of 2% Bis in 0.512ml of water. The catalytic agents used were 3.5ul Temed and 5ul of 10% ammonium persulfate. The gels were overlayed with a overlay solution H (2.40g Urea in 5.0ml water) and removed after a two hour interval. The overlay solution was replaced with 20ul of lysis buffer A (2.85g urea, 1.0ml of 10% NP-40, 200ul ampholines (pH 5-7), 50ul ampholine (pH 3.5-10), 250ul beta mercaptoethanol diluted to 5.0ml of distilled, de-ionized water) upon which a small amount of water was placed. The gels were allowed to set for two more hours. The gels were then placed in a standard tube gel electrophoresis buffer following removal of the Parafilm. The lysis buffer A was removed from the gel surface along with the water. A solution of 0.002M NaOH was then used to fill the tube gels. The upper reservoir of the gel was then filled with 0.02M NaOH while 0.01M H_3PO_4 was added to the bottom chamber. The gels were then prerun according to the following schedule: 200 volts for fifteen minutes, 300 volts for thirty minutes, and 400 volts for thirty minutes. All overlaying solutions were removed from the gel and an equivalent amount of forskolin treated and non-treated samples were loaded onto the gel. On top of the samples a gel overlay solution K (2.70g, 100ul ampholine (pH 5-7), 25ul ampholine (pH 3.5-10) diluted to 5.0ml of distilled, de-ionized water) was added. The upper and lower chamber buffers were replenished. Following sample and overlay solution loading, the gels were run for eighteen hours at

400 volts. The following day, the isoelectric focusing gels were extruded into 5ml of SDS sample buffer for thirty minutes.

b. Second Dimension

The tube gels were embedded in a 1% agarose gel and then electrophoresed onto a 10% SDS-PAGE gel for twenty-four hours at sixty volts. At this point the gels were either stained with a Biorad Rapid Silver Stain according to manufacturers' directions or transferred onto a nitrocellulose membrane for subsequent analysis upon the mass spectrometer.

9. Radiolabeling

The tunica media layer of the descending rabbit aorta was distributed among the four wells of a twelve well tissue culture plate containing one milliliter of phosphate free DMEM. Retinoic Acid was added to the medium at a final concentration of 10^{-6} M to preserve the contractile property of the vascular smooth muscle as supported by Wang et. al. (1997). Twenty-four milliliters of phosphorous-33 dispersed in phosphoric acid as purchased was then added to each well from a stock solution of ten millicuries per milliliter. The tissue pieces were then incubated overnight in an incubator with a mixed atmosphere of air and five percent carbon dioxide to allow sufficient time for phosphorous-33 to radiolabel the intracellular ATP. Following the interval of incubation the radiolabeling media was removed and tissues were rinsed three times with tris buffered saline solution. Fresh incubation media was supplied to each well in addition to the experimental agonist required to activate protein kinase. The plate was then incubated for an additional time period (two hours for phorbol and one hour for forskolin) to allow the activated kinases to catalyze the transfer of phosphorous-33 from the radiolabeled ATP to specific proteins. Each of the tissue pieces was then transferred to a

separate glass homogenizer containing one milliliter of lysis buffer in addition to phosphatase inhibitors and homogenized. Following centrifugation of the tissue mixture, the supernatant underwent immunoprecipitation to harvest the specific proteins of interest.

10. Immunoprecipitation

The rabbit VSM cells to be lysed were first washed with a phosphate buffered solution (PBS) to allow removal of serum proteins. The cell lysate was then suspended in one milliliter of cell lysate buffer (250mM NaCl, 25mM Tris-HCl pH 7.5, 5mM EDTA pH 8.0, 1% NP-40, 2µg/mL aprotinin, 1mM phenylmethylsulfonylfluoride) and incubated for twenty minutes on ice. Following incubation the cell lysate was sonicated. The cellular suspension was transferred to microfuge tubes and spun at 12000g for ten minutes at four degrees Celsius in a microfuge. The supernatant was placed within a fresh microfuge tube. Antibody against the target protein was added to the supernatant at a ratio of one microliter of antibody to fifty microliters of lysate along with fifteen microliters of protein A. The mixture was incubated for two hours at four degrees Celsius upon a shaker. The supernatant was then discarded following microfugation of one minute. The pellet was resuspended in one milliliter of wash buffer (250mM NaCl, 25mM Tris-HCl pH 7.5, 5mM EDTA pH 8.0, 0.1% NP-40, 2µg/mL aprotinin, 1mM phenylmethylsulfonylfluoride). The cell mixture was once again placed upon the shaker for one minute at four degrees Celsius. The cell lysate was microfuged for one minute at four degrees Celsius. The preceding wash step was repeated three more times. After the removal of the supernatant, the pellet was resuspended in one hundred microliters of SDS-PAGE loading buffer. A Western blot then followed SDS-PAGE. The bands of interest were subsequently extracted and analyzed on the Bruker Biflex III MALDI-TOF Mass Spectrometer.

D. Results

1. Electron Microscope Images

The control cells demonstrated a somewhat elongated shape with broad pseudopod-like structures for attachment to the glass substrate. This is typical for untreated cultured vascular smooth muscle cells (Junqueira et. al, 1995). The brightly stained regions correspond to the slightly raised perinuclear / nuclear region of the cell. The outlying areas of the cell from the perinuclear /nuclear region to the pseudopod-like structures were broad, flat and therefore near background intensity levels. (Figure 18)

Exposure of vascular smooth muscle cells to 5×10^{-6} M forskolin for a one hour interval resulted in a distinctly shaped nuclear region and thin pseudopod-like structures of high intensity. The broad pseudopod-like structures and low intensity cytosolic region were no longer evident. Instead, thin branches of high intensity projected from the nuclear region. Also, intense staining material dotted the filamentous branches extruding from the nuclear region. (Figure 19)

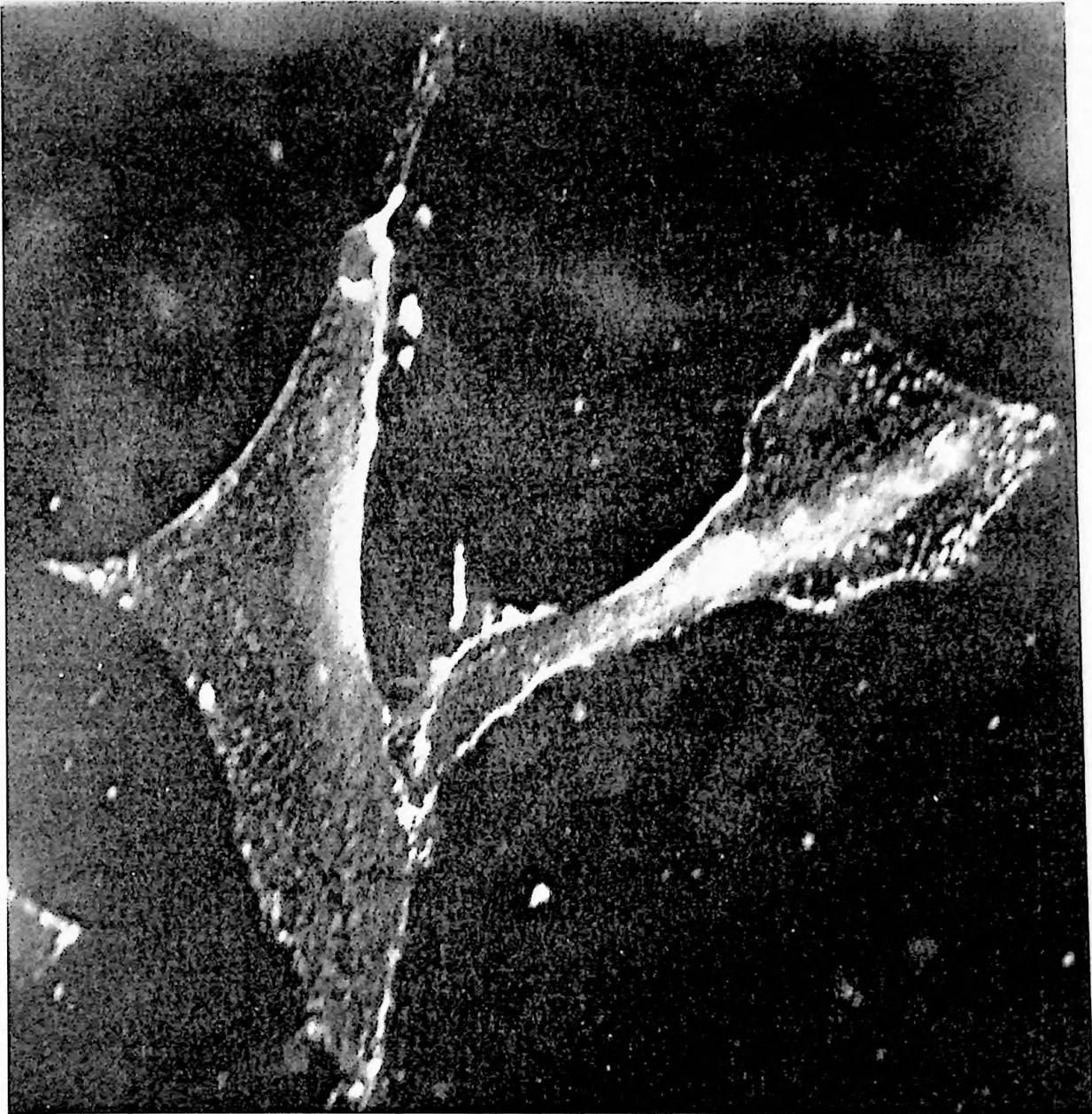


Figure 18. Vascular Smooth Muscle Cells Imaged on the Electron Microscope.

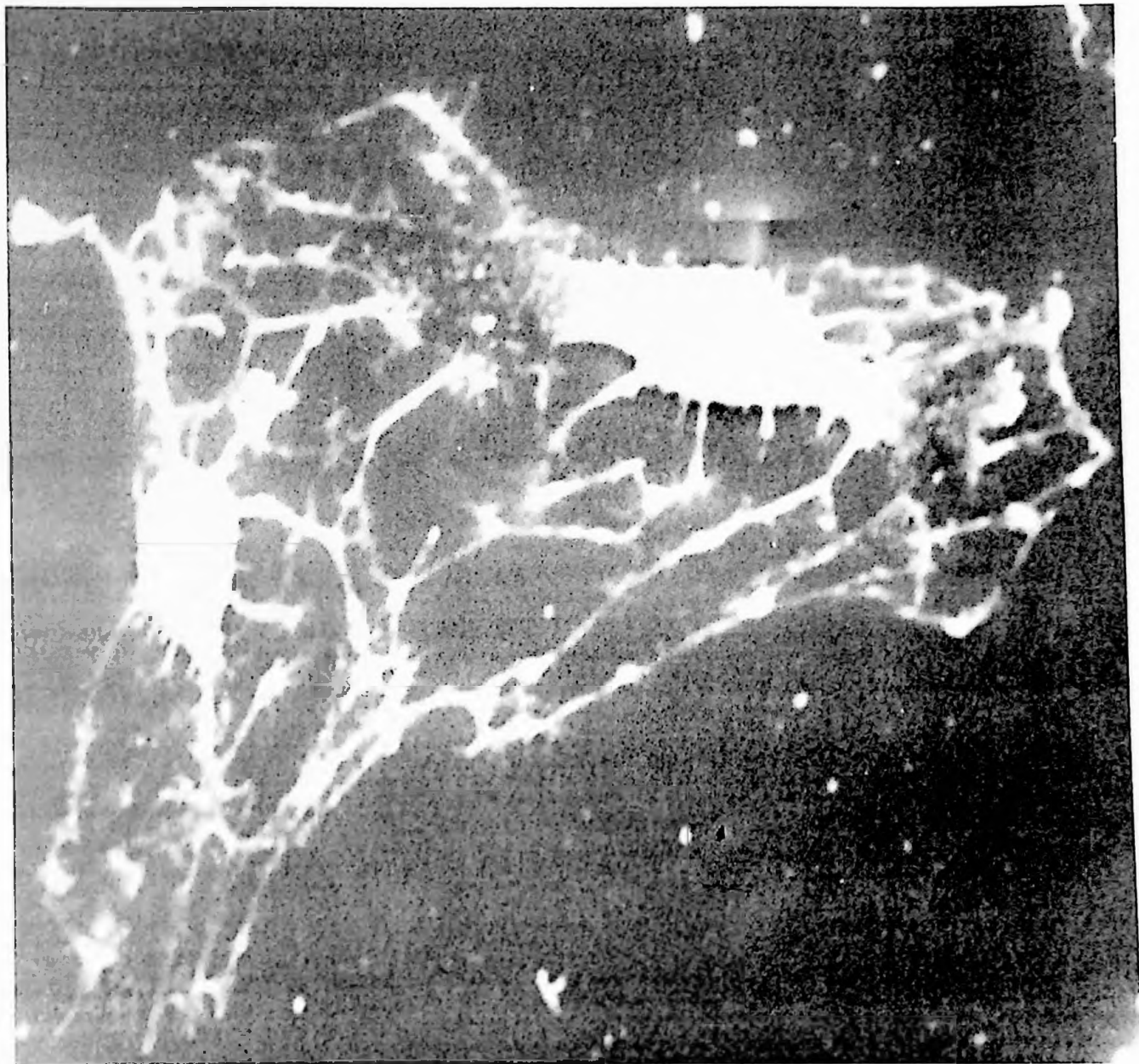


Figure 19. Electron Microscope Image of Vascular Smooth Muscle Cells Exposed to 5×10^{-6} M Forskolin for a One Hour Interval.

2. Light Microscopy Images

Control cells demonstrated the classic shape of cultured vascular smooth muscle cells, which is characterized, by a somewhat elongated shape with broad pseudopod-like structures for attachment to the glass substrate. The cytoplasm has a sheet like appearance with pseudopodia extending in multiple directions. (Figure 20)

After a thirty minute exposure to 5×10^{-6} M forskolin, subtle change in cell shape was noted compared to control cells. The treated cells became more rounded and, in some cases, thin pseudopod-like structures were evident. (Figure 21)

At an incubation interval of one hour, the vast majority of the vascular smooth muscle cells subjected to forskolin assumed a "balled up" appearance characterized by a swollen nuclear/perinuclear region with thin pseudopod-like extensions that were attached to the glass substrate. (Figure 22)

After an incubation period of three hours, the pseudopod-like structures of the forskolin-treated cells appeared to have broadened compared with the pseudopod-like structure of cells exposed to forskolin for one hour. This could be due to the partial return of the cytoplasm from the perinuclear/ nuclear region back to the pseudopod-like extensions. A sheet like "webbing" connecting the main pseudopod-like structure was apparent. This "webbing" was thought to arise from cytoplasm migration away from the perinuclear region. The perinuclear/ nuclear region still appeared to be swollen and elevated above the glass substrate attachment points. (Figure 23)

After twenty-four hours of incubation with forskolin, the cells appeared to have returned to a state of normalcy and assumed an appearance indistinguishable for untreated control cell. The thin pseudopod-like extensions and swollen perinuclear/ nuclear region were no longer evident. The cells now were broad and flat like the untreated cells. (Figure 24)

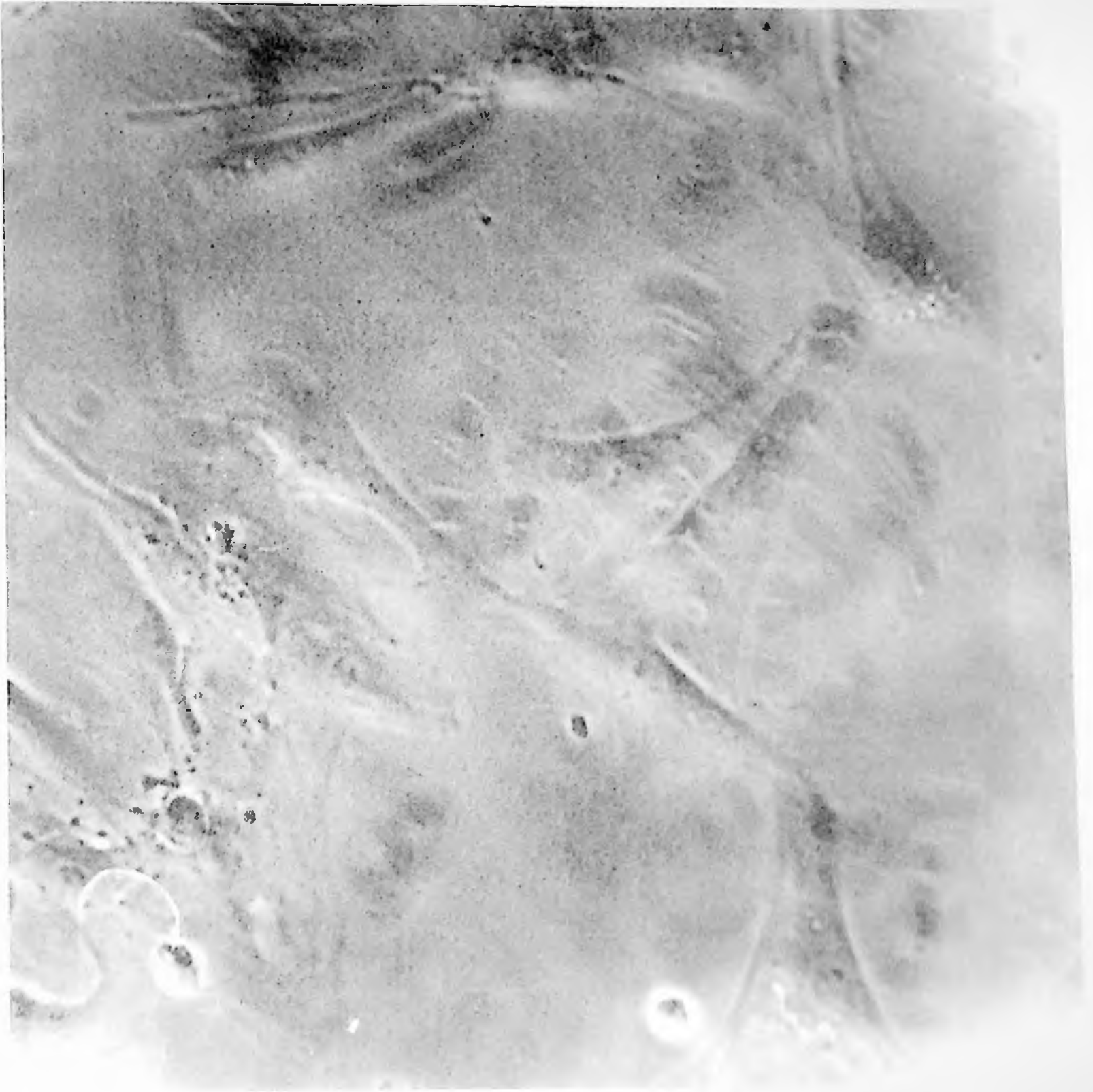


Figure 20. Vascular Smooth Muscle Control Cells Imaged on a Light Microscope.

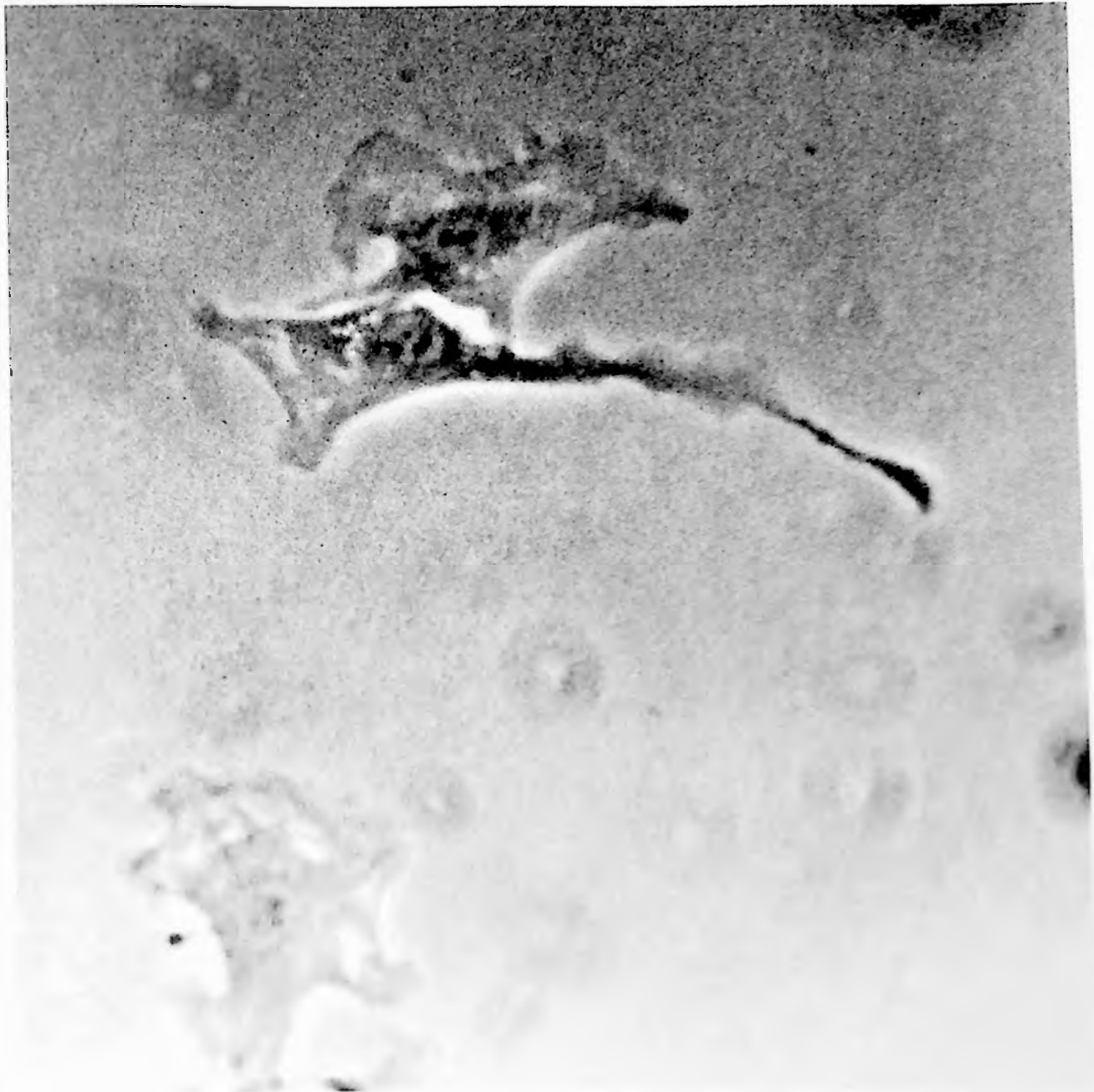


Figure 21. Light Microscopy Image of Vascular Smooth Muscle Cells Exposed to 5×10^{-6} M Forskolin for a Thirty Minute Interval.

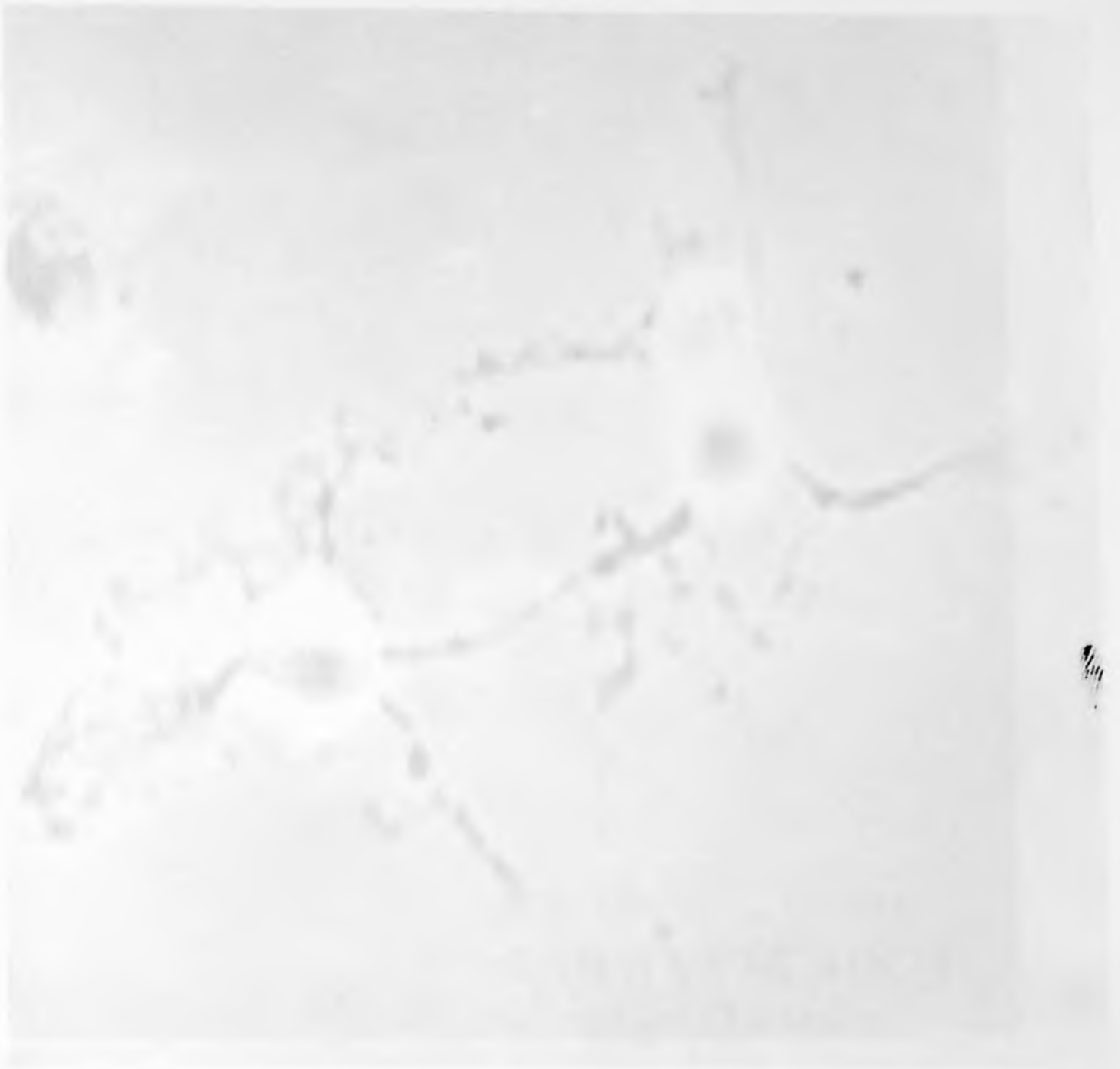


Figure 22. Light Microscopy Image of Vascular Smooth Muscle Cells Exposed to 5×10^{-6} M Forskolin for a One Hour Interval.

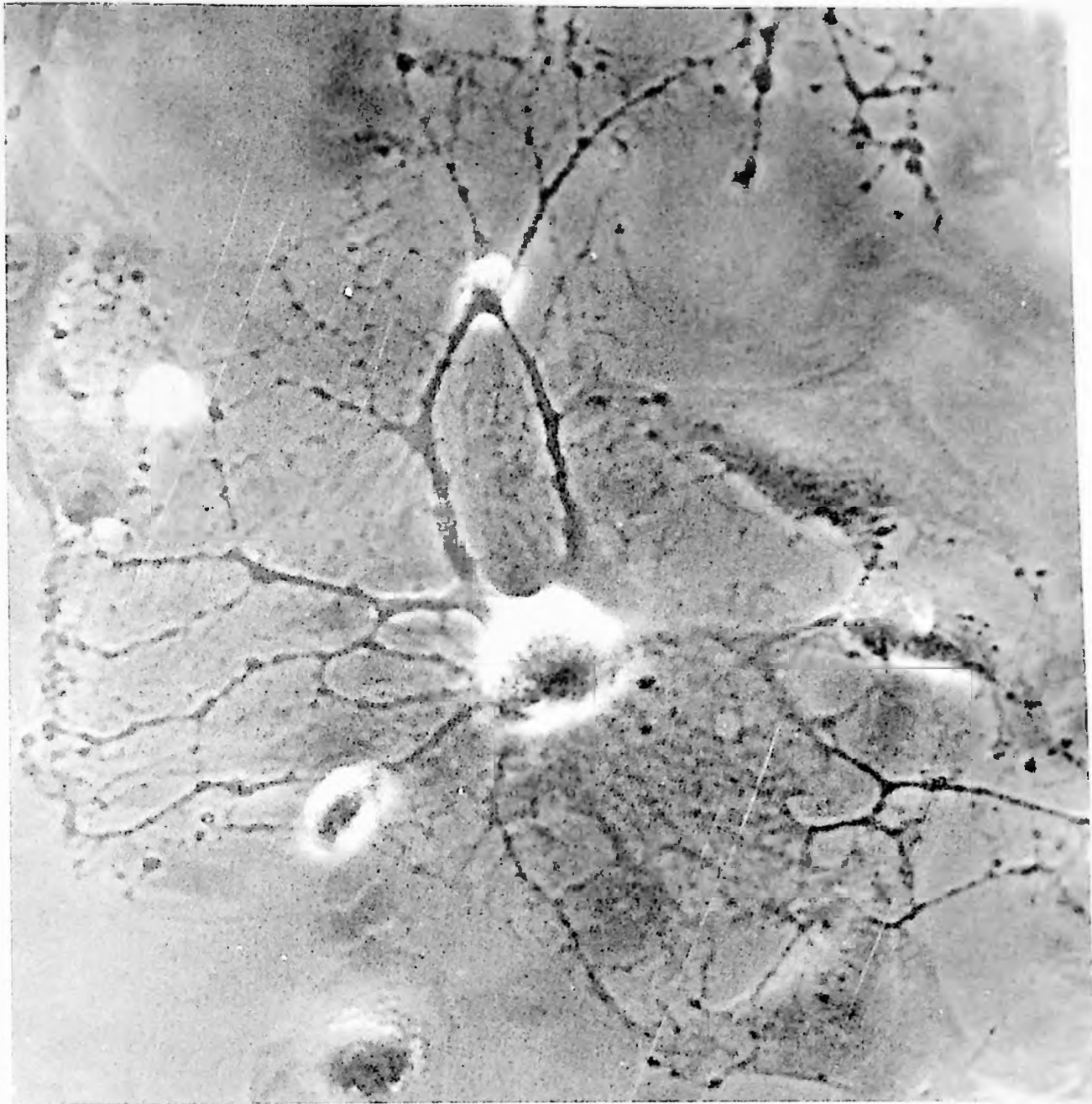


Figure 23. Light Microscopy Image of Vascular Smooth Muscle Cells Exposed to 5×10^{-6} M Forskolin for a Three Hour Interval.



Figure 24. Light Microscopy Image of Vascular Smooth Muscle Cells Exposed to 5×10^{-6} M Forskolin for a Twenty-Four Hour Interval.

3. Confocal Images

Thin straight filaments from untreated smooth muscle cells highlighted the actin cytoskeleton. The individual filaments were clearly defined and possessed directionality. (Figure 25)

Exposure of vascular smooth muscle cells to 5×10^{-6} M forskolin for ten minutes resulted in a partial loss of the actin filament structure. The actin filaments appeared as a loose network of short fragmented filaments. This may be an indication that the filamentous actin (F-actin) is disassembling into its original globular actin (G-actin) monomer building blocks. (Figure 26)

A thirty minute exposure of smooth muscle cells to forskolin resulted in a further loss of actin filament structure. Actin tended to aggregate in the perinuclear\ nuclear region and the thin straight actin filaments were no longer evident. A retraction of cytoplasm to the perinuclear\ nuclear region was suggested by an increased intensity of the staining within this region. The intense staining of the perinuclear region correlates with the increase in thickness or elevation above the glass substrate detected by the image stacking capabilities of the confocal assistant software. A second indicator of cytoplasm retraction was the development of notable pseudopod-like extensions, the movement of cytoplasm appearing to cause an indentation within the cell shape. The pseudopod-like extensions appear broad and lacy. (Figure 27)

Following a one hour exposure to forskolin, the phalloidin-staining material became highly concentrated in the nuclear region and organized actin filaments completely disappeared. The cell had the appearance of an intensely stained central region with multiple thin protoplasmic processes or pseudopod-like structures radiating outward from the nuclear region. The pseudopod-like structures were elongated with globular attachment points. (Figure 28)

Following a three hour forskolin exposure, cells exhibited a more complex pattern of cytoplasmic extensions. The nuclear region, which still retained the brightly intense swollen appearance, seemed to have develop more pseudopod-like structures. The pseudopod-like structures were no longer thin with a few globular regions but were broader in width. A complex lacy appearance characterized by multiple branches arising from the globular regions from within the pseudopod-like structures. (Figure 29)

Exposure of vascular smooth muscle cells to 5×10^{-6} M forskolin for a twenty-six hour interval resulted in an apparent return of the actin cytoskeleton to an appearance resembling that of control cells. Although some loose filaments as well as partial bundles of actin filaments were evident, the majority of the actin cytoskeleton appeared straight and elongated. No evidence of pseudopod-like structures was present. (Figure 30)

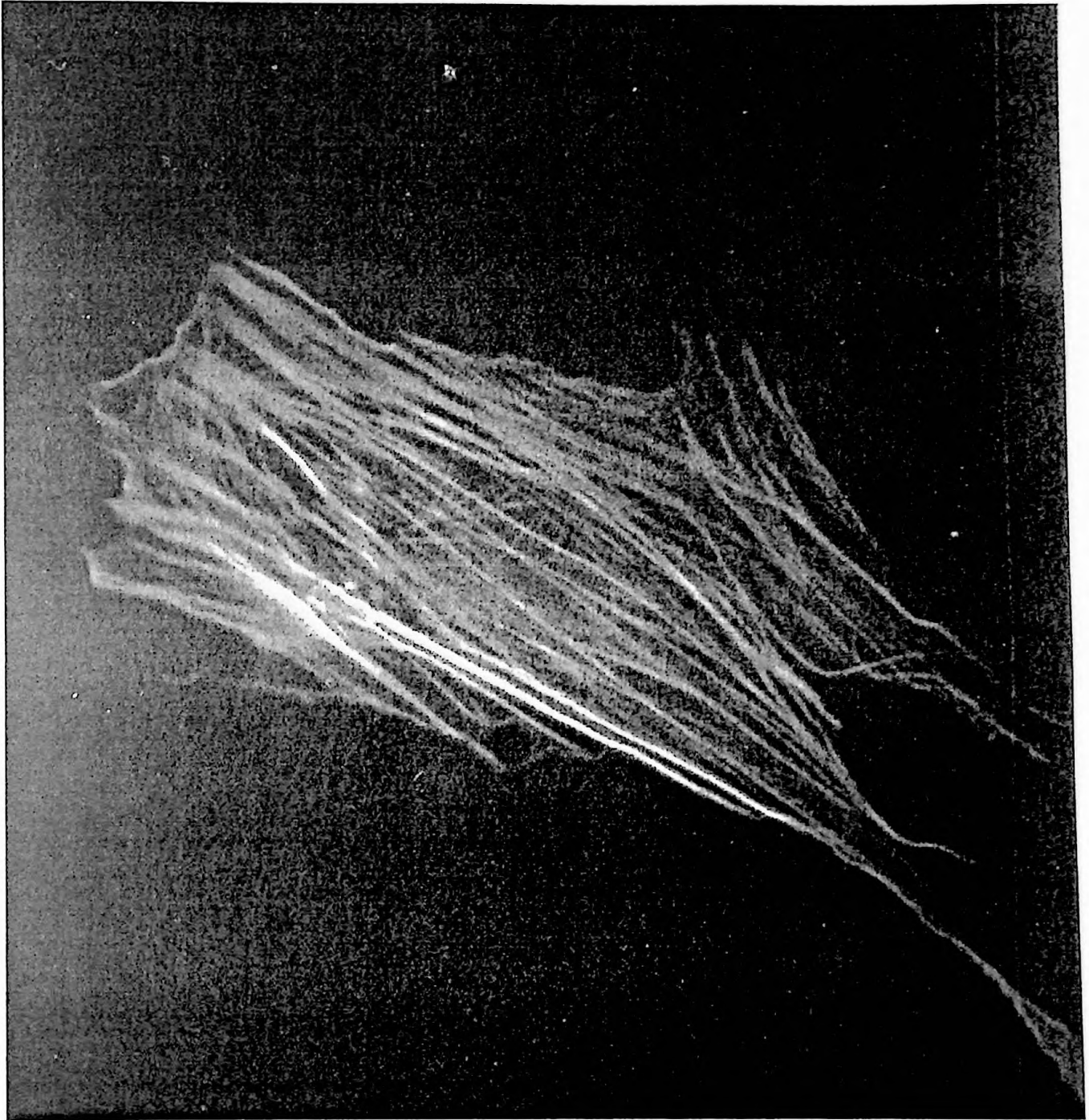


Figure 25. Vascular Smooth Muscle Control Cells Imaged on the Confocal Microscope.

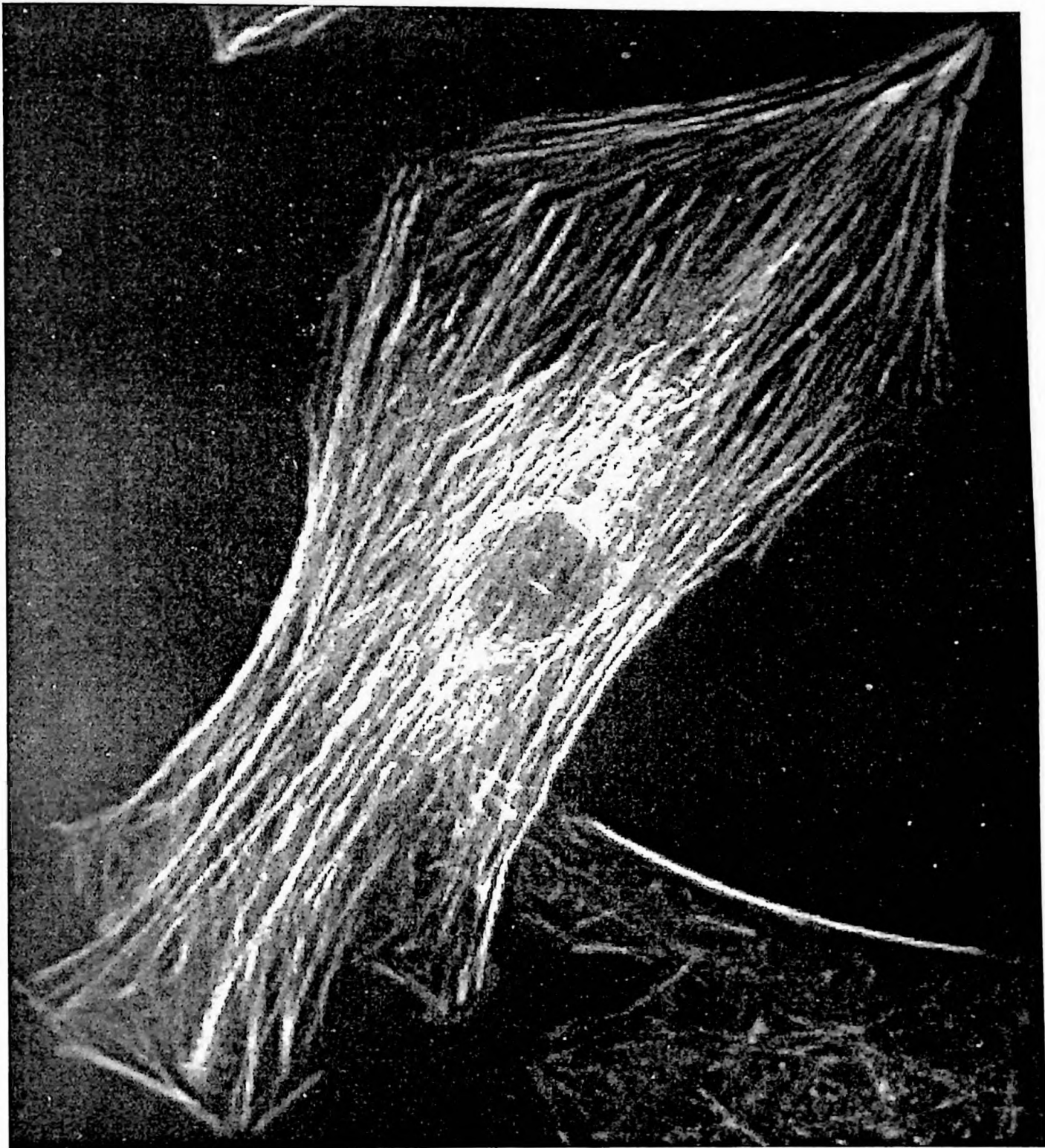


Figure 26. Confocal Microscopy Image of Vascular Smooth Muscle Cells Exposed to 5×10^{-6} M Forskolin for a Ten Minute Interval.

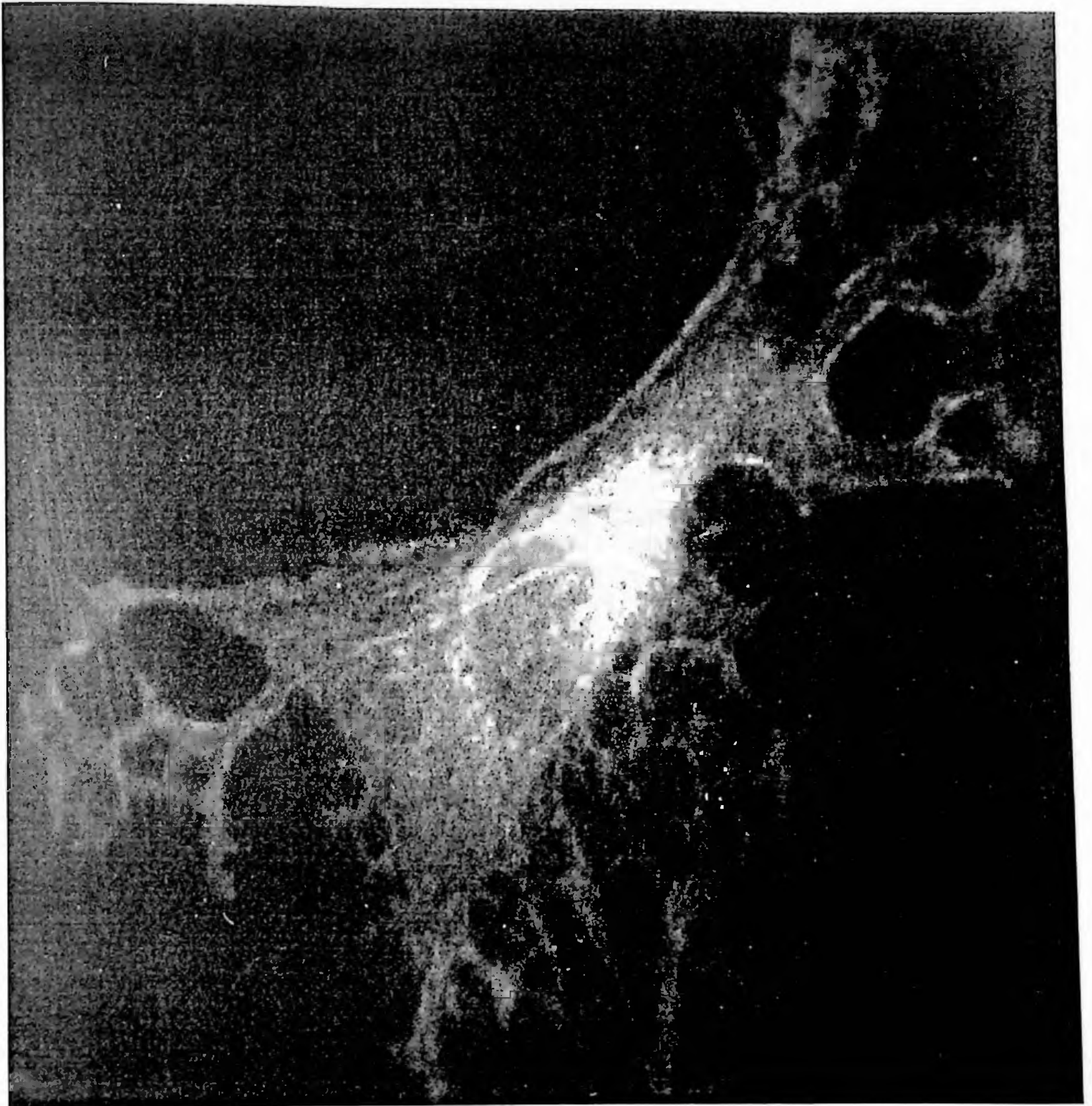


Figure 27. Confocal Microscopy Image of Vascular Smooth Muscle Cells Exposed to 5×10^{-6} M Forskolin for a Thirty Minute Interval.

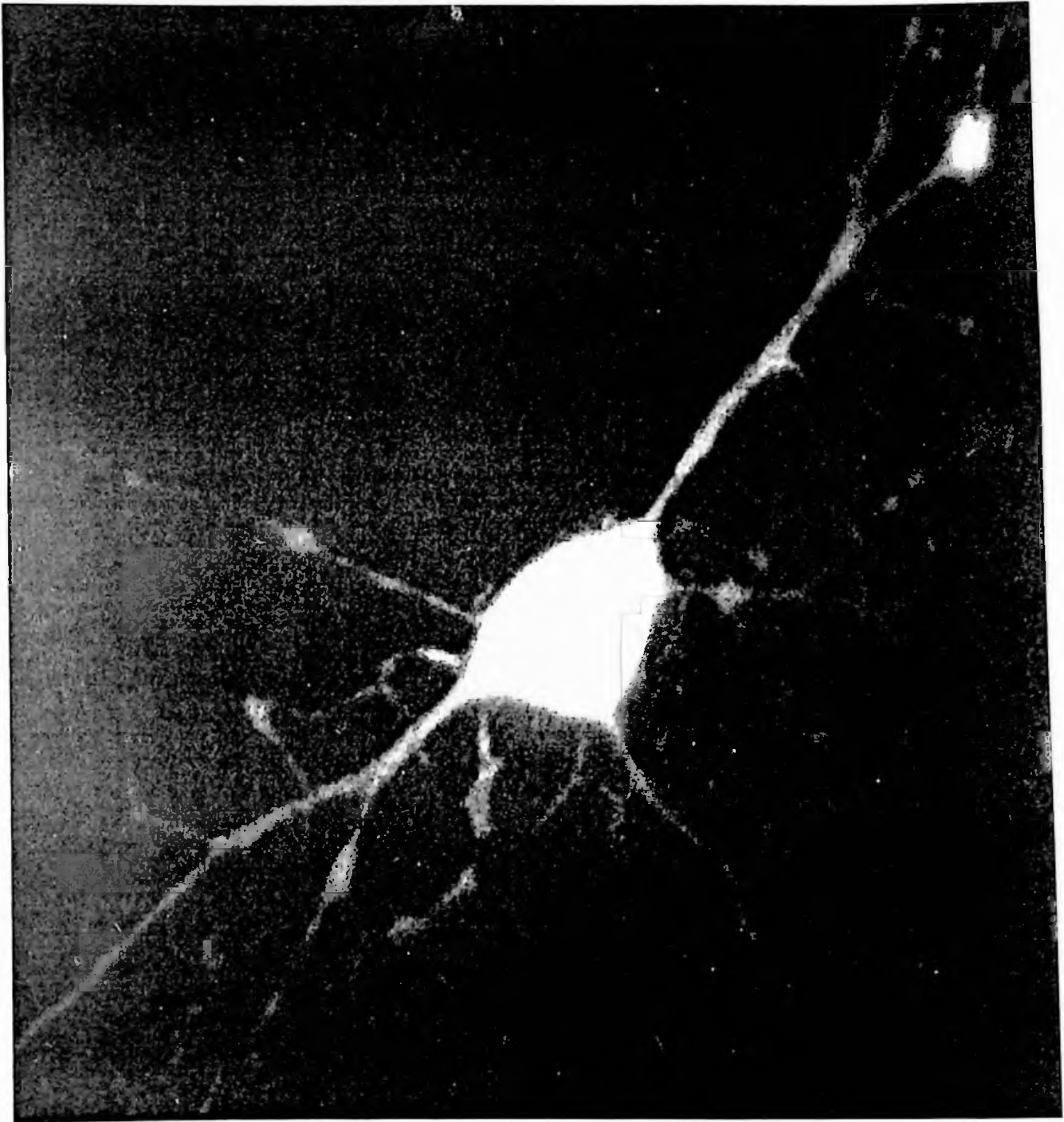


Figure 28. Confocal Microscopy Image of Vascular Smooth Muscle Cells Exposed to 5×10^{-6} M Forskolin for a One Hour Interval.

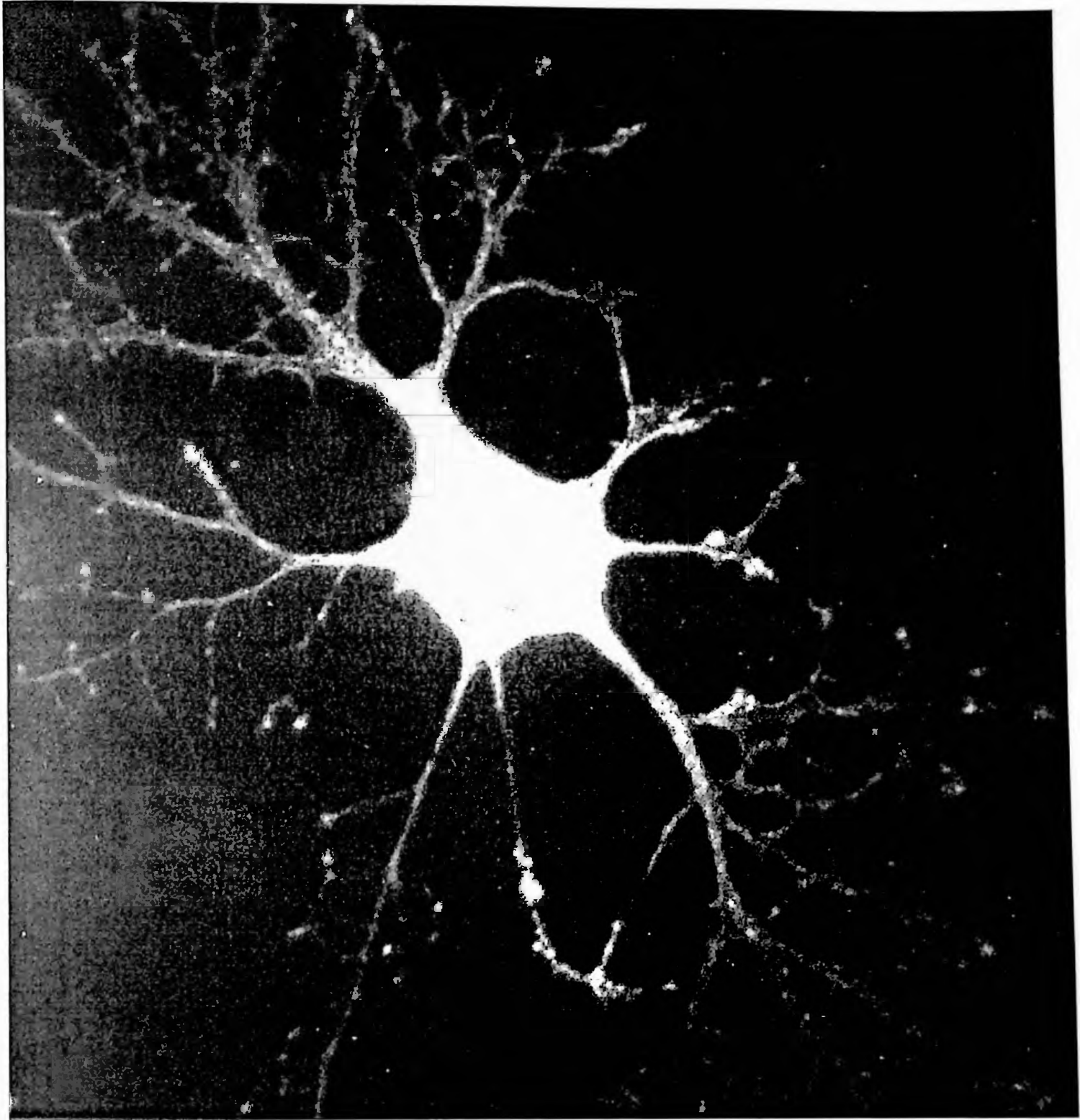


Figure 29. Confocal Microscopy Image of Vascular Smooth Muscle Cells Exposed to 5×10^{-6} M Forskolin for a Three Hour Interval.

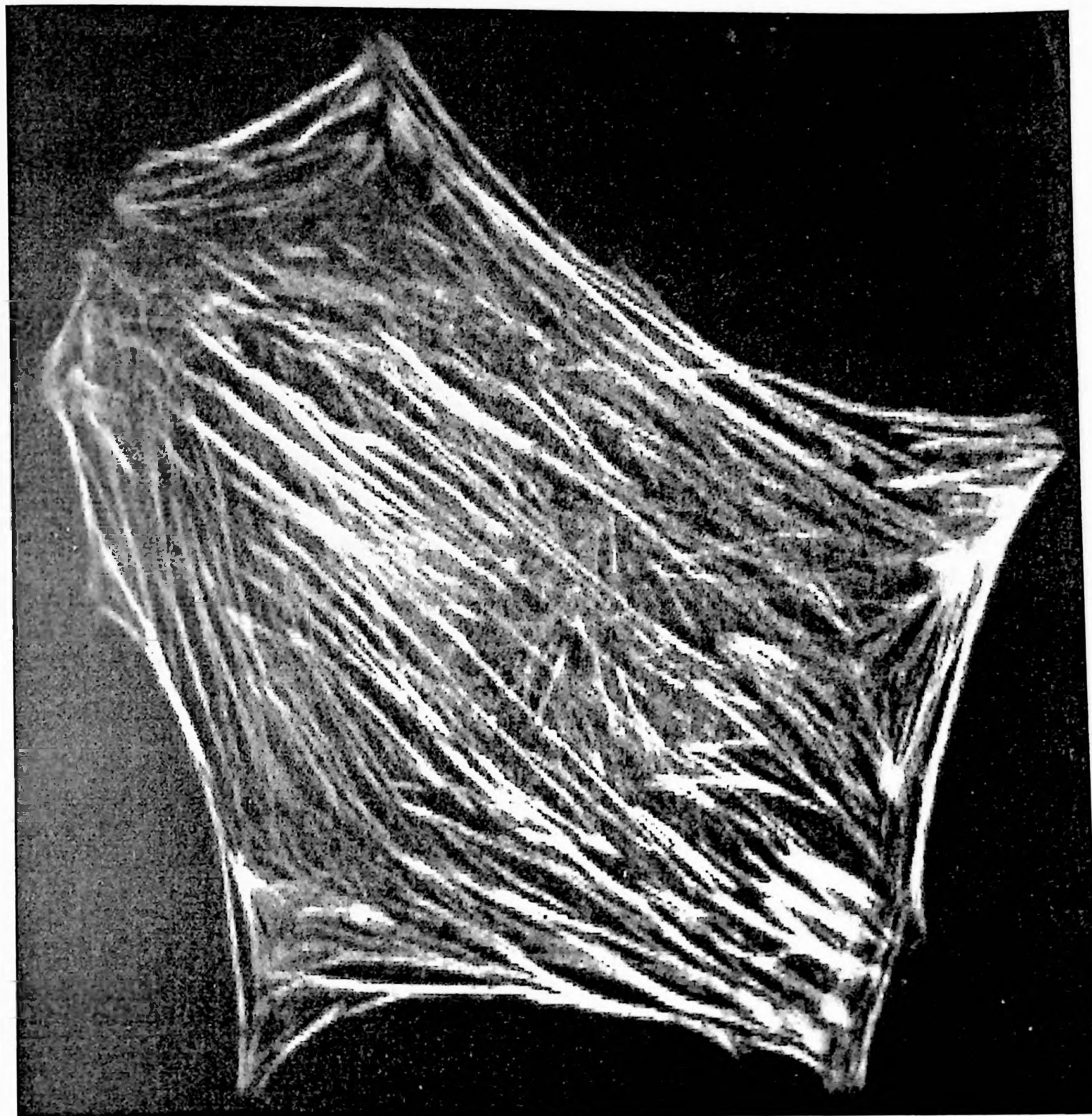


Figure 30. Confocal Microscopy Image of Vascular Smooth Muscle Cells Exposed to 5×10^{-6} M Forskolin for a Twenty-Six Hour Interval.

4. Western Blot Analysis for the Expression of Actin in VSM

The expression of actin in forskolin treated vascular smooth muscle cells was significantly greater than non-treated vascular smooth muscle cells. A visual difference within the typical actin bands determined via Western blot analysis was evident as demonstrated in figure 31. Subsequently, bands for both forskolin treated and untreated cells were measured on a densitometer. The average band volume for forskolin treated cells were 10868.05 arbitrary units, whereas untreated vascular smooth muscle cells yielded on average volume of 5078.21 arbitrary units. Although on average the expression of actin in the forskolin treated cells were more than double that of the untreated cells, the percent difference decreased as the passage of the cell increased. One possible explanation for the elevated actin expression in forskolin treated cells was an increased number of receptor sites made available for the binding of an actin antibody used in Western blot analysis. (Figure 32)



Actin

Figure 31. Western Blot for the Expression of Actin by Forskolin and Control Stimulated Vascular Smooth Cells.

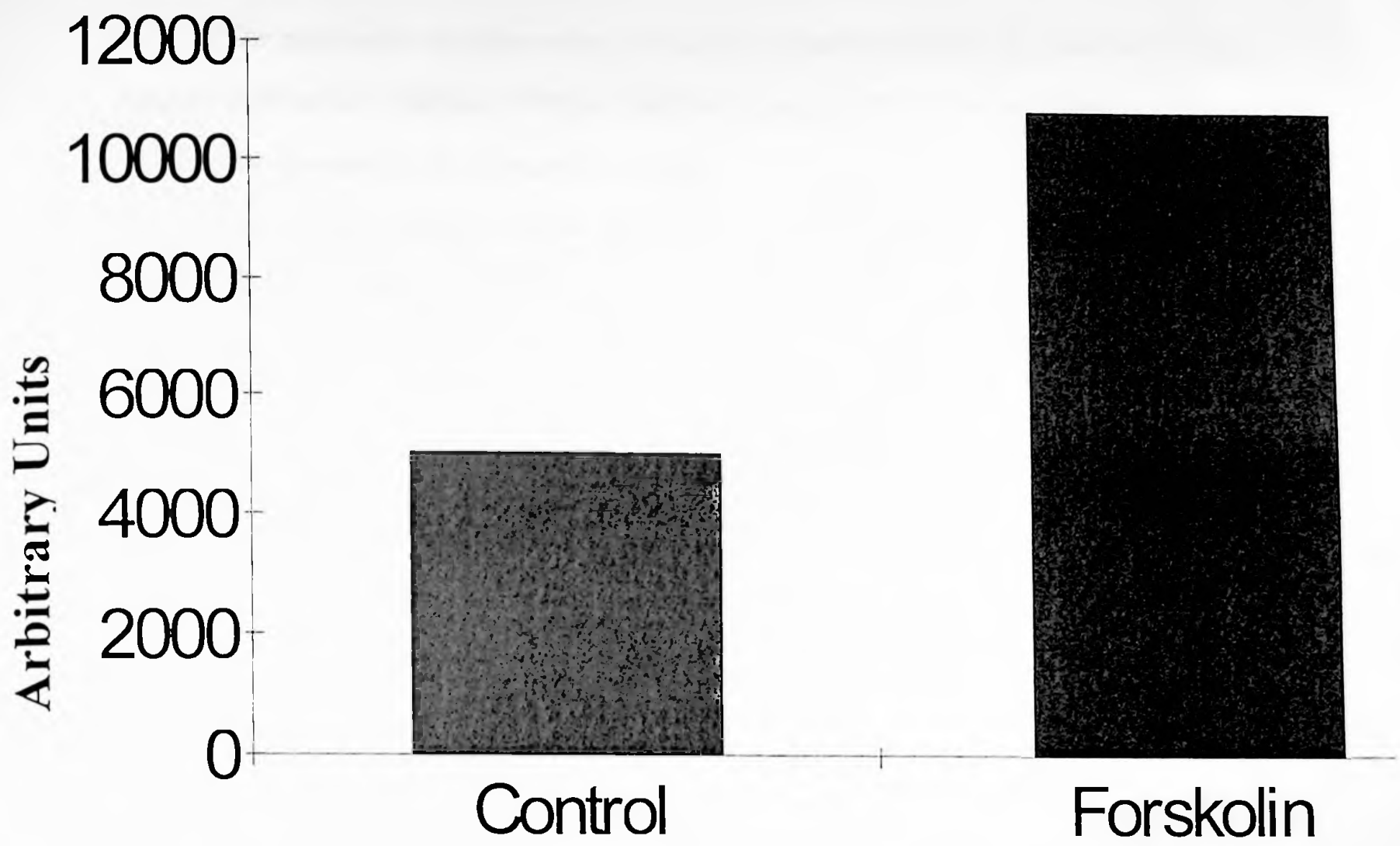


Figure 32. Expression of Actin by Control and Forskolin Stimulated Vascular Smooth Cells.

5. Western Blot Analysis of Immunoprecipitated Alpha-Actin in Stimulated VSM

The expression of alpha-actin in forskolin treated VSM were the same as the non-treated VSM cells. Phorbol (10^{-6} M in DMSO) stimulated VSM demonstrated a significant decrease in the expression of alpha-actin whereas the combination of forskolin and phorbol treated showed a slight elevation of alpha-actin expression. The average band volume for control, forskolin treated, the combination of forskolin and phorbol and phorbol treated were 3617.45, 3612.70, 3766.60 and 1975.95 arbitrary units respectively. (Figure 33 and 34)

h
26KD
80KD
52.5KD
21.9
27.9
21.5

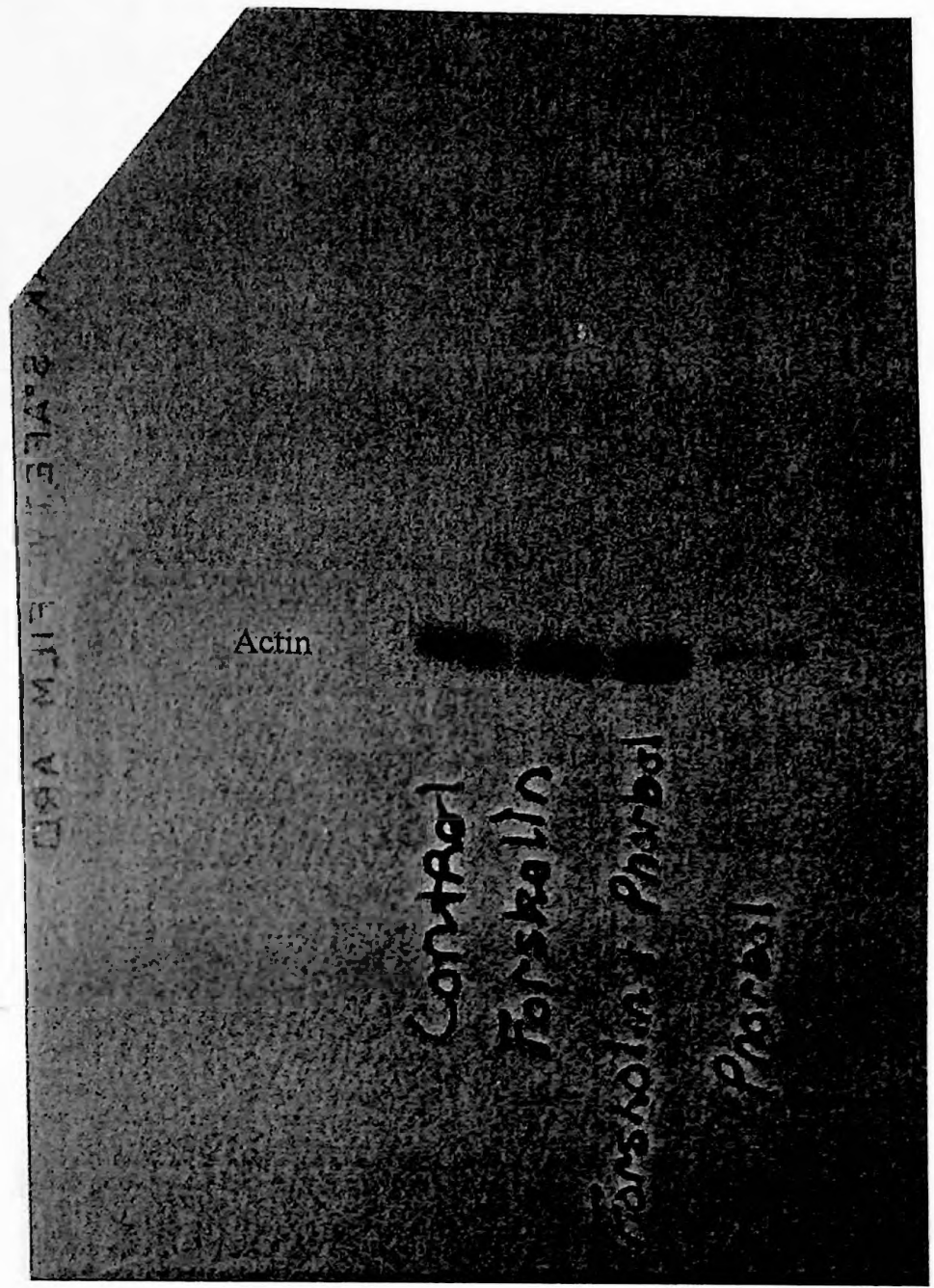


Figure 33. Western Blot of Immunoprecipitated Alpha-actin in Stimulated Vascular Smooth Muscle Cells.

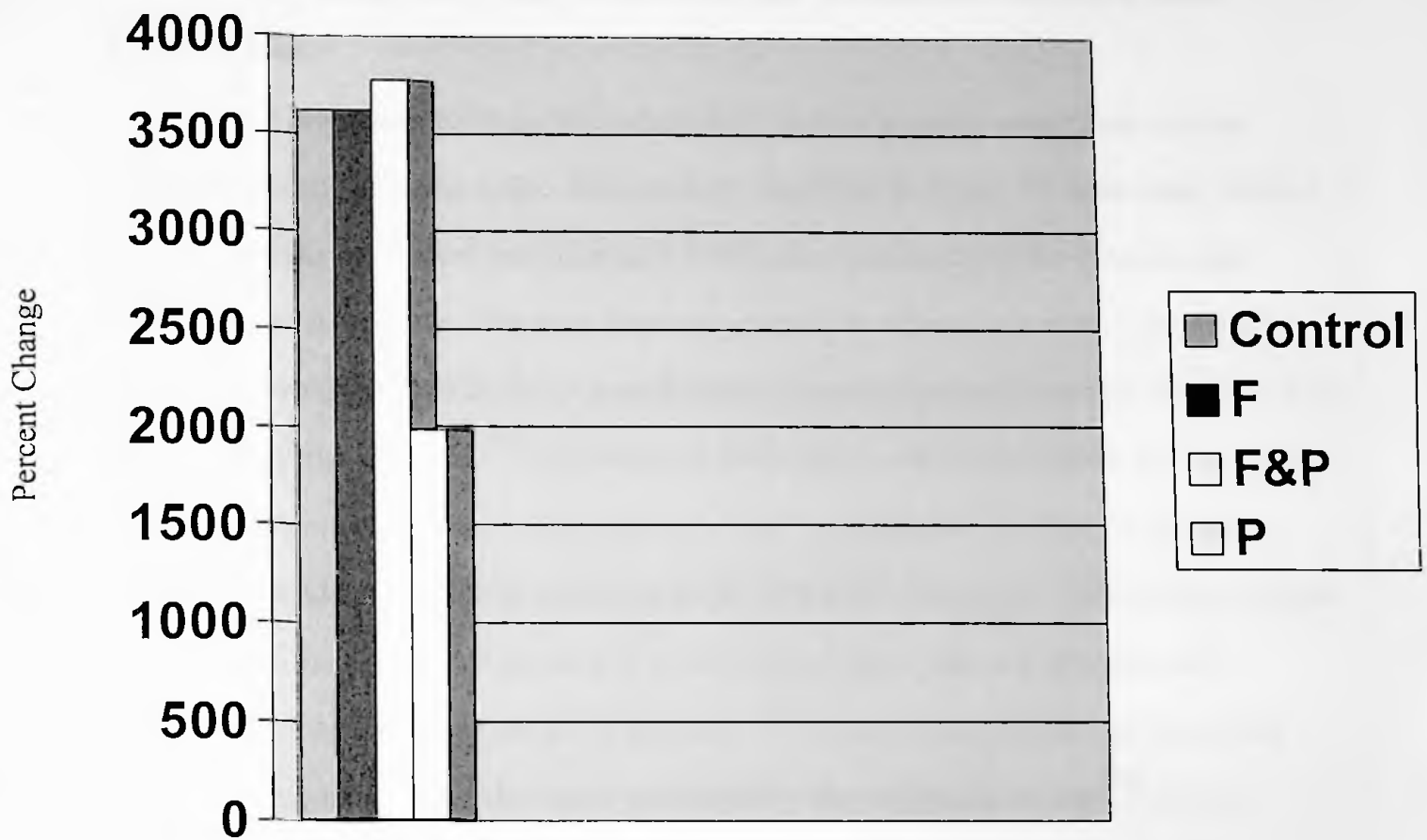


Figure 34. The Expression of Actin in Immunoprecipitated Alpha-actin in Stimulated Vascular Smooth Muscle Cells.

6. Analysis of ^{33}P Radiolabeled Immunoprecipitated Alpha-actin in Stimulated VSM in Comparison with the Coomassie Brilliant Blue Stained Gel

The Coomassie Brilliant Blue stain identified all proteins associated with the immunoprecipitate of alpha-actin. The bands as identified in figure 35, were clear, distinct and sharp. Both the treated and untreated VSM cells demonstrated the characteristic banding pattern for actin. The actin band migrated to an area with a molecular weight range of approximately 42KDa as determined by standard molecular weight markers. The radiograph of the identical ^{33}P radiolabeled alpha-actin immunoprecipitate gel identified only the proteins associated with alpha-actin that incorporated ^{33}P . (Figure 36) The number of bands presented as compared to the identical Coomassie Brilliant Blue stained gel was significantly less. The band of central focus, actin, was not present in the radiograph of the radiolabeled gel. Therefore, ^{33}P was not incorporated into the alpha-actin immunoprecipitate. The bands presented by the radiograph of the ^{33}P labeled immunoprecipitate fell within areas corresponding to the following approximate molecular weights 22KDa, 35KDa, 116KDa, 126KDa, 161KDa and two bands over 200KDa. The band volume was measured via densitometry. All bands with one notable exception, demonstrated the same relative intensity when compared to their respective bands undergoing various treatments (e.g. comparison of the fourth band in each of the various treatments). The exception was found in the third band from the top of the gel corresponding to an approximate molecular weight of 161KDa. The relative intensity of the third band undergoing stimulation with forskolin and phorbol was found to be significantly less than all other treatments (control, forskolin and phorbol).

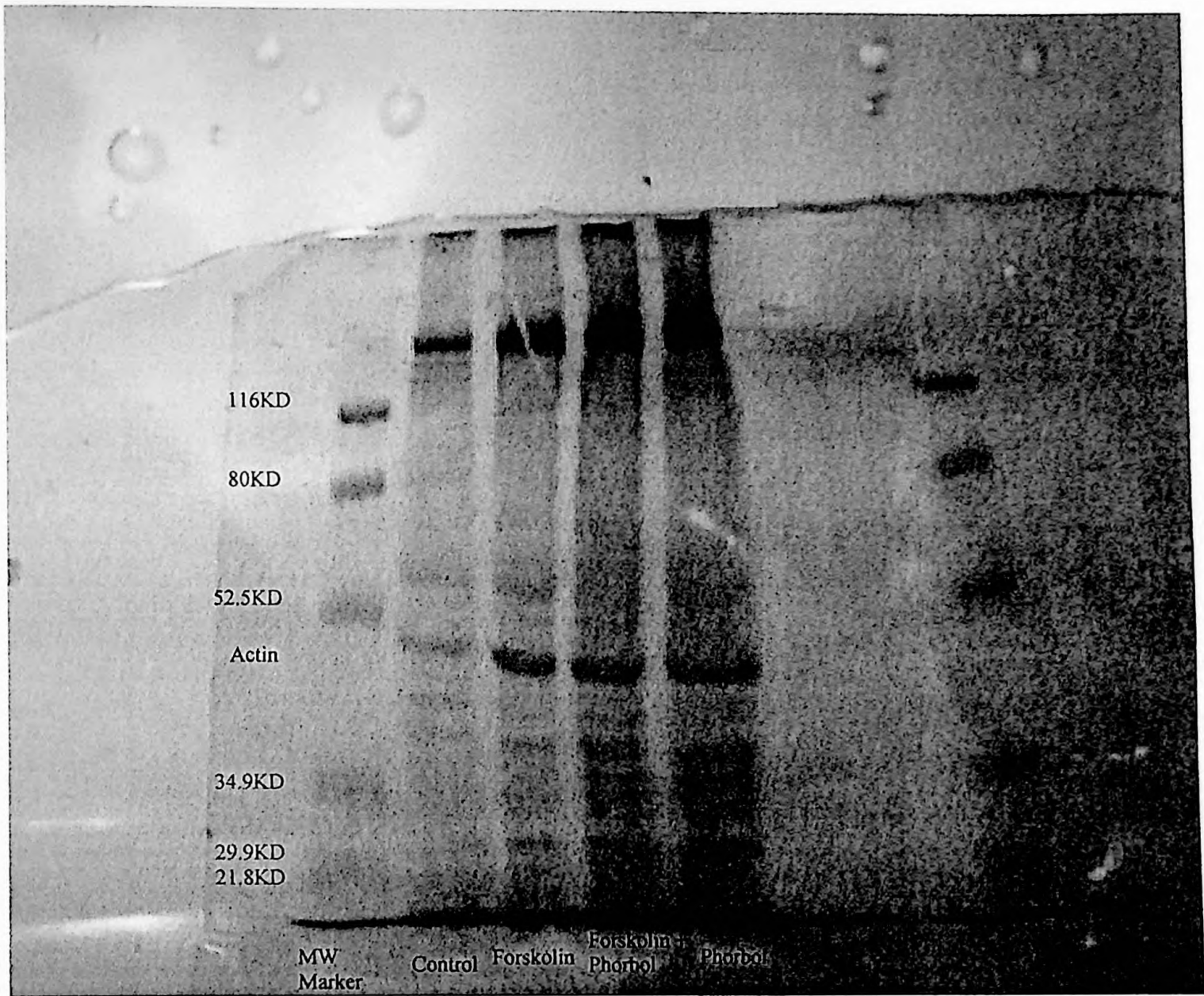


Figure 35. Coomassie Brilliant Blue Stained Immunoprecipitated Alpha-actin in Stimulated Vascular Smooth Muscle.

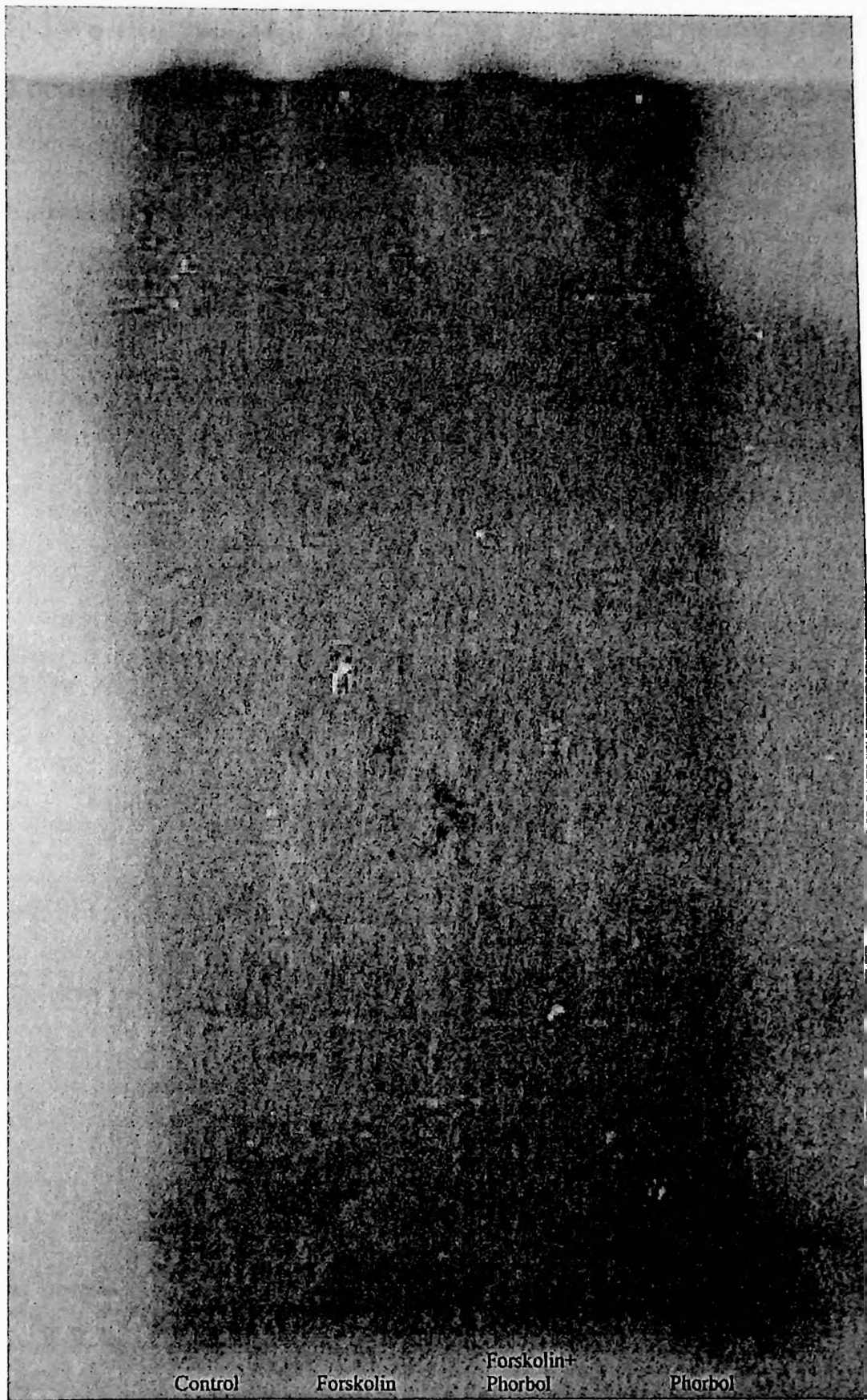


Figure 36. ^{33}P Radiolabeled Immunoprecipitated Alpha-actin in Stimulated VSM.

7. Two-dimensional Comparison of the Expression of Actin in Forskolin Treated VSM

Differences in the expression of actin in forskolin treated and untreated vascular smooth muscle cells were inconclusive.

8. Time Course Study

Time intervals of ten minutes, thirty minutes, one hour and three hours were selected to view the extent of arborization that occurred in cells exposed to forskolin at a concentration of 5×10^{-6} M. This study demonstrated that a gradual change in arborization had occurred. (Figure 37) At ten minutes approximately 88% of the cells were not affected by the presence of forskolin. The typical rat vascular smooth muscle cell resembled a control cell as demonstrated in figure 20. By thirty minutes, 26% of the cells were completely arborized and resembled cells in figure 24 in addition to an approximate 34% demonstrated partial arborization. (Figure 21) After an incubation period of one hour, approximately 71 percent of the cells were completely arborized. These cells were identical to cells presented in figure 23. Approximately 87% of the cells demonstrated complete arborization after three hours. The shape of these cells is exemplified in figure 23.

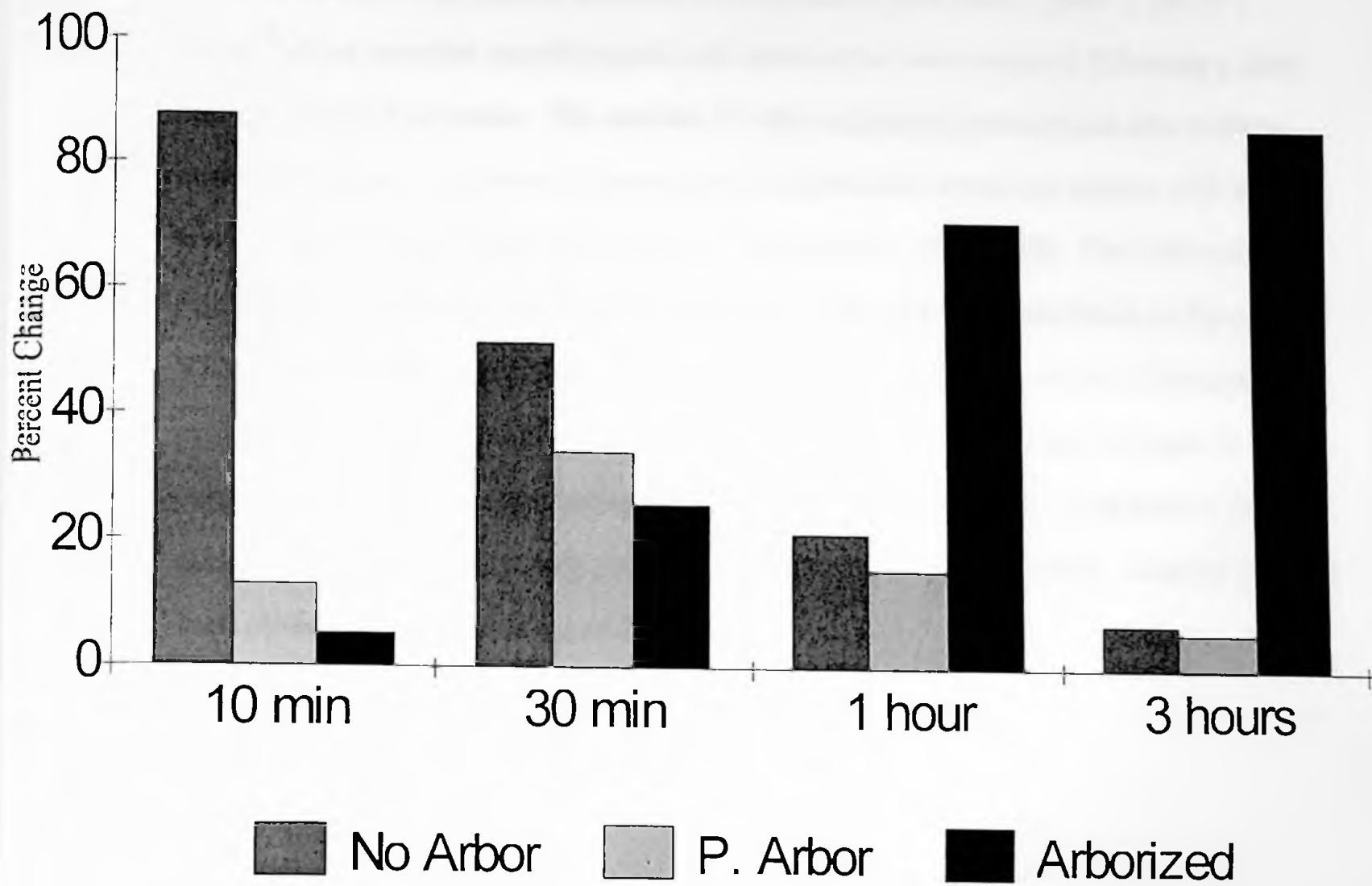


Figure 37. Forskolin Effects on Vascular Smooth Muscle Arborization. A Time Course Study.

9. Concentration Study

The effects of various forskolin concentrations (0 , 2.5×10^{-6} , 5×10^{-6} , 10×10^{-6} , 20×10^{-6} M) on vascular smooth muscle cell arborization were assessed following a thirty minute period of exposure. The number of cells undergoing arborization after a thirty minute exposure to forskolin increased in a concentration dependent manner with the greatest effect being observed with 20×10^{-6} M forskolin. (Figure 38) The VSM cells resembling control cells were considered to be unchanged as demonstrated in figure 20. VSM cells exhibiting partial arborization demonstrated partial retraction of cytoplasm as evident by obvious indentations of the cell membrane like those found in figure 21. Cells considered to be arborized demonstrated complete retraction of the cytoplasm to the perinuclear/nuclear region with extensions of pseudopod-like structures radiating outward such as those evidenced in figure 22.

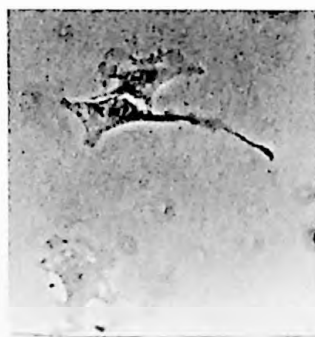
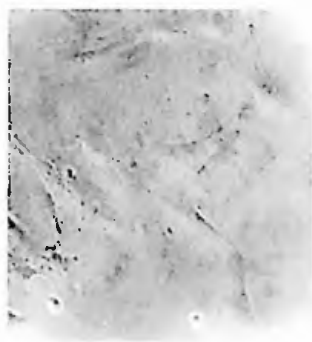
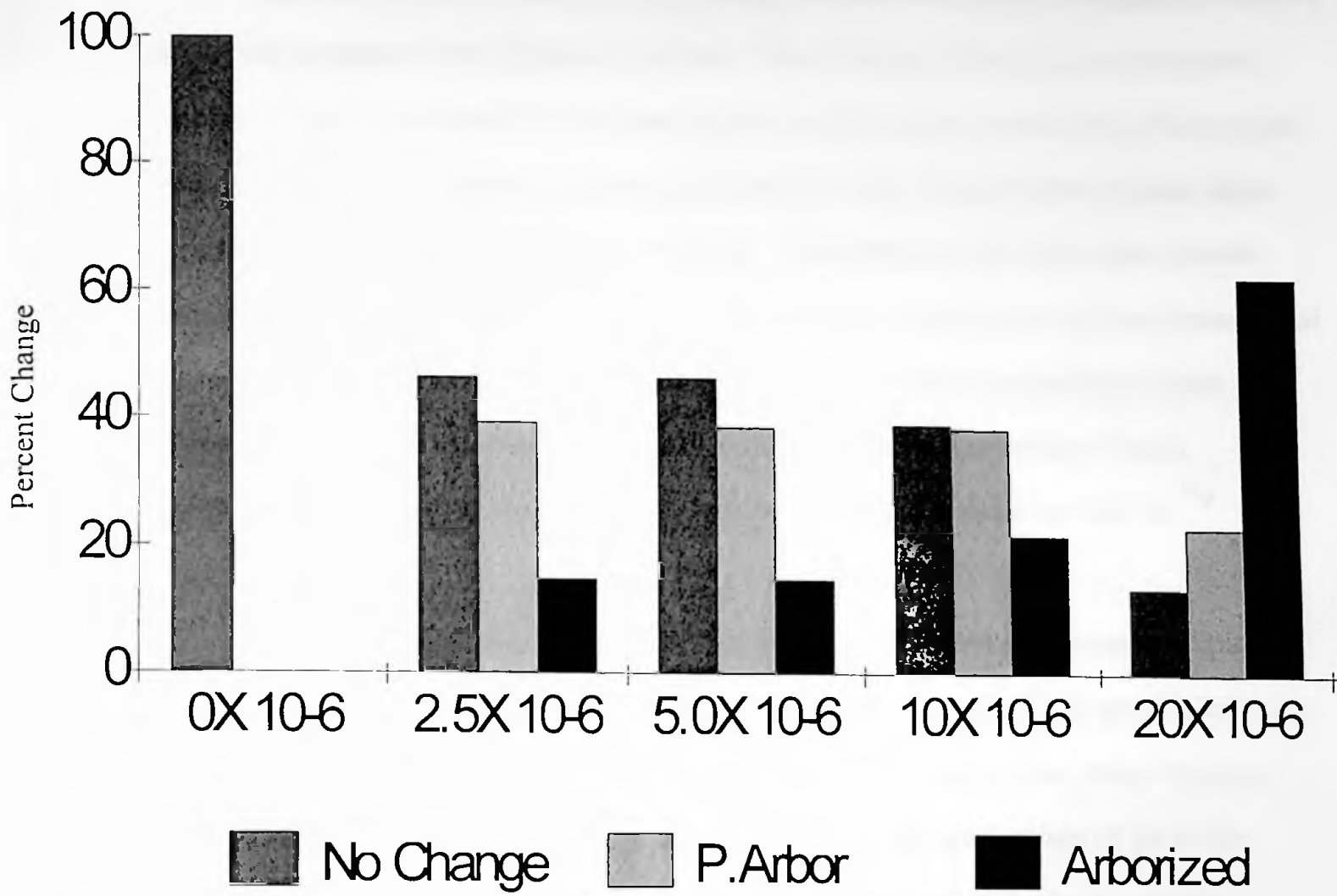


Figure 38. Forskolin Concentration Effects On Arborization Following a Thirty Minute Incubation.

E. Conclusion

Vascular smooth muscle cells following exposure to forskolin, assumed a rounded shape with extensive protoplasmic processes. The filaments of the actin cytoskeleton depolymerized as indicated by the concentration of actin stain around the nuclear region. With time the actin filaments repolymerized and the cells resumed their original shape despite their continuous exposure to forskolin. Differences in the expression of actin were evident in the forskolin treated and untreated cells through one and two dimensional electrophoresis as well as through Western blotting. The actin immunoprecipitate of forskolin treated and untreated cells demonstrated the same expression of actin. Forskolin did not induce the phosphorylation of actin as evidenced by lack of ^{33}P incorporation.

Future investigations will identify all proteins, which were immunoprecipitated along with the alpha-actin in stimulated vascular smooth muscle. Radiographic analysis of ^{33}P incorporation will identify those proteins associated with actin, which became phosphorylated. Acquiring this information along with the mechanism of forskolin stimulation will allow a greater understanding into the effect of forskolin on actin polymerization in cultured vascular smooth muscle.

F. Appendix

1. Mass Spectrometry Background

Mass spectrometry is becoming the analytical instrument of choice for the examination of biological samples. In the past, mass spectrometry was mainly used to establish the structure of a new chemical compound or to confirm the identity of an unknown. Today, the applications of mass spectrometry are numerous. The mass spectrometer reveals structural information concerning polypeptides, amino acid sequences, protein modifications and molecular weight. The mass spectrometer is capable of detecting very minute quantities of material with an approximate range of 10^{-12} mole to 10^{-15} mole for a compound with a mass of 1000 Daltons.

Basically mass spectrometers consist of an ion source, an analyzer for mass selection, an ion detector and a vacuum system. Within mass spectrometers, molecules undergo an ionization process to convert the sample into a gaseous ionic form. The ions are then sorted based upon their mass-to-charge ratios via a mass analyzer. Detectors are then employed to collect the ion flux and transform it into an equivalent electrical current. A computer data system converts the magnitude of the electrical signals as a function of the mass-to-charge ratios into the mass spectrum. A mass spectrum is a graph of ion intensity as a function of the mass-to-charge ratio.

The protein samples were first analyzed on a Finnigan LCQ Mass Spectrometer equipped with an electrospray ionization source and a quadrupole ion trap mass analyzer (figure 39) both by direct infusion and columns. Typically protein samples first undergo some sort of enzyme digestion to decompose the protein into its peptide building blocks. Peptides are considered to have 50 or less amino acids.

The sample is first introduced into the mass spectrometer through the electrospray ionization source. Electrospray is defined as the dispersing of liquid into electrically

charged droplets. The electrospray ionization source is capable of generating a charged aerosol for ion formation. Electrospray ionization of large biomolecules yields a spectrum of multi-charged ions with moderate mass-to-charge ratios. This method is commonly used in the analysis of many biological and pharmaceutical samples since it is easily compatible with common liquid separation techniques.

Information concerning the peptide and protein structure becomes evident through observed charge states. The amount of charges a protein may have is based upon the number of acidic and basic residues it contains as well as its size. The amount of protonated basic sites within a solubilized protein can be determined by the state of protonation observed with the mass spectrometer. The masses of individual molecules may be determined through ion conversion (electrical charging of the ion) by the mass spectrometer. This is performed indirectly through the mass-to-charge ratio of the ions created from the molecules. The charge on an ion is designated by the integer number Z of fundamental units of charge, and the mass-to-charge ratio m/z which represents Daltons per fundamental unit of charge. Most often, the ions created via mass spectrometry contain just one charge, $Z = 1$, thus leaving the m/z value numerically equal to the molecular (ionic) mass in Daltons.

The set of ions are analyzed in such a way that a signal is obtained for each value of mass to charge (m/z) that is represented. The intensity of each signal reflects the relative abundance of the ion producing the signal. The largest peak is called the base peak; its intensity is taken as 100, and the intensities of the other peaks are expressed relative to it. If one electron is extracted from the parent molecule then M^+ is produced, whose m/z value is the molecular weight of the compound. If the M^+ peak is the base peak then it should be easily recognizable. Often it does not represent the base peak, but once identified the molecular weight can be determined accurately. The resolution of the mass spectrometer describes the ability to separate ions of similar mass as described by

$R = M/\Delta M$. M is the ion mass. Delta mass is based upon the two resolvable peaks in a mass spectrum.

The ions are directed through the electrospray orifice into the mass analyzer by using the combination of gas flow and electric field. Ion optics can also be employed via lenses and/or an rf (radio frequency) only quadrupole (octapole). The upper limit of the vacuum in the mass spectrometer allowed is determined by the pressure tolerated by the mass analyzer. The amount of ions, which may flow through the sampling orifice, is based upon the mass spectrometer vacuum upper limit, speed of the vacuum pump and the size of the sampling orifice. A quadrupole mass analyzer has a flow rate of 100,000 L/sec.

The analyzer on the LCQ is a quadrupole ion trap, which sorts the ions by their mass-to-charge ratios. The quadrupole ion trap mass spectrometer stores ions for subsequent analysis. This device traps ions within a selected range of mass-to-charge ratios determined by the applied voltages in the space bound by the electrodes and increasing rf voltage is applied over time to sequentially eject ions of increasing mass to charge ratios through an end cap opening for detection in order to produce a mass spectrum.

Amino acid sequence information can be determined through a collision activated dissociation (CAD) mass spectrum. The spectrum is generated by first selecting the peptide of interest from the other polypeptides or contaminants in the solution via rf voltage. The selected peptides of interest are excited by an rF voltage and undergo collisions with helium, which is present in the trap. The use of helium provides a collisional dampening effect of ions through the low molecular weight of helium atoms. During the collision process, translational energy becomes converted into vibrational energy building up to a level in which the peptide of interest fragments at the weakest bond. This fragmentation results in a spectrum, which may be analyzed to determine the

amino acid sequence.

The Matrix Assisted Laser Desorption Ionization Time of Flight Mass Spectrometer (MALDI-TOF) provides accurate mass determinations and primary sequence information in addition to enhancing the ease and sensitivity in which large biomolecules may be analyzed. The time of flight mass spectrometer has an elevated upper mass limit of over 300,000 Daltons allowing for the analysis of large biomolecules. The time of flight mass spectrometer uses the differences in flight time through a drift region to separate ions of different masses. The foundation of the time of flight mass spectrometer is exemplified when a spatially and temporally well defined group of ions, differing in m/z ratios, becomes subjected to identical electric fields and allowed to drift in a region of constant electric field. The time required to transverse the region is depends upon the m/z ratios.

The solid sample placed in the ionization chamber is ablated via a pulsed laser to produce ions. The ions, upon extraction, enter a drift tube. The reflection, located at the end of the drift tube, is comprised of a series of grids or rings, which serve as an ion mirror. The reflectron compensates for the differences in flight times of the same m/z ions of slightly different kinetic energies via an ion reflector. This enables the ion packets to be focused in time and space at the detector and allows the resolution of the mass spectrometer to be improved. (Figure 40)

The information derived from the mass spectrum may then be entered into a protein data base search such as protein prospector (<http://www.protein-prospector.ucla.edu>). These data bases allow known information concerning a protein of interest to be entered into the search such as the molecular weight, mass spectrum peaks and the isoelectric focusing points. Peptide mass searching is a means of identifying proteins whose sequence is already located within the given database. These systems employ algorithms to match the known set of peptide masses to the protein of interest

provided the same cleavage reagents were employed. A score or ranking is then calculated to provide a measure of likeness between the known and experimental peptide masses. Most often more than one database is employed for conformation purposes.



Figure 10: The diagram illustrates the process of peptide mass fingerprinting. It shows the relationship between experimental peptide masses and a database of known peptide masses. The process involves comparing the experimental masses to the database masses to identify potential matches. The diagram is very faint and difficult to read.

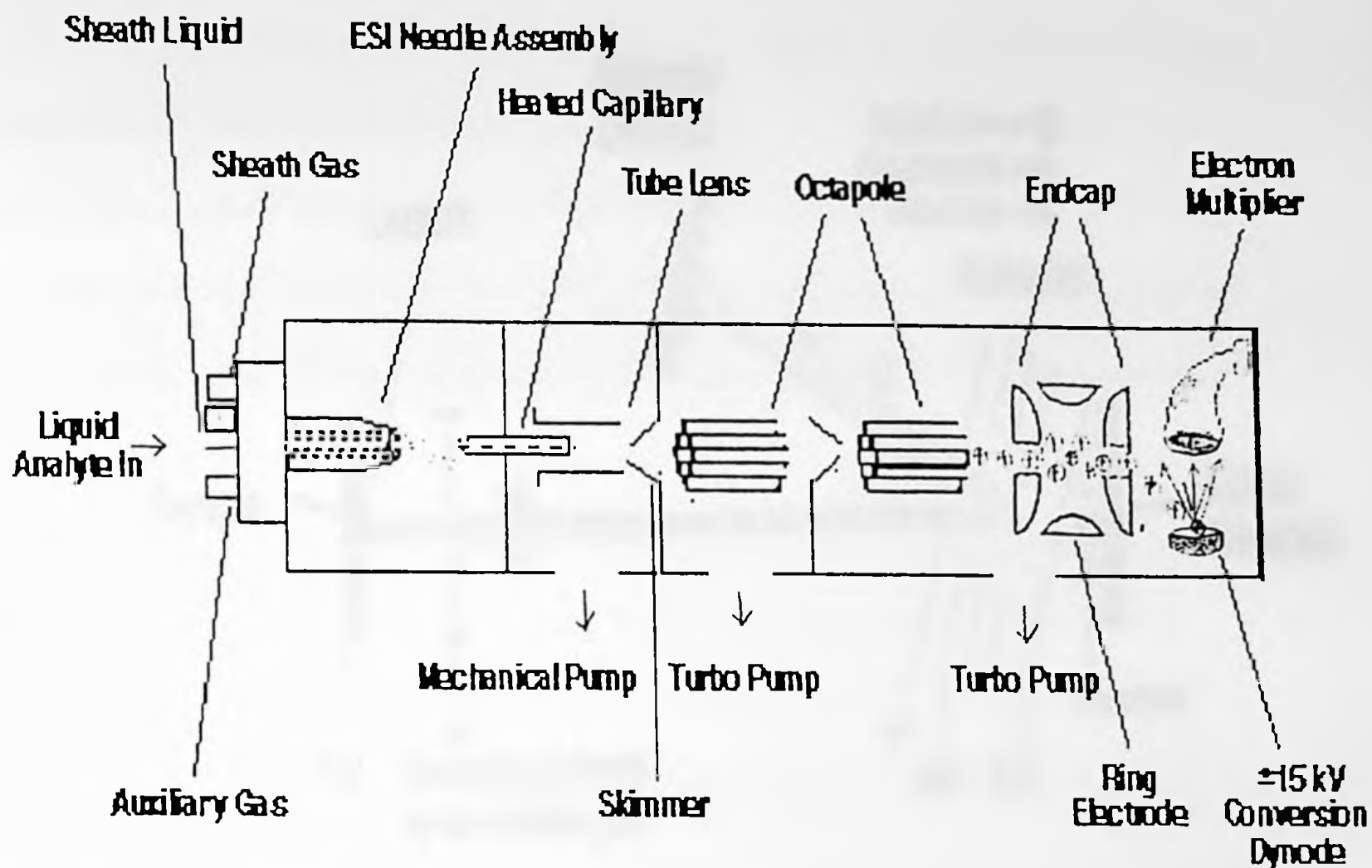


Figure 39. The Finnigan LCQ Mass Spectrometer. The sample is introduced through the electrospray ionization source, which is capable of generating a charged aerosol for ion formation. The ions are then directed into the mass analyzer by using the combination of gas flow and electric field. The analyzer on the LCQ is a quadrupole ion trap, which sorts the ions by their mass-to-charge ratios.

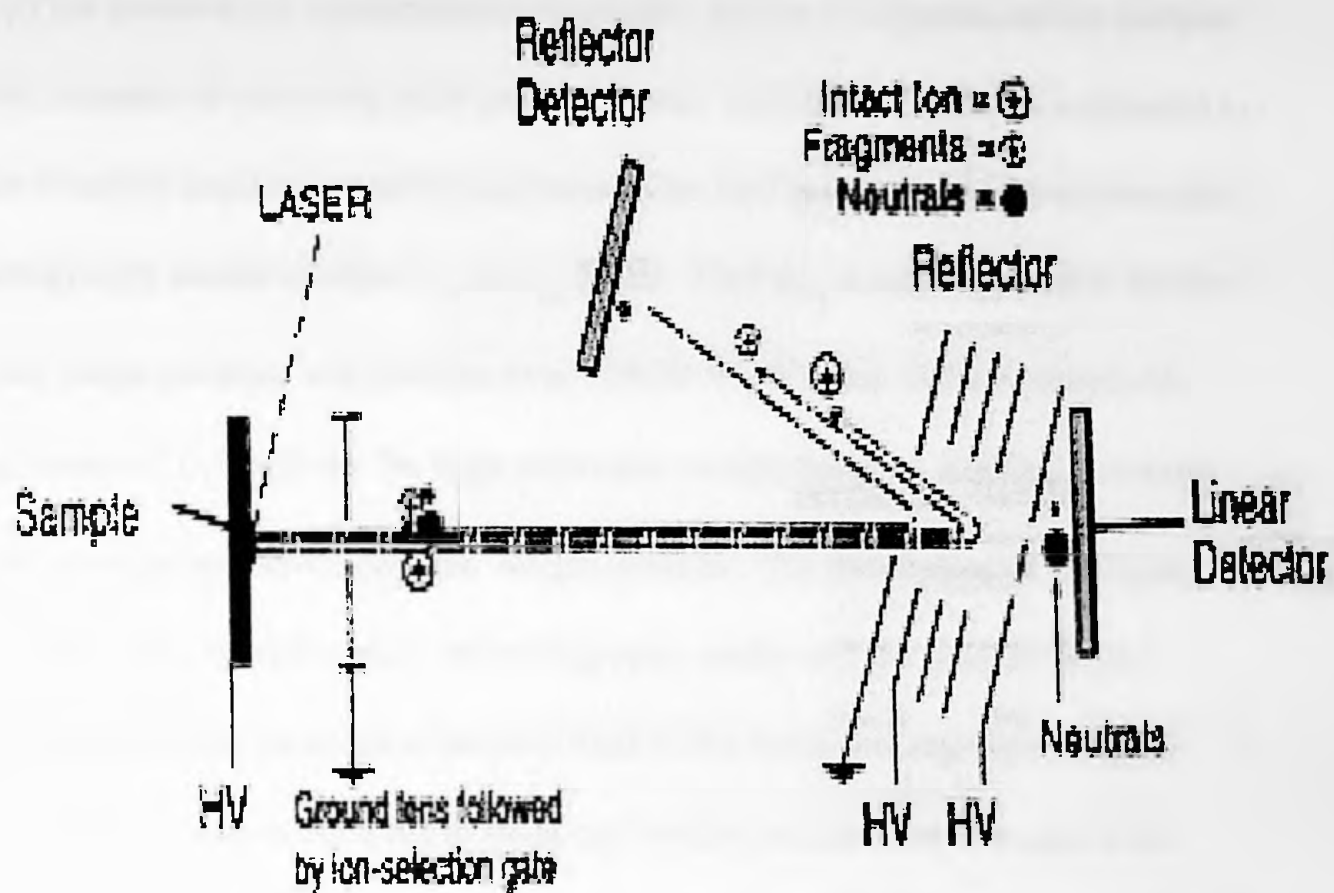


Figure 40. The Matrix Assisted Laser Desorption Ionization Time of Flight Mass Spectrometer (MALDI-TOF MS). The solid sample placed in the ionization chamber is ablated via a pulsed laser to produce ions. The ions, upon extraction, enter a drift tube. The reflection, located at the end of the drift tube, is comprised of a series of grids or rings, which serve as an ion mirror. The reflectron compensates for the differences in flight times of the same m/z ions of slightly different kinetic energies via an ion reflector. This enables the ion packets to be focused in time and space at the detector and allows the resolution of the mass spectrometer to be improved.

2. Millipore ZipTip

ZipTips enhance the concentration of peptide, protein or oligonucleotide samples and provide a means of removing salts and detergents. ZipTips may also be employed to fractionate complex peptide or protein mixtures. The ZipTip contains an absorptive bed of chromatography media of either C₄ or C₁₈ beads. ZipTip_{C₄} is most applicable for low intermediate range proteins and proteins over 100,00 NMWL due to the hydrophobic absorbing nature of C₄ beads for the high molecular weight proteins. ZipTip_{C₁₈} is most suitable for peptides and low molecular weight proteins. The foundation of Millipore ZipTips resides upon reverse phase chromatography media and the peptide-buffer solution. Essentially, the peptides of interest bind to the beads and the supernatant containing the unwanted contaminants (salts and buffer) are removed through wash solutions. This is followed by the elution of the desired peptide onto the MALDI sample plate for subsequent analysis.

3. Mass Spectrometry Sample Preparation

Following subsequent visualization and extraction of the protein of interest via immunoblot techniques, salts and detergents (SDS, glycine, and tris) were removed via water. The bands were incubated in a stripping buffer (7.813g B-mercaptoethanol, 9.85g Tris-HCL, 2g SDS diluted to 1L of distilled, de-ionized water at a pH of 6.7) for thirty minutes at 37C to remove any remaining antibody used for protein identification. After removing and rinsing off the strip buffer, the bands were blocked in a polyvinylpyrrolidone (PVP-40) solution (0.5% PVP-40 solution in 0.6% acetic acid) for

thirty minutes at 37C to saturate any free sites upon the membrane surface. The PVP-40 solution was removed from the membrane bands via copious amounts of water. The bands were then rinsed with digestion buffer (100mM ammonium acetate, pH 8) and submerged in digestion buffer containing 0.1 to 0.5ug Promega trypsin overnight at 37C. The protein digestion process was terminated the following day with acetic acid to yield a final concentration of 1%. The digestion solution was then extracted and concentrated for use in the mass spectrometer.

4. Trypsin In-Gel Digestion of Proteins

The SDS-PAGE gels were stained for forty-five minutes in a solution containing 0.1% Coomassie Brilliant Blue, forty-five percent methanol and nine percent acetic acid in Milli-Q grade water. The protein bands of interest were excised, placed in individual one and a half milliliter Eppendorf tubes and dehydrated in acetonitrile for ten minutes following destaining in five percent methanol and seven and a half percent acetic acid in Milli-Q grade water for one and a half hours. The acetonitrile was removed and the gel pieces were placed in a Savant SC110 SpeedVac until dry. The gel pieces were covered with 10mM dithiothreitol (DTT) in 100mM NH_4HCO_3 (pH 8.0) for one hour at 56C for protein reduction. Following removal of DTT, an equal amount of 55mM iodoacetamide in 100mM NH_4HCO_3 was added for an additional forty-five minutes at room temperature. The gel pieces were then washed several times with 100mM NH_4HCO_3 for ten minutes. The gel pieces were once again dehydrated with acetonitrile, rehydrated with 100mM NH_4HCO_3 , followed by an additional acetonitrile dehydration step. The gel pieces were then placed in the speedvac. The aqueous solution was extracted from the gel pieces and discarded. The gel pieces were rehydrated in a buffer containing 50mM NH_4HCO_3 and sequencing grade modified trypsin (1ug/ul) from Promega for three hours

at 37C. Following centrifugation at 9000 RPM/g for five minutes, the supernatant was collected. An additional change of 20mM NH_4HCO_3 was added to the gel pieces and collected following centrifugation at 9000 RPM/g for five minutes. In addition, three changes of five percent formic acid in fifty percent acetonitrile with incubation periods of twenty minutes at 37C were also applied to the sample. The sample was then concentrated via speedvac until a final volume of approximately thirty to fifty microliters was obtained.

5. Reversed-Phase ZipTip Sample Preparation

The ZipTip obtained from Millipore was equilibrated for sample binding by the aspiration of a wetting solution (50% acetonitrile in Milli-Q grade water) into the tip. The wetting solution was discarded and the aspiration repeated. The ZipTip was washed twice with an equilibration solution (0.1% trifluoroacetic acid in Milli-Q grade water). The peptides created by the trypsin in-gel digestion of proteins were bound to the ZipTip by seven to ten cycles of aspiration\dispersion of the sample. A wash solution consisting of 0.1% trifluoroacetic acid in Milli-Q grade water was twice used to wash the ZipTip. The wash solution was discarded. The ZipTip bound peptides were eluted directly onto the MALDI-TOF mass spectrometer sample plate via elution solution (50% acetonitrile in 0.1% trifluoroacetic acid). Alpha-Cyano-4-hydroxycinnamic acid obtained from Sigma was applied upon the peptide sample.

6. MALDI-TOF Mass Spectrum Analysis

Bruker Biflex III MALDI-TOF Mass Spectrometer (Bruker-Franzen Analytik GmbH, Bremen, Germany) was used to obtain all MALDI mass spectra. Ionization was accomplished via a nitrogen laser (337 nanometer beam, 3 nanosecond pulse width, 3 Hz) set at attenuation between fifty and seventy-five. A total acceleration voltage of 26.3 KV

and a reflecting voltage of 30KV was used in the operation of the mass spectrometer in the reflection mode. A peptide standard mixture using the known mass of synthetic peptides externally calibrated the Bruker Biflex III. The following peptides, bradykinin, angiotension I (human), fibrinogen related peptide and renin substrate (human), obtained from Advanced ChemTech were used to create a peptide standard mixture at a concentration of picomole per microliter. The peptide mixture was placed directly onto the MALDI-TOF mass spectrum sample plate. Alpha-Cyano-4-hydroxycinnamic acid was placed upon the peptide standard. The Bruker Biflex III MALDI-TOF mass spectrometer was calibrated in the digest reference mode using the following peaks 1060.57 for bradykinin, 1296.5 for angiotension I (human) and 1645.92 for renin substrate (human).

7. Actin Standard

Rabbit Muscle Actin obtained from ICN Biomedicals was dissolved in SDS-PAGE sample buffer. The rabbit muscle actin was run on a twelve and a half percent SDS-PAGE gel obtained from Biorad for one hour at one hundred volts. The trypsin in-gel digestion of proteins as well as reverse-phase ZipTip sample preparation protocols as previously described were followed for MALDI-TOF mass spectrum analysis.

8. Mass Spectrum Identification

The following peaks 711.34, 1161.0, 1164.74, 1401.51, 1580.67, 1949.92, 1958.0, 2179.25, 2253.99 and 3064.0 identified on the mass spectrometer corresponded to the alpha-actin vascular smooth muscle peaks as determined by MS-Digest results (<http://prospector.ucsf.edu>).

9. Troubleshooting

The most critical aspect to good MALDI-TOF mass spectrums is considered to be the sample preparation itself. The quality of a uniform matrix assisted laser desorption ionization sample is dependent upon many variables such as the preparation of the analyte sample itself (e.g. exposure to strong ionic detergents, removal of salts), the dilution of the sample, the choice of matrix solution, the compatibility of matrix and analyte solutions and the presence of contaminants etc.

Many protocols available for protein/peptide harvesting require the use of buffers containing high concentrations of salts, chaotropes (e.g. urea and guanidinium) and detergents needed for proteolytic digestion, which hamper spectra acquisition. The salts present in the sample solution will form adduct peaks which compete with the molecular protein/ peptide ion peaks and cause an overall broadening of signal. This results in reduced mass accuracy and signal intensity. The presence of various buffer components such as urea and tris may prevent or reduce the optimal level of crystallization of the MALDI-matrix. When urea is of high concentration, its prominence overshadows any matrix crystals, which may have formed yielding very small, or no peptide signals. The presence of such concentrated buffers inhibit the incorporation of peptides into the growing matrix crystal. In addition, the greater the basicity of the buffer, the greater the ionization interference will be.

Sample dilution is another frequently encountered problem after harvesting and subsequent processing of the proteins of interest. Depending on the protocols used to obtain the final solution containing the protein of interest, various manipulations may be performed to enhance the amount of protein harvested or allow reduction in the amount of buffer required. For instance, the harvesting of hydrophobic proteins can be improved

by employing greater concentrations of urea or guanidine. These contaminants can subsequently be removed by Millipore-ZipTips. The addition of extra washing steps may greatly facilitate the removal of these unwanted buffers.

The removal of contaminants can be performed using reverse-phase chromatography resin such as C₄ or C₁₈ beads located within Millipore ZipTips. This process allows the peptide of interest to remain bound to the resin while contaminants and unwanted buffers are washed away. In addition, this procedure allows the peptides to be concentrated and separated by their physical properties, thus improving the level of sensitivity.

Errors within the proteolytic digestion process provide an additional complication for peptide mass searching. Proteolytic enzymes, which fail to completely cleave its substrate to completion or cleaves at sites other than their intended location (e.g. trypsin cleaves at sites C-terminal to lysine or arginine (if not preceded by proline)), will result in peptide masses that do not match those provide by data bases. Some data bases will take this scenario into account by providing an additional parameter for the number of missed cleavage sites, but this will increase the number of potential protein possibilities. In addition, some proteolytic enzymes may autodigest creating, for example, trypsin derived peptides. These proteolytic derived peptides may suppress the ionization of the peptide of interest or produce a spectrum, which overlaps that which was created by the experimental protein.

The next most common source of error is analysis of the information derived from the mass spectrum. The most important aspect in achieving a successful peptide-mass search is obtaining the highest mass accuracy possible. In order to assure the correct representative mass of the peptides within the sample mixture, an internal calibration should be performed. Most of the commercially available instruments today are capable of accuracy ranges within five parts per million. Peptide masses achieved within this

range allow the assignment of monoisotopic masses for use in peptide mass searches. (A monoisotopic mass is the mass of the most abundant isotope of a particular peptide.) This capability greatly decreases the number of unlikely potential proteins. Therefore, one can easily see that an error within the instrument calibration itself could have erroneous effects on the potential protein match outcomes.

If the highest ranking results obtained from the peptide-mass search do not match with the experimental peptide masses, the following reasons may account for the difference: the correct protein was identified but additional peptides were generated by nonspecific proteolytic cleavage, posttranslational modification occurred or other unwanted proteins were in the sample mixture. Other possibilities include a sequence homologue from the same or different species was identified or the sample protein of interest was a novel protein not yet identified in the data bases.

G. Works Cited

- Adelstein, R. S., M. A. Conti, D. R. Hathaway, and C. B. Klee. 1978. Phosphorylation of smooth muscle myosin light chain kinase by the catalytic subunit of adenosine 3'-5'-monophosphate-dependent protein kinase. *J. Biol. Chem.* 253: 8347-8350.
- Benzonana, G., O. Skalli and G. Gabbiani. 1988. Correlation Between the Distribution of Smooth Muscle or Non-muscle Myosin and Alpha-smooth Muscle Actin in Normal and Pathological Soft Tissue. *Cell Motility Cytoskeleton II*, 260-274.
- Birukov, K. G., M. G. Rogers, V. P. Shrinsky, V. E. Koleliansky, J. H. Campbell and G. R. Campbell. 1993. Synthesis and Expressions of Smooth Muscle Phenotype Markers in Primary Culture of Rabbit Aortic Smooth Muscle Cells: Influence of Seeding Density and Media and Relation to Cell Contractility. *Exp. Cell. Res.* 204, 46-53.
- Brelje, T.C., M.W. Wessendorf, R.L. Sorenson. 1993. Multicolor Laser Scanning Confocal Immunofluorescence Microscopy: Practical Application and Limitations. *Methods in Cell Biology*, Vol. 38.
- Chaldokov, G. N., T. Nabika, T. Nara and Y. Yamori. 1989. Cyclic AMP and cytochalasin B-induced arborization in cultured aortic smooth muscle cells: its cytopharmacological characterization. *Cell Tissue Res.* 432-442.
- Chamley, J. H., G. R. Campbell, J. D. McConnell and U. Groschel-Stewart. 1977. Comparison of Vascular Smooth Muscle Cells From Adult Human, Monkey and Rabbit in Primary Culture and in Subculture. *Cell Tissue Res.* 177, 503-522.
- Daly, John W. (1984) Forskolin, Adenylate Cyclase, and Cell physiology: An Overview. *Advances in Nucleotide and Protein Phosphorylation Research Vol 17.* 81-89.
- de Souza, Noel J., Alihoussein N. Dohadwalla and Jurgen Reden. 1983. Forskolin: A Labdane Diterpenoid with Antihypertensive, Positive Inotropic, Platelet Aggregation Inhibitory, and Adenylate Cyclase Activating Properties. *Medicinal Research Reviews.* 3(2); 201-219.
- Devlin, Thomas M. (editor). 1997. *Textbook of Biochemistry with Clinical Correlations.* 4th. Ed. Wiley-Liss. Inc.
- Electrospray Ionization Mass Spectrometry, Fundamentals Instrumentation and Applications.* Editor Richard B. Cole. Ch. 1 On the Mechanism of Electrospray Mass Spectrometry. Paul Kebarle and Yeughaw Ho. John Wiley and Sons, Inc. 1997. New York.
- Electrospray Ionization Mass Spectrometry, Fundamentals Instrumentation and Applications.* Editor Richard B. Cole. Ch.3 ESI Source Design and Dynamic Range Considerations. Andries P. Bruins. John Wiley and Sons, Inc. 1997. New York.
- Electrospray Ionization Mass Spectrometry, Fundamentals Instrumentation and Applications.* Editor Richard B. Cole. Ch. 4 Solution, Gas-phase and Instrumental Parameters Influences on Charge-state Distributions in Electrospray Ionization Mass Spectrometry. Guangdi Wang and Richard B. Cole.

- John Wiley and Sons, Inc. 1997. New York.
- Electrospray Ionization Mass Spectrometry, Fundamentals Instrumentation and Applications. Editor Richard B. Cole. Ch.6 Electrospray Ionization Time-of-Flight Mass Spectrometry. Igor V. Chernushevich, Werner Ens, and Kenneth G. Standing. John Wiley and Sons, Inc. 1997. New York.
- Fatigati, V. and R. A. Murphy. 1984. Actin and Tropomyosin Variants in Smooth Muscle. Dependence on Tissue Type. *J. Biological Chem.* 259: 14383-14388.
- Gabbiani, G. O. Kacher, W. S. Bloom, J. Vandekerckhove and K. Weber. 1984. Actin Expression in Smooth Muscle Cells of Rat Aortic Intimal Thickening, Human Atheromatous Plaque and Cultured Rat Aortic Media. *J. Clin. Invest.* 73, 148-152.
- Gabbiani, G., E. Rungger-Bradle, C. De Chastonay and W. W. Franke. 1982. Vimentin Containing Smooth Muscle Cells in Aortic Intimal Thickening After Endothelial Injury. *Lab. Invest.* 47, 265-269.
- Garrett, Reginald H. and Charles M. Grisham. 1999. *Biochemistry*. 2nd Ed. Saunders College Publishing.
- Larson, D. M., K. Fujiwara, R. W. Alexander and M. A. Gimbrone. 1984. Myosin in Cultured vascular Smooth Muscle Cells: Immunofluorescence and Immunochemical Studies of Alterations in Antigenic Expression. *J. Cell. Biol.* 99, 1582-1589.
- Hicks, M.J., M. Shigekawa and A. M. Katz. 1979. Mechanism by which Cyclic Adenosine 3':5'-Monophosphate-Dependent Protein Kinase Stimulates Calcium Transport in Cardiac Sarcoplasmic Reticulum. *Circ. Res.* 44: 384-391.
- Jiang, He and N. L. Stephens. 1994. Calcium and Smooth Muscle Contraction. *Molecular and Cellular Biology.* 135:1-9.
- Johnson, Gary L., Harvey R. Kaslow, Zvi Farfei and Henry R. Bourne. 1980. Genetic Analysis of Hormone-Sensitive Adenylate Cyclase. *Advances to Cyclic Nucleotide Research.* 13;1-33.
- Jones, A.W., D.B. Bylund and L. R. Forte. 1983. cAMP-dependent Reduction in Membrane Fluxes During Relaxation of Arterial Smooth Muscle. H309-H311.
- Kanoh, S., M. Ito, E. Niwa, Y. Kawano and D. Hartshorne. 1993. *Biochemistry.* 32, 8902-8907.
- Kelley, C., P. D'Amore, H. Hechtman and D. Shepro. 1988. Vasoactive hormones and cAMP affect pericyte contraction and stress fibers in vitro. *Journal of Molecular and Cell Biology.* 184-194.
- Kramer, G. L. and Hardman, J. G. (1980). cyclic nucleotides and blood vessel contraction. In "Handbook of Physiology: The Cardiovascular System" (David F. Bohr, Andrew P. Somyo, and Harvey V. Sparks, Eds.), Vol. II, pp. 39-179-199. American Physiological Society, Bethesda, MD.
- Lindner, E., A. N. Dohadwalla, and B.K. Bhattacharya. 1978. Positive inotropic and blood pressure lowering activity of a diterpene derivative isolated from *coleus forskolii*: forskolin. *Arzneim. Forsch.* 28(1): 284-289.
- Matthews, Christopher K. and K. E. Van Holde. 1996. *Biochemistry*. 2nd Ed. Benjamin Cummings Publishing Company.

- McCumbee, W. D. and E. I. Mangiarua. 1991. Effects of cyclic adenosine 3'-5'-monophosphate on amino acid transport and incorporation into protein in the rat aorta. *Can. J. Physiol. Pharmacol.* 69: 1001-1008.
- McDaniel, N.L., C. M. Rembold, H. M. Richard and R. A. Murphy. 1990. Cyclic AMP Relaxes Swine Arterial Smooth Muscle Predominantly By Decreasing Cell Ca²⁺ Concentration. *Journal of Physiology.* 439: 147-160.
- Mewes, Thorsten, Silke Dutz, Ursula Ravens and Karl H. Jakobs. 1993. Activation of Calcium Currents in Cardiac Myocytes by Empty B-Adrenoceptors. *Circulation.* 88(6); 29-16-2922.
- Nabika, T., Y. Nara, L. Yamori, W. Lovenburg and J. Endo. 1985. Angiotension II and phorbol ester enhance isoprotenerol- and vasoactive intestinal peptide (VIP)-induced cyclic AMP accumulation in vascular smooth muscle cells. *Biochem. Biophys. Res. Commun.* 131: 30-36.
- Nakamura, H. and K. I. Ohtsubo. 1992. Ultrastructure Appearance of Atherosclerosis in Human and Experimentally-induced Animal Models. *Electron Microsc. Rev.* 5, 129-170.
- Sawtell, N. M. and J. L. Lessard. 1989. Cellular Distribution of Smooth Muscle Actins During Mammalian Embryogenesis: Expression of the Alpha-vascular but not the Gamma-Enteric Isoform in Differentiating Striated Myocytes. *J. Cell Biol.* 109, 2929-2937.
- Schorderet-Slatkine, S. and E. Baulieu. 1982. *Endocrinology.* 111: 1385-1387.
- Seamon, K. and J.W. Daly. 1981. Activation of adenylate cyclase by the diterpene forskolin does not require the guanine nucleotide regulatory protein. *J. Biol. Chem.* 256 (19): 9799-9801.
- Seamon, K. B. and J. W. Daly. 1981. Forskolin: A Unique Diterpene Activator of Cyclic AMP-generating Systems. *Journal of Cyclic Nucleotide Research.* 7(4); 201-224.
- Seamon, K. B., Padgett, W. and Daly, J. W.: Forskolin- unique diterpene activator of adenylate cyclase in membranes and in intact cells. *Proc. Natl. Acad. Sci.* 78, 3363-3367 (1981)
- Shirinsky, V. P., K. G. Birukov, V. E. Koleliansky, M. A. Glukhova, E. Spanidis, R.E. Rogers, J. D. Campbell and G. R. Campbell. 1991. Density-related Expression of Caldesmon and Vinculin in Cultured Rabbit Aortic Smooth Muscle Cells. *Exp. Cell. Res.* 194, 186-189.
- Smith, J. B., S. D. Dwyer and L. Smith. 1989. Decreasing extracellular Na⁺ concentration triggers inositol polyphosphate production and Ca²⁺ mobilization. *J. Biological Chemistry.* 264: 831-837.
- Stary, H. C., A. B. Chandler, S. Glagov, J. R. Guyton, W. Insull, M. E. Rosenfeld, S. A. Schaffer, G. J. Schwatz, W. D. Wagner and R. W. Wissler. 1994. A Definition of Intial, Fatty Streak and Intermediate Lesions of Atherosclerosis. A Report from the Committee on Vascular Lesions of the Council on Arteriosclerosis, American Heart Association. *Circulation* 89, 2462-2478.
- Thyberg, J. Differentiated properties and proliferation of arterial smooth muscle cells in culture. *International review of Cytology.* 169: 183-265.

- Wang, S., G. Wright, W. Geng and G. L. Wright. 1997. Retinol influences contractile function and exerts an anti-proliferative effect on vascular smooth muscle cells through an endothelium-dependent mechanism. *Pflugers Arch-Eur J Physiol.* 434:669-677.
- Wright, G. and A. Battistella-Patterson. 1998. Involvement of the cytoskeleton in calcium-dependent stress relaxation of rat aortic smooth muscle. *Journal of Muscle Research and Cell Motility.* 19: 405-414.